B6985

Encl to
9-21-84 ltr
to Brooks

Benchmark Problems for Waste Package Computer Codes

Draft Report

Submitted to:

Division of Waste Management
Office of Nuclear Materials
Safety & Safeguards
U.S. Nuclear Regulatory Commission
Washington, D.C. 20555
NRC FIN B6985

Submitted by:

CorSTAR Research, Inc.
7315 Wisconsin Avenue
Suite 702 North
Bethesda, Maryland 20814

NUREG/CR-XXXX

Benchmark Problems for Waste Package Computer Codes

Draft Report

Manuscript Completed:
Date Published:

Prepared by:
W. Coffman, D. Vogt, M. Mills

CorSTAR Research, Inc.
7315 Wisconsin Avenue
Suite 702 North
Bethesda, MD 20814

Prepared for:
Division of Waste Management
Office of Nuclear Material Safety and Safeguards
U.S. Nuclear Regulatory Commission
Washington, D.C. 20555
NRC FIN B6985

ABSTRACT

This report provides benchmark problems for computer codes that can be used for analysis of a high-level waste package. Problems with analytical solutions, hypothetical waste package design problems, and problems simulating field experiments are presented. Types of problems include heat transfer, stress analysis, radiation shielding, corrosion and leaching, and near-field geochemistry. Specific phenomena addressed include thermal conduction, convection, and radiation; elastic and plastic stress analysis; creep; particle transport for shielding analysis; empirical analysis of corrosion and leaching; and elevated temperature geochemistry.

CONTENTS

CONTENTS (continued)

LIST OF FIGURES

List of Figures (continued)

List of Figures (continued)

List of Figures (continued)

LIST OF TABLES

List of Tables (continued)

List of Tables (continued)

List of Tables (continued)

List of Tables (continued)

ACKNOWLEDGMENTS

We gratefully acknowledge the assistance of and for their critical review of this manuscript. The completion of the manuscript was made possible by the diligent efforts of Ms. Helen Romm and Ms. Marilyn Singer. This study was performed for the U.S. Nuclear Regulatory Commission under contract NRC-02-81-026. The NRC Project Officers were Dr. Daniel Fehringer and Mrs. Pauline Brooks.

1.0 INTRODUCTION

1.1 Background

The effective management of high-level radioactive wastes is essential to protect public health and safety. The Department of Energy (DOE), through responsibilities inherited from the Energy Research and Development Administration (ERDA) and the Atomic Energy Commission (AEC), and the authority granted in the Nuclear Waste Policy Act, is charged with the safe disposal of these wastes. The Nuclear Regulatory Commission (NRC), through authority granted by the Energy Reorganization Act of 1974, which created the NRC, and the Nuclear Waste Policy Act, is responsible for the regulation of high-level waste management.

The Environmental Protection Agency (EPA) has the authority and responsibility for setting general standards for radiation in the environment. The NRC is responsible for implementing these standards in its licensing actions and for ensuring that public health and safety are protected. The NRC has promulgated technical criteria for regulating the geologic disposal of HLW which incorporate the EPA standard. (The draft EPA standard was published in the Federal Register dated December 29, 1982.) NRC's technical criteria are intended to be compatible with a generally applicable environmental standard. The performance objectives and criteria address the functional elements of geologic disposal of HLW and the analyses required to provide confidence that these functional elements will perform as intended. These technical criteria are described in Chapter 10, Code of Federal Regulations, Part 60 (10 CFR 60).

In discharging its responsibility, the NRC must review DOE repository performance assessments and independently evaluate the performance of the repositories that the DOE seeks to license. Because of the complexity and multiplicity of these performance assessments, computerized simulation modeling is used. Computer simulation models provide a means to evaluate the most important processes that will be active in a repository, thereby permitting assessment and prediction of repository behavior. Another factor necessitating the use of models is that the time frames associated with high-level waste management range from decades to tens of thousand of years.

Accordingly, the NRC is developing models and computer codes for use in supporting these regulations and in reviewing proposed nuclear waste management systems. Independently, the DOE is also developing models and computer codes for use in assessing repository sites and designs. The analytical model and code development effort must include a procedure for independent evaluation of the tool's capability to simulate real processes. Codes must be evaluated to determine their limitations and the adequacy of supporting empirical relations and laboratory tests used for the assessment of long-term repository performance.

1.2 Scope of This Report

This report is one in a series that deals with the independent evaluation of computer codes for analyzing the performance of a high-level radioactive waste repository. The codes used for repository performance assessment have been divided into the following categories: (1) repository siting, (2) radiological assessment, (3) repository design, (4) waste package performance, and (5) overall systems.

Repository siting requires consideration of events at a distance from the repository. Far-field processes include saturated flow, unsaturated flow, surface water flow (flooding routing), solute transport, heat transport, combined solute and heat transport, geochemistry, and geomechanical response.

Radiological assessment includes the development of source terms, the calculation of radionuclide concentrations in the environment, and the analysis of food pathways, dose-to-man, and expected mortality rates.

Repository design covers areas often called the "near-field." The processes in the repository design area include heat transport, flow in fractured media, and rock mechanics.

The waste package code area deals with the very near-field, primarily the interactions that take place within the waste package and the waste package's interactions with the repository host rock. Included are heat transfer, stress analysis, and chemical interactions such as corrosion.

Overall systems include subcategories of the other categories. For example, overall systems codes may consider aspects of radiological assessment, waste package performance, economic cost (e.g., cost/benefit analysis), repository performance, natural multibarrier performance, or probabilistic aspects of repository performance.

The first step in computer code benchmarking is to select the codes potentially useful for thermal and structural analysis. The next step is to summarize the nature of each selected code and then to prepare benchmark problems for code testing. As a prerequisite to designing benchmark problems, the data that will be used in the problems should be summarized. Thus, three reports will be issued for waste package codes: (1) a model summary report (already prepared), (2) a data set report, and (3) a report describing the benchmark problems to be used in code testing. This report is the benchmark problem report for waste package codes.

1.3 Processes Considered

The processes considered in waste package analysis include: heat transfer, engineering mechanics, radiation shielding, corrosion, leaching, and estimation of the waste package geochemical environment. This report provides benchmark problems for each of these areas.

Heat transfer analysis is required to estimate the temperature rise in the initial period of repository operation and during the period following repository decommissioning. The temperature is important because it must be controlled to allow retrieval of wastes within 50 years, if required. For the longer term performance of the waste package systems, temperatures must be controlled to limit the degradation of or physical and chemical changes to the waste package, canister, and engineered barriers.

Heat transfer phenomena considered include conduction, convection, and radiation. Thermal analysis may include either steady-state or transfer conditions and may be either linear or non-linear. Non-linear analysis may be needed to model materials with temperature-dependent properties such as specific heat or thermal conductivity and heat flow with non-linear boundary conditions. Results of thermal analyses in the form of temperature distributions may be used as the input to stress analysis codes to estimate thermal-induced stresses.

Engineering mechanics analyses will be required to estimate the stress and deformation of the waste package after emplacement. Stresses and displacements may be caused by hydrostatic and lithostatic pressure, swelling of backfill material, creep, and thermal loading. Dynamic analyses may be required to estimate loads on the waste package and its contents during shipping or in accidents. Both static and dynamic analyses must be considered for linear as well as non-linear material behavior to assess the performance of the waste package during handling, operation, emplacement, and the decommissioning and long-term storage of waste.

Radiation shielding analyses will be required to estimate the radiation field surrounding the waste package during transportation, repository handling operations, and during the post-emplacement phases. During transportation handling, the radiation field around the waste package must be known in order to estimate the potential dose-to-man. Following emplacement of the waste package, radiation shielding analyses are required to estimate the radiation dose to the host rock and any packing material surrounding the waste package. Dose to geologic and packing materials must be considered to determine whether those materials will be estimation of the waste package geochemical environment. This report provides benchmark problems for each of these areas.

Heat transfer analysis is required to estimate the temperature rise in the initial period of repository operation and during the period following repository decommissioning. The temperature is important because it must be controlled to allow retrieval of wastes within 50 years, if required. For the longer term performance of the waste package systems, temperatures must be controlled to limit the degradation of or physical and chemical changes to the waste package, canister, and engineered barriers.

Heat transfer phenomena considered include conduction, convection, and radiation. Thermal analysis may include either steady-state or transfer conditions and may be either linear or non-linear. Non-linear analysis may be needed to model materials with temperature-dependent properties such as specific heat or thermal conductivity and heat flow with non-linear boundary conditions. Results of thermal analyses in the form of temperature distributions may be used as the input to stress analysis codes to estimate thermal-induced stresses.

Engineering mechanics analyses will be required to estimate the stress and deformation of the waste package after emplacement. Stresses and displacements may be caused by hydrostatic and lithostatic pressure, swelling of backfill material, creep, and thermal loading. Dynamic analyses may be required to estimate loads on the waste package and its contents during shipping or in accidents. Both static and dynamic analyses must be considered for linear as well as non-linear material behavior to assess the performance of the waste package during handling, operation, emplacement, and the decommissioning and long-term storage of waste.

Radiation shielding analyses will be required to estimate the radiation field surrounding the waste package during transportation, repository handling operations, and during the post-emplacement phases. During transportation handling, the radiation field around the waste package degraded by cumulative or instantaneous radiation dose. Radiation dose may also be important in estimating the geochemical environment, especially if the dose rate is high and causes significant radiochemical changes in the very near field surrounding the waste package.

No widely accepted analytical methods exist to estimate corrosion and leaching of waste package canister or waste form materials from first principles. Most of the existing work on waste canister corrosion and waste form leaching is based on the use of experimental data to formulate empirical relationships describing the waste canister and waste form performance over time. The problems presented in this report are designed as verification problems for the code WAPPA proposed by DOE for use in the assessment of overall waste package performance.

Geochemical analysis of the very near-field will be needed to determine the environment in which the waste canister and waste form will perform. The corrosion and leaching behavior of waste package materials is highly dependent on concentrations of chemical species in the very near field. An accurate assessment of chemical speciation will require treatment of elevated temperatures. This generally will require the use of a geochemical analysis code.

1.4 Previous Work

The most extensive testing of codes useful in waste package performance assessment has been done during the development of the individual codes. The documentation available with most codes generally contains from 2 up to as many as 100 problems that have been solved by the code and checked against analytical solutions. These verification problems almost always show excellent agreement with theoretical problems because these are the types of problems used during code development to find "bugs" in the code and to correct the code. In addition, the developers are likely to be more familiar with the code capabilities than are future users and can thus set up a problem consistent with the solution method.

Although most of the routines in a code should have been tested by the developer before the code's release, codes should also be tested by an independent user on a problem or problems developed independently. Studies with this as an objective include the following:

- Westinghouse Electric Corporation Advanced Energy System Division conducted a five-year study of spent fuel dry storage testing at the Engine Maintenance, Assembly, and Disassembly (EMAD) facility on the Nevada Test Site. This project gathered field data on spent fuel temperature profiles in a geometry similar to that which may be encountered in a waste package.

- General Electric gathered data on the radiation field surrounding PWR and BWR fuel assemblies in both air and water at its GE Morris facility. These data were used to compare actual measured data with results predicted by QAD-IV.

- An extensive comparison of geochemical codes conducted under the auspices of the American Chemical Society.

1.5 Model Verification and Validation

The testing of waste package performance assessment models can be divided conceptually into two phases, code verification and code validation. As used in this report, code verification refers to testing the performance of the code. Code validation refers to testing the code against actual physical data obtained from field tests.

Two types of problems can be used for code verification. Problems with known analytical solutions can be used to test the code's numerical solution methods. These will indicate the accuracy of the code and also point out areas where the code may be in error. The second type includes hypothetical waste package problems. These can be used to determine whether the code can simulate interactions likely to occur in a waste package design.

The validation of codes involves gathering data from field tests and comparing the results of the computer model to these field data. The advantage of field validation is that both the code and the mathematical model are tested against the actual physical performance of the waste package concept being modeled. Although this should be an ideal method of testing a code, in reality, this is not the case because several sources of error are possible in the field validation process. These include inaccuracies associated with:

- Inadequate field test data
- The measurements themselves
- Transcription or transmission of data
- Difficulty in modeling boundary conditions as they occur in the field
- Non-homogeneity of materials
- Approximations necessary for numerical modeling

The code validation process provides an estimate of the ability of an analytical method to predict the overall response of the system and assists in quantifying data inaccuracies in code predictions.

1.6 Problem Specifications

The problems described in this report fall into three categories: problems for which analytical or semi-analytical solutions are available, hypothetical problems, and problems based on laboratory or field studies. Problems for which analytical or semi-analytical solutions are available provide a direct means for verifying the correctness of formulation and the accuracy of basic segments of a code's solution algorithm.

Since analytical solutions are based on several restrictive assumptions and are limited to simple cases, several realistic problems, some of which correspond to actual field simulations, have been included in the test series to verify segments of numerical codes that may not otherwise be tested. Two modes of evaluation are available for these problems. First, answers can be compared to simulations using other codes; if major differences in results arise, further investigation is needed. Second, spatial and temporal discretizations can be refined to see if numerical results are convergent. It should be noted that convergence is a necessary but not conclusive indicator of code accuracy.

Besides providing a means of testing a code's solution algorithm, these problems (especially the hypothetical problems and problems based on field or laboratory studies) provide a means of exposing other difficulties that may arise in the practical application of a code. The sources of these other difficulties include inconsistencies between input instructions and the code's actual input requirements, cumbersome input requirements, incompatibilities between codes where output from one code is needed as input to another, and poor output format (for example, too few significant figures).

The description of each problem, in general, consists of the following:

- Problem statement
- Objectives
- Analytical solution, semi-analytical solution, or physical description
- Assumptions
- Input specifications
- Output specifications
- Comments

The problem statement describes the problem and the processes and conditions being considered. The objective section explains what feature of the code the problem will test. If an analytical or semi-analytical solution is available, the solution is described in the next segment. For the hypothetical and validation problems, the physical system being simulated is described. The assumption section specifically lists the assumptions.

The input specifications restate the physical description in terms that can be included in the model. They include values for all necessary physical properties. All required input data must be accurately and completely stated so that results can be reproduced accurately.

Output specifications include the desired solution's specified spatial locations and times. In some cases these results are best presented in graphic form. Comments include any anticipated problems or other information that might be useful to those running the codes.

Grid sizes and time steps have not been specified for problems. This will permit the use of different values for different codes, so as to optimize the use of each code.

The hypothetical problems presented here have not been actually run. Before a problem can be adopted for use as a benchmark problem, it is important to run it on one or more codes. This is necessary to verify that the problem is well posed and reasonably tractable and to adjust values of input parameters to obtain outputs that will be most sensitive to imperfections in the codes.

2.0 THERMAL ANALYSIS CASE PROBLEMS

This section is primarily concerned with heat transfer by conduction. Heat transfer by convection and radiation are also considered to complete the thermal analysis required for a waste package and to estimate accurately the thermal loads to be used for mechanical analyses. Mathematical model representing these forms of heat transfer consist of differential equations together with appropriate boundary and initial conditions that express conservation of energy and describe the temperature over the region of interest. In the most generalized form, the equations model transient and non-uniform heat transfer with non-linear material properties. The generalized form of the heat transfer equations can be solved analytically or semi-analytically only if simplifications are made.

The literature contains well-established analytical and numerical solutions ranging from the very simple to the complex. For example, in the verification of ANSYS code alone, the developers used over 40 problems ranging in complexity from one-dimensional conduction through a wall to the three-dimensional cooling of a fin (Reference DE-82). Benchmark problems have been selected that represent the code features required for waste package analysis. These features include conduction (linear and non-linear), radiation, convection, and heat transfer in one and two dimensions.

2.1 Steady-State Radial Conduction Heat Transfer in a Hollow Cylinder — Temperature Distribution Solution
(Similar to problem solved by Kreith, Reference KR-58, pp. 25-27)

Problem Statement. This problem is designed to determine the steady-state radial temperature distribution in a hollow cylinder of inside radius r_i and outside r_o when a region of radius r_w ($r_w \geq r_i$) has a known volumetric heat generation rate of q''' that is spatially uniform and the outside surface ($r = r_o$) temperature has a known value of T_o.

A sketch of the geometry is shown in Figure 2.1-1.

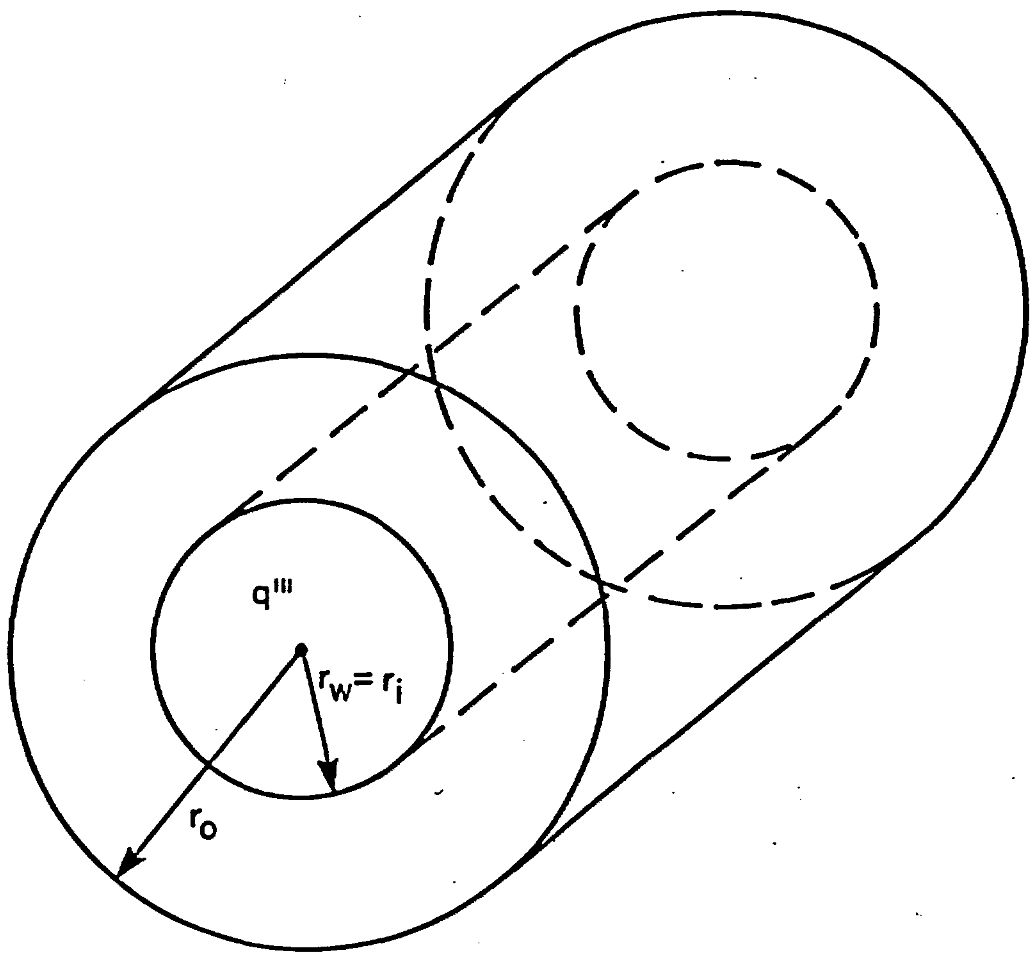

Figure 2.1-1

Hollow Cylinder with Steady-State Radial Conduction for Which the Radial Temperature Distribution Will Be Determined

The thermal conductivity of the material in the annulus is assumed to be constant and independent of temperature.

The differential equation is

$$\frac{d}{dr}\left(r\frac{dT}{dr}\right) = 0 \tag{1}$$

in the region ($r_i \leq r \leq r_o$). The boundary conditions are:

$$\text{at } r = r_o \qquad T = T_o \tag{2}$$

$$\text{at } r = r_i \qquad Q = -k2\pi r_i \ell \frac{dT}{dr}\bigg|_{r = r_i} \tag{3}$$

where

T = temperature [θ]*

r = radial position [ℓ]

r_i = inside radius of hollow cylinder [ℓ]

r_o = outside radius of hollow cylinder [ℓ]

k = thermal conductivity of cylinder material [e/tℓθ]

ℓ = length of cylinder [ℓ]

Q = heat cylinder flow rate to the hollow on the inside surface [e/t]

* When an equation is presented, the generalized dimensions of the quantities are given in brackets. They are: ℓ = length or distance; t = time; f = force; m = mass; θ = temperature change or temperature; e = energy (which is equal to the product of fℓ).

The heat flow rate to the hollow cylinder at steady-state is related to the heat generation rate per unit volume within the solid cylindrical region of radius r_w by

$$Q = q''' \pi r_w^2 \ell \tag{4}$$

where

q''' = volumetric heat generation rate in the heat source region ($0 \leq r \leq r_w$) $[e/t\ell^3]$

r_w = outside radius of cylindrical heat generating region $[\ell]$

Objectives. The solution to this problem can be used to verify the accuracy of a program's thermal model. This is the heat conduction problem that the WAPPA model (Reference CO-84) solves for each engineered barrier surrounding the waste form.

Analytical Solution. The analytical solution for the temperature distribution in the region $r_i \leq r \leq r_o$ is:

$$T = T_o + \frac{Q}{2\pi k \ell} \quad \ell n\left(\frac{r_o}{r}\right) \tag{5}$$

This solution can also be written in terms of the heat generation rate in the region $0 \leq r \leq r_w$ as:

$$T = T_o + \frac{q''' r_w^2}{2 \quad k} \ell n \frac{r_o}{r} \tag{6}$$

where $r_w \leq r_i$.

Using the last expression, the temperature at the inside surface ($r = r_i$) is given by

$$T_i = T_o + \frac{q''' r_w^2}{2k} \ln\frac{r_o}{r_i} \qquad (7)$$

This equation is used successively over the engineered barriers in WAPPA proceeding inward from the outermost annular region.

Assumptions.

- The hollow cylinder material has a unique value for thermal conductivity that is independent of temperature.
- Axial heat conduction is negligible in comparison to radial heat conduction.
- The heat generation is uniform over the cylinder of radius r_w.

Input Specifications.

- Geometry (similar to the defense high-level waste cast-iron overpack, Reference ON-83, pp. 33 and 199)
  - waste region radius $r_w = 30.5$ cm
  - hollow cylinder inside radius $r_i = 30.5$ cm
  - hollow cylinder outside radius $r_o = 67.5$ cm
- Material properties
  - thermal conductivity $k = 0.5$ w/cm°C
- Boundary conditions
  - hollow cylinder outside temperature $T_o = 200$°C
  - waste region volumetric heat generation rate $q''' = 0.001291$ w/cm^3

Output Specifications. The temperature distribution $T(r)$ in the hollow cylinder $r_i \leq r \leq r_o$ is to be determined.

Values at discrete points from $r_i \leq r \leq r_o$ are presented below as determined for the input quantities and Equation 6.

r (cm)	T (°C)
30.5	200.954
35.0	200.789
40.0	200.628
45.0	200.487
50.0	200.360
55.0	200.246
60.0	200.141
67.5	200.0

2.2 Steady-State Radial Conduction Heat Transfer in a Series of Concentric Cylindrical Annuli for a Specified Heat Flow Rate and Outside Surface Temperature

(Similar to problem solved by Holman, Reference HO-81, pp. 28, 29)

Problem Statement. This problem concerns the steady-state radial temperature distribution and interface temperatures for a series of three concentric cylindrical annular sections. Each section has a unique value of thermal conductivity that is independent of temperature. The temperature is assumed to be a continuous function from one annular section to another (no reduced conductance region between sections). There is a known steady radial heat flow rate and a known constant temperature at the outside surface of the outermost annular section. A sketch of the geometric configuration is shown in Figure 2.2-1

The governing equation in region c ($r_3 \leq r \leq r_4$) is

$$\frac{d}{dr}\left(r\frac{dT}{dr}\right) = 0 \tag{8}$$

and the boundary conditions are

$$r = r_4 \quad T = T_4 \tag{9}$$

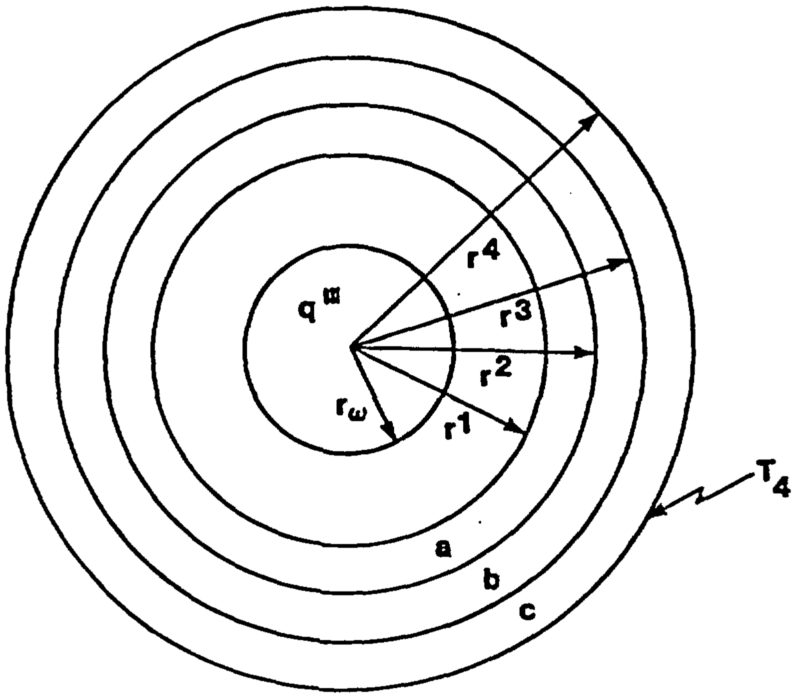

Figure 2.2-1

Three Concentric Cylindrical Annuli a, b, and c in Which the Temperature Distribution Is to Be Determined for Known Volumetric Heat Generation Rate q''' in the Region (0 r r_w) and Known Value of Surface Temperature T_4

$$r = r_3 \qquad Q = -k_c\, 2\, r_3 \left.\frac{dT}{dr}\right|_{r = r_3} \tag{10}$$

where

T = temperature [θ]

r = radial position [ℓ]

r_4 = outside radius of region c [ℓ]

r_3 = inside radius of region c [ℓ]

ℓ = length of cylinder [ℓ]

k_c = thermal conductivity of material of region c [$e/t\ell\theta$]

ℓ = length of cylinder (the analysis could be done on a per unit length basis as it is one-dimensional) [ℓ]

Q = heat flow radially out through the section [e/t]

The heat flow rate to the hollow cylinder at steady-state is related to the heat generation rate per unit volume within the waste region of radius r_W by

$$Q = q''' \pi r_w^2 \ell \tag{11}$$

where

q''' = volumetric heat generation rate in the waste region [$e/t\ell^3$]

r_W = outside radius of cylindrical waste region [ℓ]

The same differential equation applies to regions b and a. After the equation is solved within region c, T_3 at $r = r_3$ is known, and the boundary conditions for region b are

$$r = r_3 \qquad T = T_3 \tag{12}$$

$$r = r_2 \qquad Q = -k_b \, 2\pi r_2 \ell \frac{dT}{dr}\bigg|_{r = r_2} \tag{13}$$

Similarly, after the solution is obtained in region b, T_2 at $r = r_2$ is known. The boundary conditions for region a are

$$r = r_2 \qquad T = T_2 \tag{14}$$

$$r = r_1 \qquad Q = -k_a \, 2\pi r_1 \ell \frac{dT}{dr}\bigg|_{r = r_1} \tag{15}$$

Objectives. The solution can be compared to a WAPPA thermal model solution for a waste package with engineered barriers.

Analytical Solution. The analytical solution for the continuous temperature distribution is

$$T = T_4 + \frac{q''' r_w^2}{2k_c} \ln\frac{r_a}{r} \qquad (r_3 \leq r \leq r_4) \tag{16}$$

$$T = T_3 + \frac{q''' r_w^2}{2k_b} \ln\frac{r_3}{r} \qquad (r_2 \leq r \leq r_3) \tag{17}$$

$$T = T_2 + \frac{q''' r_w^2}{2k_a} \ln\frac{r_2}{r} \qquad (r_1 \leq r \leq r_2) \tag{18}$$

The surface temperature values are

$$T_3 = T_4 + \frac{q''' r_w^2}{2k_c} \ln(\frac{r_4}{r_3}) \tag{19}$$

$$T_2 = T_3 + \frac{q'''r_w^2}{2k_b} \ln\left(\frac{r_3}{r_2}\right) \qquad (20)$$

$$T_1 = T_2 + \frac{q'''r_w^2}{2k_a} \ln\left(\frac{r_2}{r_1}\right) \qquad (21)$$

Assumptions.

- Each region has a unique value for thermal conductivity that is independent of temperature.
- The axial heat conduction and temperature gradient are negligible in comparison to the radial.
- The temperature is continuous from one annular region to another (no reduced conductance region between regions).

Input Specifications. (Similar to defense high level waste cast steel overpack, see Reference ON-83, pp. 33, 159)

- Geometry (see Figure 2.2-1)
  - radii

    waste region outer radius = r_w = 30.5 (cm)
    region a inner radius = r_1 = 30.5 (cm)
    region a outer radius = r_2 = 43.0 (cm)
    region b outer radius = r_3 = 54.0 (cm)
    region c outer radius = r_4 = 65.0 (cm)

- Material properties
  - thermal conductivity

    region a value = k_a = 53.4 (w/m°C)
    region b value = k_b = 54.5 (w/m°C)
    region c value = k_c = 55.6 (w/m°C)

- Boundary conditions
  - region c outside temperature = T_4 = 170 (°C)
  - waste region volumetric heat generation rate = q''' = 0.001315 (w/cm^3)

Output Specifications. The region a, b, and c boundary temperatures T_1, T_2, and T_3 are to be determined. These values can be compared with the values given below.

Radial Position r (cm)	Temperature (°C)
r_1 = 30.5	170.853
r_2 = 43.0	170.460
r_3 = 54.0	170.204
r_4 = 65.0	170.0

2.3 Transient Temperature Response of a Solid Cylinder with Constant Thermal Conductivity

Problem Statement. This problem is concerned with the thermal response of an infinite solid cylinder (radial conduction only) of radius a, initially at a uniform temperature T_i which is equal to the atmospheric temperature. The atmospheric temperature is suddenly changed to a constant value of T_f. Subsequent to this change at time zero, the change in the temperature distribution in the cylinder is to be calculated with time. See Figure 2.3-1.

The energy conservation equation for only transient radial conduction in the region $(0 \leq r \leq a)$ is

$$\frac{1}{r}\frac{\partial}{\partial r}\left(r\frac{\partial T}{\partial r}\right) = \frac{1}{\alpha}\frac{\partial T}{\partial t} \tag{22}$$

where the thermal conductivity is considered to be invariant and where

T = temperature [θ]

r = radial position [ℓ]

t = time [t]

α = thermal diffusivity [ℓ^2/t]

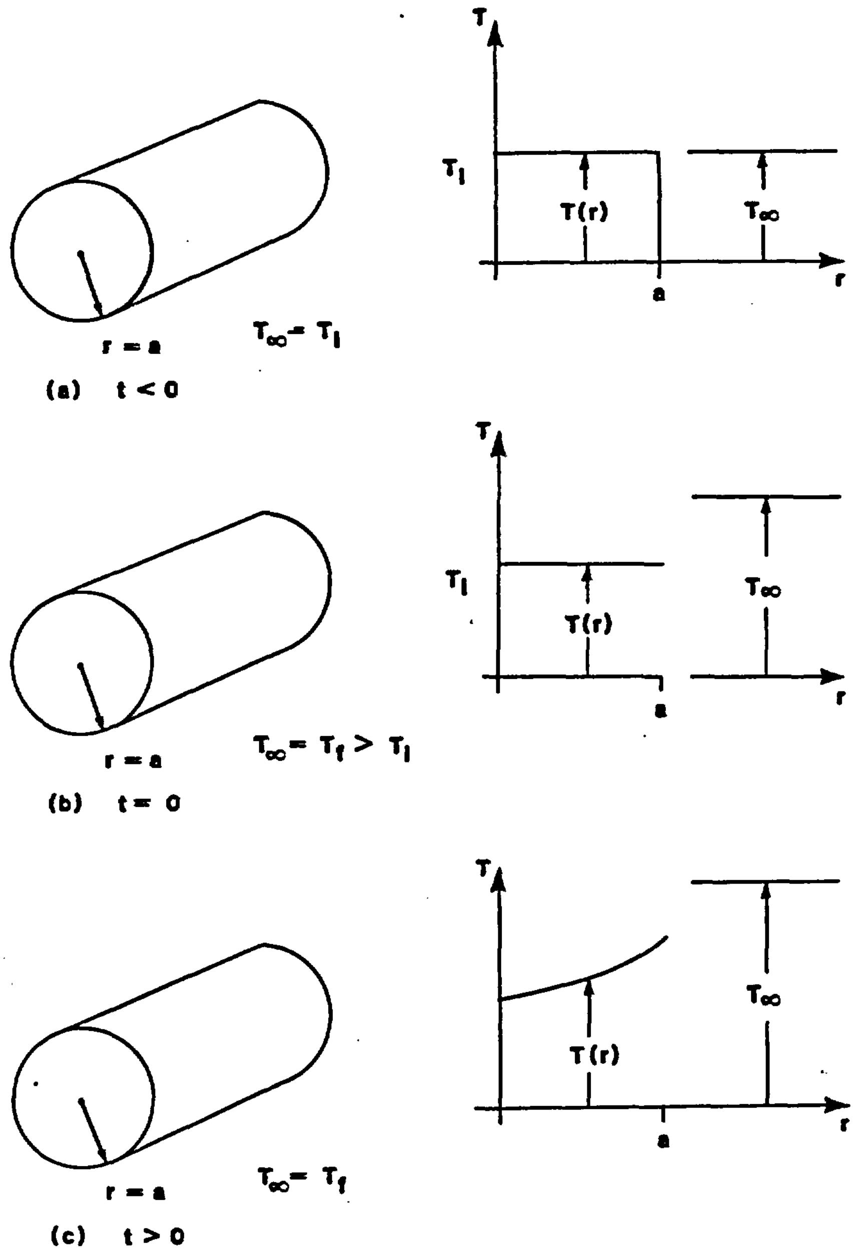

Figure 2.3-1

Cylinder of Radius a Initially in Temperature Equilibrium with Surrounding Atmosphere at Temperature T_i. At Time Zero the Surrounding Atmospheric Temperature Is Increased to a Value $T_\infty = T_f$

At the surface of the cylinder, heat may be convected between the cylinder and the atmospheric fluid. The characteristic temperature of the atmospheric fluid is T_∞. The initial condition is

$$t < 0 \qquad T(r) = T_i \qquad (0 \le r \le a) \tag{23}$$

and the surrounding atmospheric temperature is

$$t < 0 \qquad T_\infty = T_i \tag{24a}$$

$$t \ge 0 \qquad T_\infty = T_f \tag{24b}$$

The boundary conditions are

$$\text{at} \quad r = a, \quad -k \frac{\partial T}{\partial r} = h(T - T_\infty) \tag{25}$$

$$\text{at} \quad r = 0, \quad \frac{\partial T}{\partial r} = 0 \tag{26}$$

where

k = thermal conductivity of cylinder material [$e/t\ell\theta$]

h = convective heat transfer coefficient between the cylinder outer surface and the atmosphere [$e/t\ell^2\theta$]

Objectives. The purpose of this problem is to establish a reference solution for transient radial conduction in a cylinder. It will be representative of waste package transient cooling when there is an abrupt change in atmospheric conditions. The solution applies to thermal conditions where the associated thermal stresses may be important.

Analytical Solution. The solution to Equation 22 for the stated initial and boundary conditions (Reference CA-59) is

$$\frac{T(r,t) - T_\infty}{T_i - T_\infty} = \frac{2ha}{k} \sum_{n=1}^{\infty} \frac{e^{-d\lambda_n^2 t} \; J_o(\lambda_n r)}{\left[\lambda_n^2 a^2 + (\frac{ha}{k})^2\right] J_o(\lambda_n a)} \tag{27}$$

where λ_n are the characteristic values found from solving

$$(\lambda_n a) \; J_1(\lambda_n a) + (\frac{ha}{k}) \; J_o(\lambda_n a) = 0 \tag{28}$$

and wh

$J_($ $\lambda_n a$ f first kind and order
nt variable y

J f first kind and order
one of independent variable y

This analytical solution involves evaluation of the terms of an infinite series until the terms of the convergent series become negligible. A more rapid solution can be obtained by the use of charts developed by Heiser (Reference HE-47), Boelter et al. (Reference BO-42), and Kreith (Reference KR-58). These charts are shown in Figure 2.3-2. They treat r/r_a from 0 to 1.0 in increments of 0.2 (six charts). Each chart presents 11 combinations of values of k/h_a in the range from 0 to 10.

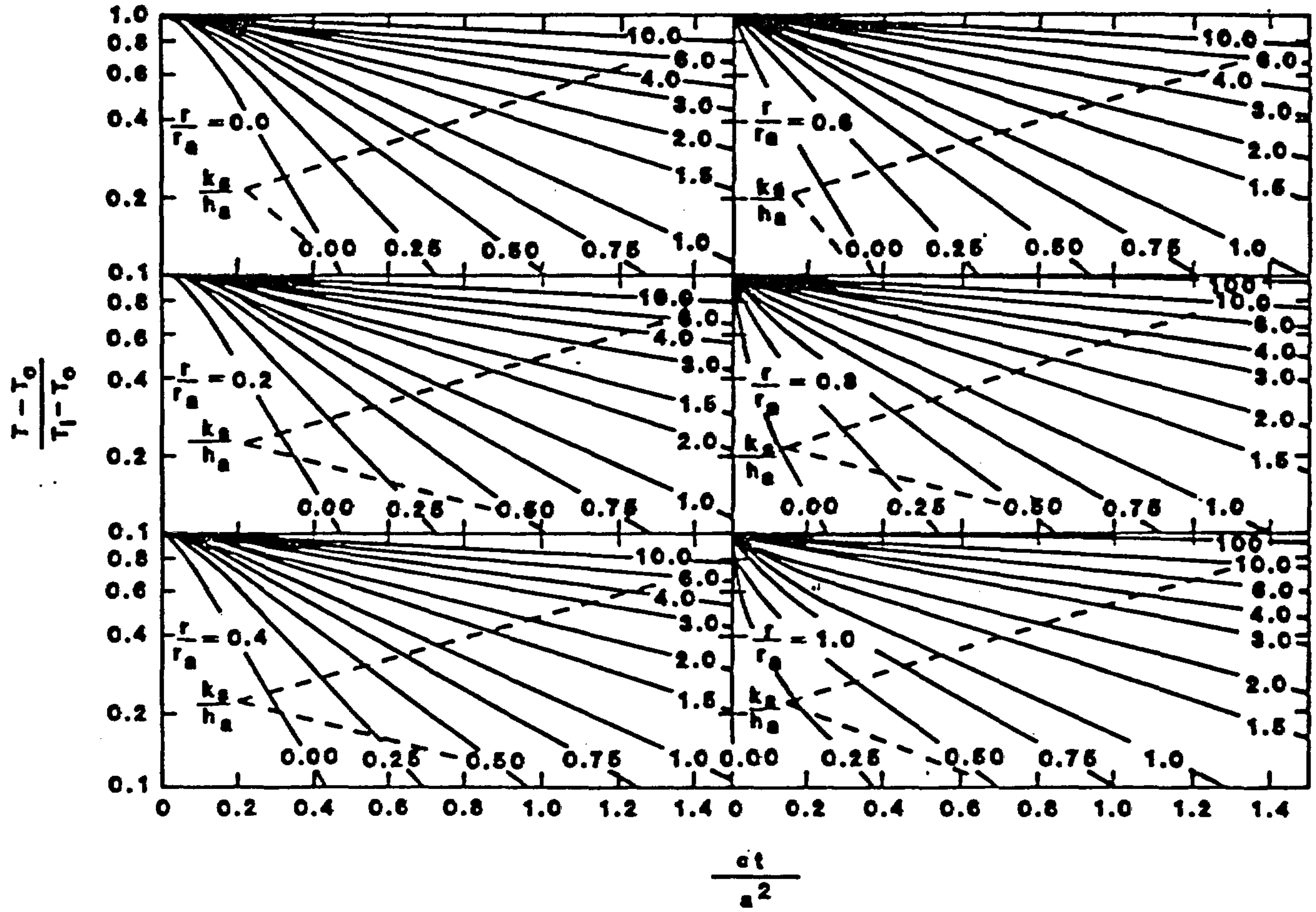

Figure 2.3-2

Dimensionless Temperature Distribution in a Long Circular Cylinder Subjected to a Sudden Change in Environmental Temperature

Assumptions.

- The surface convection heat transfer coefficient is a known constant.
- The atmospheric temperature is constant for $t > 0$ and therefore independent of the thermal energy transferred to the cylinder.
- Thermal conductivity and thermal diffusivity are independent of temperature and thus constant through the transient.

Input Specifications.

- Geometry
  - cylinder radius, $a = 1.0$ (ft)
- Material properties
  - thermal diffusivity of cylinder material, $\alpha = 0.014$ (ft^2/hr)
  - thermal conductivity of cylinder material, $k = 0.700$ (Btu/hr-ft-^oF)
- Parameters
  - convective heat transfer coefficient, $h = 2.8$ (Btu/hr-ft^2-^oF)
- Boundary conditions
  - initial temperature of cylinder and pre-step ($t \leq 0$) atmospheric temperature, $T_i = 300(^oF)$
  - post step ($t > 0$) atmospheric temperature, $t_f = 400$ (^oF)

Values of temperature as a function of radial position and time are given in the following table in terms of the thermal and geometric parameters:

				T(r)	(°F)
	t(hrs)	0.0	14.29	28.57	42.86
r (ft)	$\alpha t/a^2$ / r/a	0.0	0.2	0.4	0.6
0	0.0	300	330.07	366.75	383.46
0.2	0.2	300	332.42	366.99	384.06
0.4	0.4	300	339.32	370.55	385.78
0.6	0.6	300	350.26	376.07	388.45
0.8	0.8	300	361.30	382.96	391.78
1.0	1.0	300	380.02	390.50	395.42

For this problem, the first six roots of Equation 28, λ_n are:

n	λ_n
1	1.9081
2	4.6018
3	7.5201
4	10.5423
5	13.6125
6	16.7073

Summations using the first two roots in Equation 27 will give values of temperature accurate to 0.01°C.

Output Specifications. This problem solves for the temperature response as a function of radius and time. The solution can be compared with the values in the preceding table.

2.4 One-Dimensional Transient Temperature Distribution with Phase Change

Problem Statement. This problem simulates the transient temperature response of a fluid initially at $0^{o}C$ as one wall is lowered to a temperature of $-45^{o}C$ causing a freezing interface to propagate into the liquid. Temperatures are to be calculated as a function of time and distance from the surface boundary. The purpose of this problem is to provide a basis for examining the modeling assumptions and algorithms used by codes for the calculation of temperatures during phase changes for materials with significant latent heats.

Physical Description. A one-dimensional slab is occupied by a liquid at $0^{o}C$. At the beginning of the transient (t=0), the edge is instantaneously lowered to a temperature of $-45^{o}C$. The freezing temperature of the liquid is $-0.01^{o}C$. As heat is removed from the liquid, the freezing front propagates away from the cold surface and into the liquid (see Figure 2.4-1).

Problem Solution. Conductive heat transfer with phase change is governed by the following differential equation

$$k \frac{\partial^2 T}{\partial x^2} = \rho c \frac{\partial T}{\partial t} + L \tag{29}$$

where

T = temperature and the units of temperature are [θ]

x = position measured into the solid/fluid region from the cold edge [ℓ]

ρ = mass density of the fluid and of the solid [m/ℓ³]

c = specific heat of the fluid and of the solid [e/m]

k = thermal conductivity of the fluid and of the solid [e/tℓ]

L = heat of fusion [e/ℓ³]

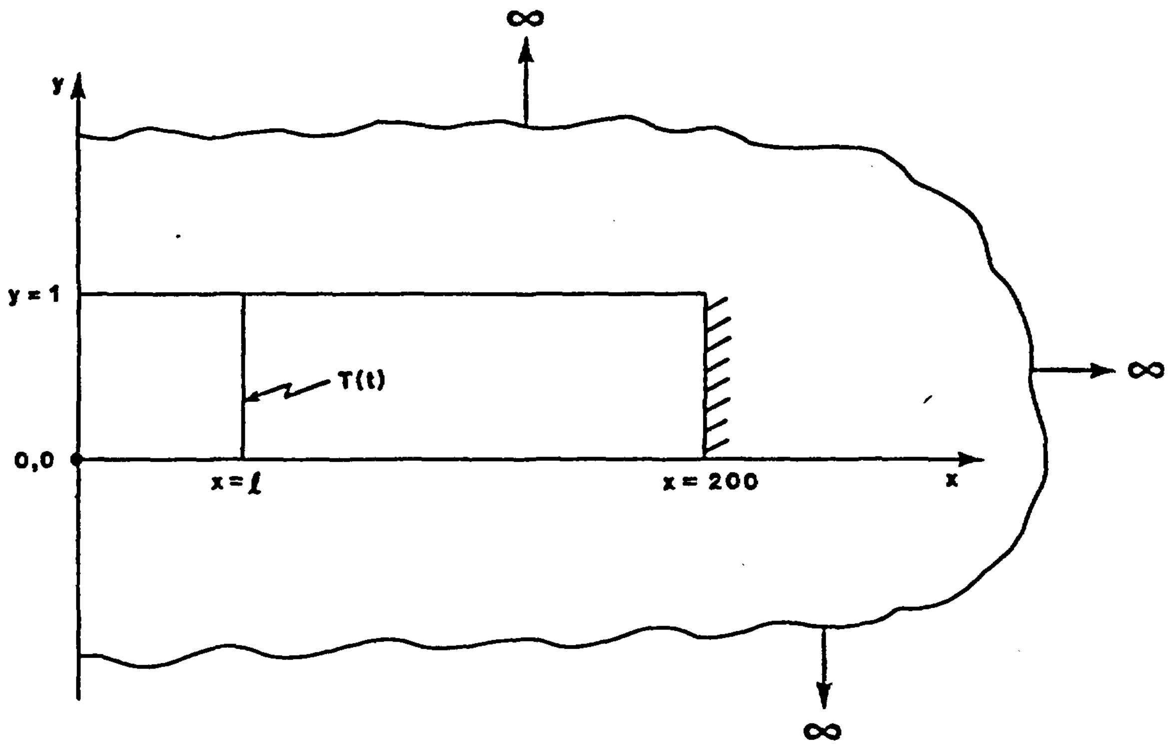

$t < 0$	$0 \leq x \leq \infty$	$T = 0°F$
$t \geq 0$	$x = 0$	$T = -45°F$
$0 \leq t \leq t_{max}$	$x = 200$	$\frac{\partial T}{\partial x} = 0$

where t_{max} is the maximum time to be analyzed

Figure 2.4-1

Slab from Semi-Infinite Freezing Liquid with One Boundary at T = -45°F

Reference CA-59 provides a solution for this problem of:

$$T(x,t) = T_o(1 - \text{erf}\left[\frac{x}{2(at)^{1/2}}\right]/\text{erf}(\lambda)) \quad \text{for } x < 2\lambda(at)^{1/2}$$

$$T(x,t) = T_1 \qquad\qquad \text{for } x \geq 2\lambda(at)^{1/2}$$

where

$T(x,t)$ = temperature

x = distance from the boundary

t = time

T_1 = initial temperature of the liquid

T_o = boundary temperature

a = thermal diffusivity ($a = k/\rho c$)

λ = an equation parameter that satisfies

$$\lambda\, e^{\lambda^2}\, \text{erf}\lambda = \frac{C(T_1 - T_o)}{L\pi^{1/2}}$$

c = specific heat

ρ = density

k = thermal conductivity

L = heat fusion

Table 2.4-1 provides a list of values of the parameter λ as a function of specific heat, temperature difference, and latent heat. When the value of λ is relatively small ($\lambda \leq 0.2$), it can be approximated by

$$\lambda^2 = C(T_1 - T_o)/2L$$

Assumptions. In modeling the problem, it can be assumed that at a point 200 centimeters into the fluid undergoing the phase change, the temperature remains constant at the initial fluid temperature.

The following input parameter values should be used:

$k = 528$ cal/cm sec ^oC

$\rho = 0.92$ g/cm^3

$c = 0.48$ cal/g ^oC

$a = 1196$ sec.cm^2

$L = 144$ cal/g

$T_1 = 0^oC$

$T_0 = -45^oC$

$\frac{C(T_1-T_0)}{L\pi^{1/2}} = 0.0846$

$\lambda = 0.267$

Calculated results can be compared with the values in Table 2.4-2.

Output Specifications. The outputs for this problem are the temperature as a function of time and distance. The temperatures are to be calculated at positions 1, 2, 5, 10, 20, 50, and 100 centimeters from the boundary at times of 0.25, 0.5, 1, 2, 5, 10, 20, 50, and 100 seconds.

Table 2.4-1

Values of the Parameter

$\frac{C(T_0-T_1)}{L\pi^{1/2}}$	λ
0.01	0.09386
0.02	0.13236
0.03	0.16164
0.04	0.18611
0.05	0.20749
0.06	0.22667
0.07	0.24415
0.08	0.26029
0.09	0.27534
0.10	0.28945
0.20	0.39902
0.30	0.47737
0.40	0.53937
0.50	0.59095
0.60	0.63520
0.70	0.67396
0.80	0.70845
0.90	0.73951
1.0	0.76755
2.0	0.96121
3.0	1.0773
4.0	1.1596
5.0	1.2230
6.0	1.2742
7.0	1.3172
8.0	1.3540
9.0	1.3863
10.	1.4149
20.	1.5974
30.	1.6992
40.	1.7694
50.	1.8226
60.	1.8653
70.	1.9009
80.	1.0314
90.	1.9579

Table 2.4-2

Time-Dependent Temperature Distribution in a One-Dimensional Slab Undergoing Phase Change

Time (seconds)	Distance (cm)	Temperature ^{o}C
0.25	1	-40.01
0.25	2	-35.03
0.25	5	-20.23
0.25	10	0.00
0.25	20	0.00
0.25	50	0.00
0.25	100	0.00
0.50	1	-41.47
0.50	2	-37.95
0.50	5	-27.42
0.50	10	-10.20
0.50	20	0.00
0.50	50	0.00
0.50	100	0.00
1.0	1	-42.51
1.0	2	-40.01
1.0	5	-32.55
1.0	10	-20.03
1.0	20	0.00
1.0	50	0.00
1.0	100	0.00
2.0	1	-43.24
2.0	2	-41.47
2.0	5	-36.19
2.0	10	-27.42
2.0	20	-10.02
2.0	50	0.00
2.0	100	0.00
5.0	1	-43.88
5.0	2	-42.77
5.0	5	-39.42
5.0	10	-33.86
5.0	20	-22.81
5.0	50	0.00
5.0	100	0.00
10.0	1	-44.21
10.0	2	-43.42
10.0	5	-41.06
10.0	10	-37.12
10.0	20	-29.27
10.0	50	- 6.23
10.0	100	0.00

Table 2.4-2 (continued)

Time (seconds)	Distance (cm)	Temperature °C
20.0	1	-44.44
20.0	2	-43.88
20.0	5	-42.21
20.0	10	-39.42
20.0	20	-33.86
20.0	50	-17.35
20.0	100	0.00
50.0	1	-44.61
50.0	2	-44.21
50.0	5	-43.03
50.0	10	-41.06
50.0	20	-37.12
50.0	50	-25.36
50.0	100	- 6.23
100.0	1	-44.75
100.0	2	-44.50
100.0	5	-43.75
100.0	10	-42.51
100.0	20	-40.01
100.0	50	-32.55
100.0	100	-20.23

2.5 Hypothetical Problem to Simulate the Steady-State Temperature Distribution in a Waste Package

Problem Statement. This problem is intended as an extension of Cases 2.1 and 2.2 to include the waste region and an arbitrary number of annular regions. It can be used to determine the steady-state radial temperature distribution in a series of n concentric hollow cylinder (annular sections) which:

- Surround a solid cylinder with a spatially uniform heat generation rate, representative of the waste form
- Have regionally varying values of thermal conductivity
- Have interfaces with a common temperature value (there is no high thermal resistance at the interface between regions). Similarly, the interface between the solid cylinder and the smallest hollow cylinder has a unique value of temperature (no high thermal resistance acts at an interface).

The radial heat flow rate across a cylindrical surface of a radius within the range of radii of the hollow cylinders can be determined algebraically from the outside dimension of the solid cylinder and its volumetric heat generation rate. This algebraic relationship is used along with Fourier's law for conduction to obtain a boundary condition at the inside surface of each annular section in terms of the temperature gradient at that radius. Also, a known temperature exists at the outer surface of the largest annular section. Solutions for the temperature distribution are obtained progressively from the largest annular section to the smallest. For the solid section, the boundary conditions are:

- The temperature on the outside surface is known
- The radial temperature gradient at the center is zero

A sketch of the geometric configuration is shown in Figure 2.5-1.

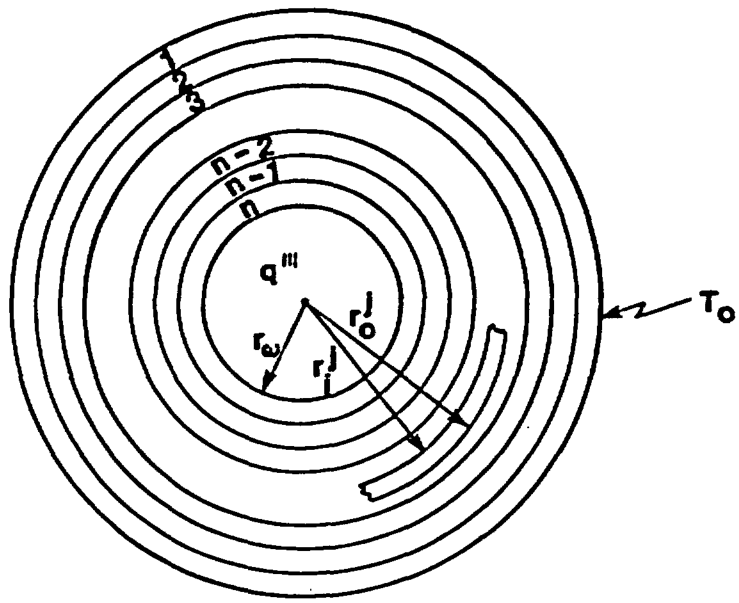

Figure 2.5-1

N Concentric Cylindrical Annuli with Known Outside Temperature T_O, Surrounding a Waste Region of Radius r_W in Which a Known Volumetric Heat Generation Rate of q''' Exists. Each Region Can Have a Unique But Constant Thermal Conductivity Value

For each of the n annular regions, the governing equation is

$$\frac{d}{dr}\left(r\,\frac{dT}{dr}\right) = 0 \tag{30}$$

in terms of the general region j where ($r_i{}^j \leq r \leq r_o{}^j$). The boundary conditions are:

$$r = r_o{}^j \qquad T = T_o{}^j \tag{31}$$

$$r = r_i{}^j \qquad Q = -k^j \;\; 2\pi \;\; r_i{}^j \;\; \left.\frac{dT}{dr}\right|_{r\,=\,r_i{}^j} \tag{32}$$

where

T = temperature

r = radial position

$r_i{}^j$ = inside radius of j^{th} annular region

$r_o{}^j$ = outside radius of j^{th} annular region

k^j = thermal conductivity of material of region j

ℓ = length of cylinder (the analysis could be done on a per unit length basis as it is one-dimensional)

Q = heat flow radially out through the section

The heat flow rate through each hollow cylinder at steady-state is related to the heat generation rate per unit volume within the waste region of radius r_w by

$$Q = q''' \pi r_w^2 \ell \tag{33}$$

where

q''' = volumetric heat generation rate in the waste region ($0 \leq r \leq r_w$)

r_w = outside radius of cylindrical waste region

ℓ = length of cylindrical waste region

The same differential equation and boundary conditions apply to all annular regions. After a solution is obtained for region j, the temperature at $T_i{}^j$ is evaluated and

$$T_o{}^{j+1} = T_i{}^j \tag{34}$$

is used as the boundary condition for region j+1.

For constant thermal conductivity, the differential equation expressing the energy conservation principle in the waste region ($0 \leq r \leq r_w$) is

$$\frac{d}{dr}\left(r \frac{dT}{dr}\right) + \frac{q''' r}{k^w} = 0 \tag{35}$$

where

k^w = thermal conductivity of the waste region and the other symbols are as previously defined. The mathematical statement of the boundary conditions is:

$$r = r_w \qquad T = T_i^n \tag{36}$$

$$r = 0 \qquad \frac{dT}{dr} = 0 \tag{37}$$

where T_i^n is known from evaluating the last solution obtained for annular region n.

Objectives. This problem is useful in representing a multi-region waste package including the waste and the engineered barriers. It can be used to evaluate WAPPA multi-region thermal analysis capabilities. Also, it can be used to evaluate ANSYS and HEATING thermal analysis methods.

Analytical Solution. For the j^{th} annular region where $1 \leq j \leq n$, the solution for the continuous temperature distribution in that region ($r_i^j \leq r \leq r_o^j$) is

$$T = T_o^j + \frac{q''' r_w^2}{2k^j} \ln \frac{r_o^j}{r} \tag{38}$$

which can be evaluated at the inside radius of the j^{th} region, $r = r_i^j$, to give

$$T_i^j = T_o^j + \frac{q''' r_w^2}{2k^j} \ln \frac{r_o^j}{r_i^j} \tag{39}$$

where all terms on the right side are known. By using Equation 34 and incrementing j in Equations 38 and 39, the temperature distribution in the $j+1^{th}$ region and the temperature at the inside surface of the j+1 region can be determined.

The solution to Equation 35 for the temperature distribution in the waste region ($0 \leq r \leq r_w$) for the boundary conditions of Equations 36 and 37 is:

$$T = T_i^n + \frac{q'''}{4k^w}(r_w^2 - r^2) \tag{40}$$

and the maximum temperature occurs at r = 0 and is

$$T_{max} = T_i^w = T_i^n + \frac{q''' r_w^2}{4k^w} \tag{41}$$

where all terms on the right side of Equation 39 are known.

Assumptions.

- Each region has a unique value of thermal conductivity that can be specified at the beginning of the problem and is constant throughout the region.
- The axial heat conduction and temperature gradient are negligible in comparison to the radial.
- The heat generation is uniform throughout the waste region.

Input Specifications.

- Geometry (see Figure 2.5-1)
  - radii (for n = 7)

$r_o^6 = r_i^7 = 60.$ (cm)

$r_o^5 = r_i^6 = 55.$ (cm)

$r_o^4 = r_i^5 = 50.$ (cm)

$r_o^3 = r^{i^2} = 45.$ (cm)

$r_o^2 = r_i^3 = 40.$ (cm)

$r_o^1 = r_i^2 = 35.$ (cm)

$r_i^1 = r_o^W = 30.5$ (cm)

$r_i^W = 0$

- Material Properties
  - thermal conductivity

    $k^7 = 51$ (w/m°C)

    $k^6 = 52$ (w/m°C)

    $k^5 = 53$ (w/m°C)

    $k^4 = 54$ (w/m°C)

    $k^3 = 55$ (w/m°C)

    $k^2 = 56$ (w/m°C)

    $k^1 = 57$ (w/m°C)

    $k^W = 1.0$ (w/m°C)

- Boundary conditions
  - Largest annular region outside temperature = $T_o^7 = 170$ (°C)
  - Waste region volumetric heat generation rate = $q''' = 0.001315$ (w/cm^3)

<u>Output Specifications</u>. The temperatures at $r = 0$, r_i^1, r_i^2, r_i^3, r_i^4, r_i^5, r_i^6, and r_i^7 are to be determined.

Temperatures determined using the analytical solution from Equations 39 and 41 are given in Table 2.5-1.

Table 2.5-1

Analytical Solution for Temperature Distribution

r (cm)	k (w/m^{o}C)	T (^{o}C)	Equation
65		170.00	
	51.0		
60		170.096	(10)
	52.0		
55		170.198	(10)
	53.0		
50		170.308	(10)
	54.0		
45		170.427	(10)
	55.0		
40		170.558	(10)
	56.0		
35		170.704	(10)
	57.0		
30.5		170.852	(10)
	1.0		
0.0		201.434	(12)

2.6 Hypothetical Radial Heat Transfer Analysis of PWR Fuel Assembly in a Vertical Canister

Problem Statement. A series of tests has been conducted to measure the thermal response of 12-foot-long PWR fuel assemblies in a vertical cylindrical canister. The tests were conducted at the Engine Maintenance, Assembly and Disassembly (E-MAD) facility on the Nevada Test Site.

A single PWR fuel assembly was enclosed in a 0.375 inch thick canister, with a 14-inch outside diameter, made from 304 stainless steel pipe. An elevation view of the canister is shown in Figure 2.6-1. The cross section of the fuel assembly section is shown in Figure 2.6-2.

Objectives. It is intended that the steady-state radial temperature profile be determined. The boundary conditions and fuel canister loading are similar to those that may exist in a high-level waste repository.

Analytical Solution. The problem will be used to assess the ability of an analysis program to represent and simulate conditions encountered in the field. No analytical solution is available.

Input Specifications. The dimensions of the canister are shown in Figure 2.6-1. The canister is fabricated from 304 stainless steel. Separate cases are provided for different fuel assembly powers, canister outside temperatures, and fill gases. Tables 2.6-1 and 2.6-2 summarize the conditions under which data have been gathered. Fuel assembly thermal output as a function of time is given in Figures 2.6-3 and 2.6-4.

The thermal properties, including thermal conductivity and surface emissivity, will be taken from the waste package data summary report.

Output Specifications. Temperatures at thermocouple locations given in Figures 2.6-5 and 2.6-6 and Table 2.6-3 will be determined and compared with measured values given in Tables 2.6-4 through 2.6-15 and Tables 2.6-16 through 2.6-27.

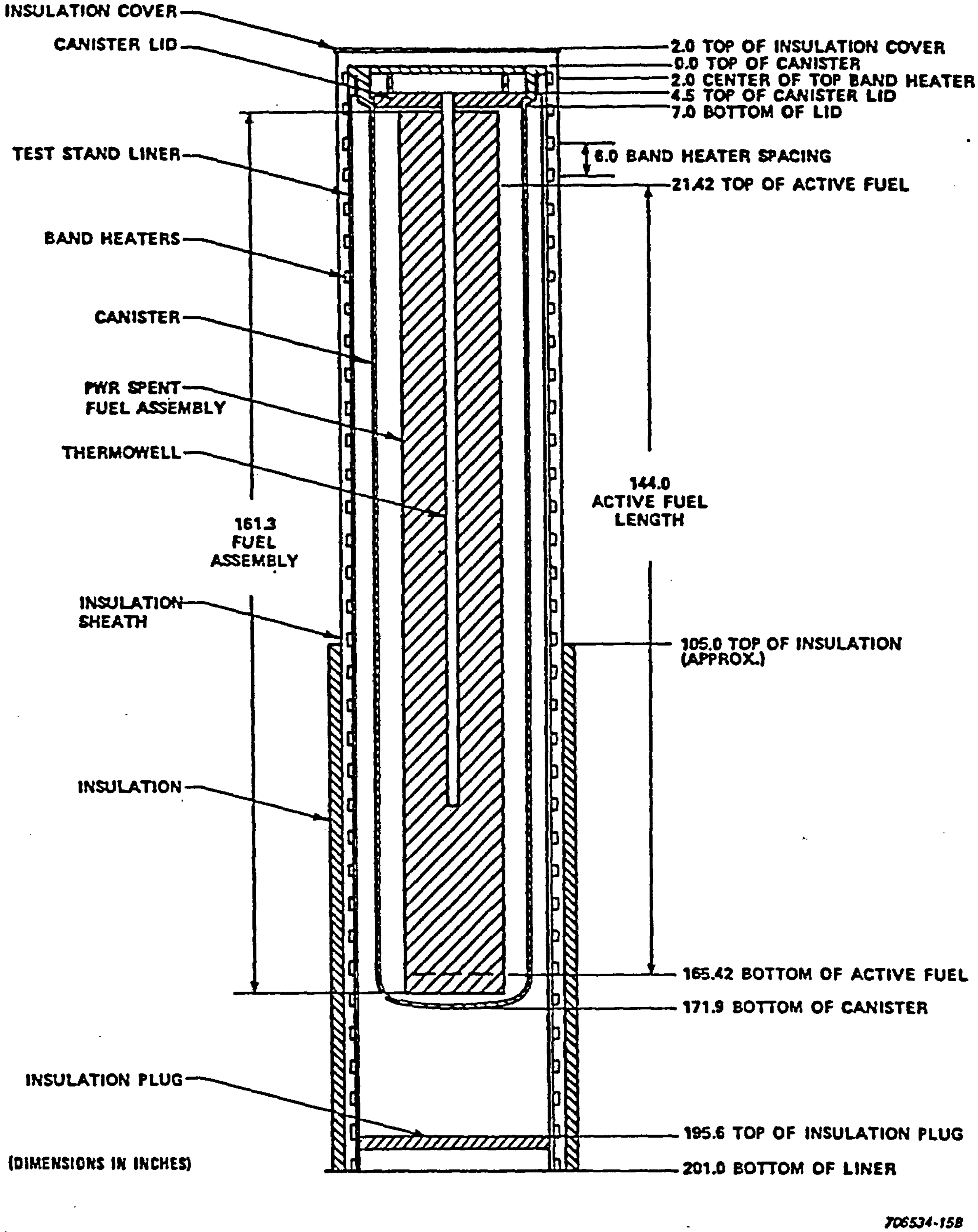

Figure 2.6-1

Elevation View of PWR Fuel Assembly Loaded into Canister

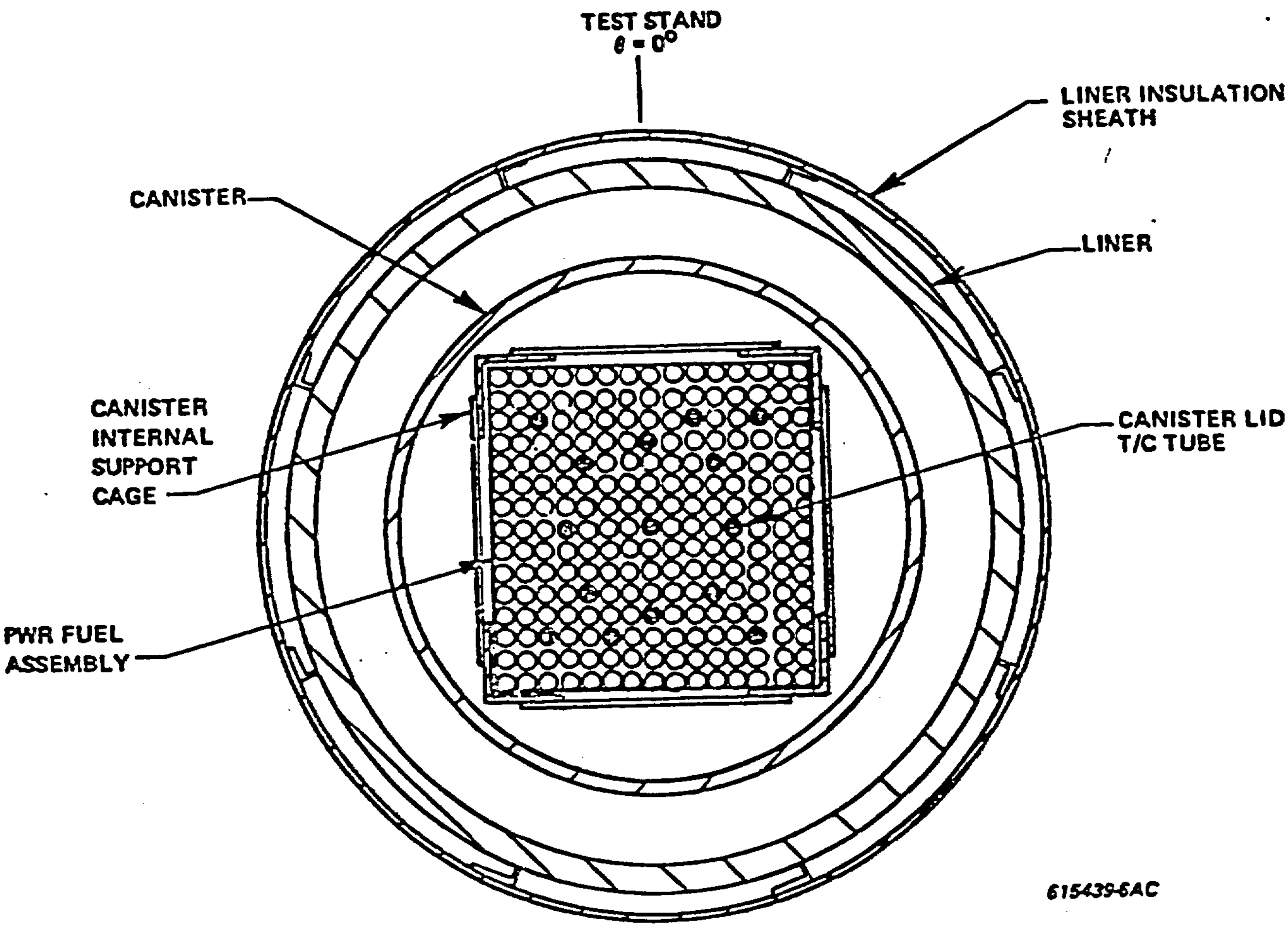

Figure 2.6-2

Cross-Section View of PWR Fuel Assembly Loaded into Canister

Table 2.6-1

Fuel Assembly B43 Temperature Test Summary

Test Condition	Backfill	Date Completed	Data Table	Fuel Assembly Thermal Power-kW
250°F Uniform Canister Profile	Helium	12/6/79	2.6-5	0.760
300°F Uniform Canister Profile	Helium	12/7/79	2.6-8	0.760
400°F Uniform Canister Profile	Helium	12/11/79	2.6-11	0.755
500°F Uniform Canister Profile	Helium	12/17/79	2.6-14	0.755
500°F Uniform Canister Profile	Vacuum	12/20/79	2.6-13	0.755
250°F Uniform Canister Profile	Air	1/4/80	2.6-6	0.745
300°F Uniform Canister Profile	Air	1/14/80	2.6-9	0.740
400°F Uniform Cansiter Profile	Air	1/17/80	2.6-12	0.740
500°F Uniform Canister Profile	Air	1/24/80	2.6-15	0.735
400°F Uniform Canister Profile	Vacuum	1/30/80	2.6-10	0.730
250°F Uniform Canister Profile	Vacuum	2/8/80	2.6-4	0.730
300°F Uniform Canister Profile	Vacuum	2/11/80	2.6-7	0.725

Table 2.6-2

Fuel Assembly D15 Temperature Test Summary

Test Condition	Backfill	Date Completed	Data Table	Fuel Assembly Thermal Power-kW
350°F Uniform Canister Profile	Air	10/8/80	2.6-16	1.340
400°F Uniform Canister Profile	Air	10/10/80	2.6-18	1.340
500°F Uniform Canister Profile	Air	10/17/80	2.6-23	1.330
500°F Uniform Canister Profile	Vacuum	10/20/80	2.6-21	1.325
500°F Uniform Canister Profile	Helium	10/22/80	2.6-22	1.320
400°F Uniform Canister Profile	Helium	10/27/80	2.6-17	1.315
400°F Uniform Canister Profile	Vacuum*	10/31/80	*	*
450°F Uniform Canister Profile	Vacuum*	11/3/80	*	*
450°F Uniform Canister Profile	Helium	11/5/80	2.6-19	1.305
450°F Uniform Canister Profile	Air	11/7/80	2.6-20	1.300
550°F Uniform Canister Profile	Air	11/12/80	2.6-26	1.295
550°F Uniform Canister Profile	Vacuum	11/14/80	2.6-24	1.290
550°F Uniform Canister Profile	Helium	11/17/80	2.6-25	1.285
600°F Uniform Canister Profile	Helium	11/20/80	2.6-27	1.280

*Test backfill was not vacuum; data therefore not included

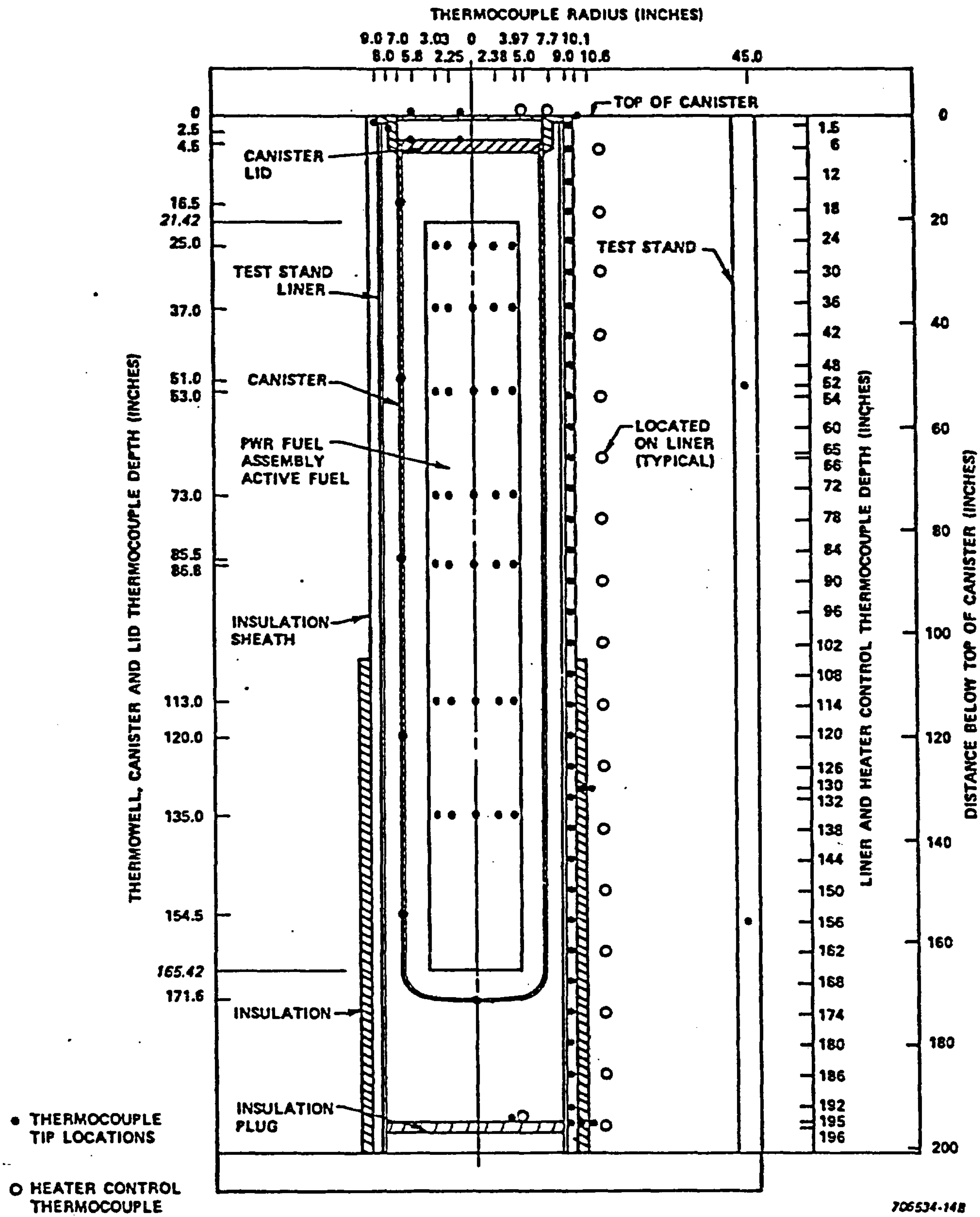

Figure 2.6-3

Canister Thermocouple Locations

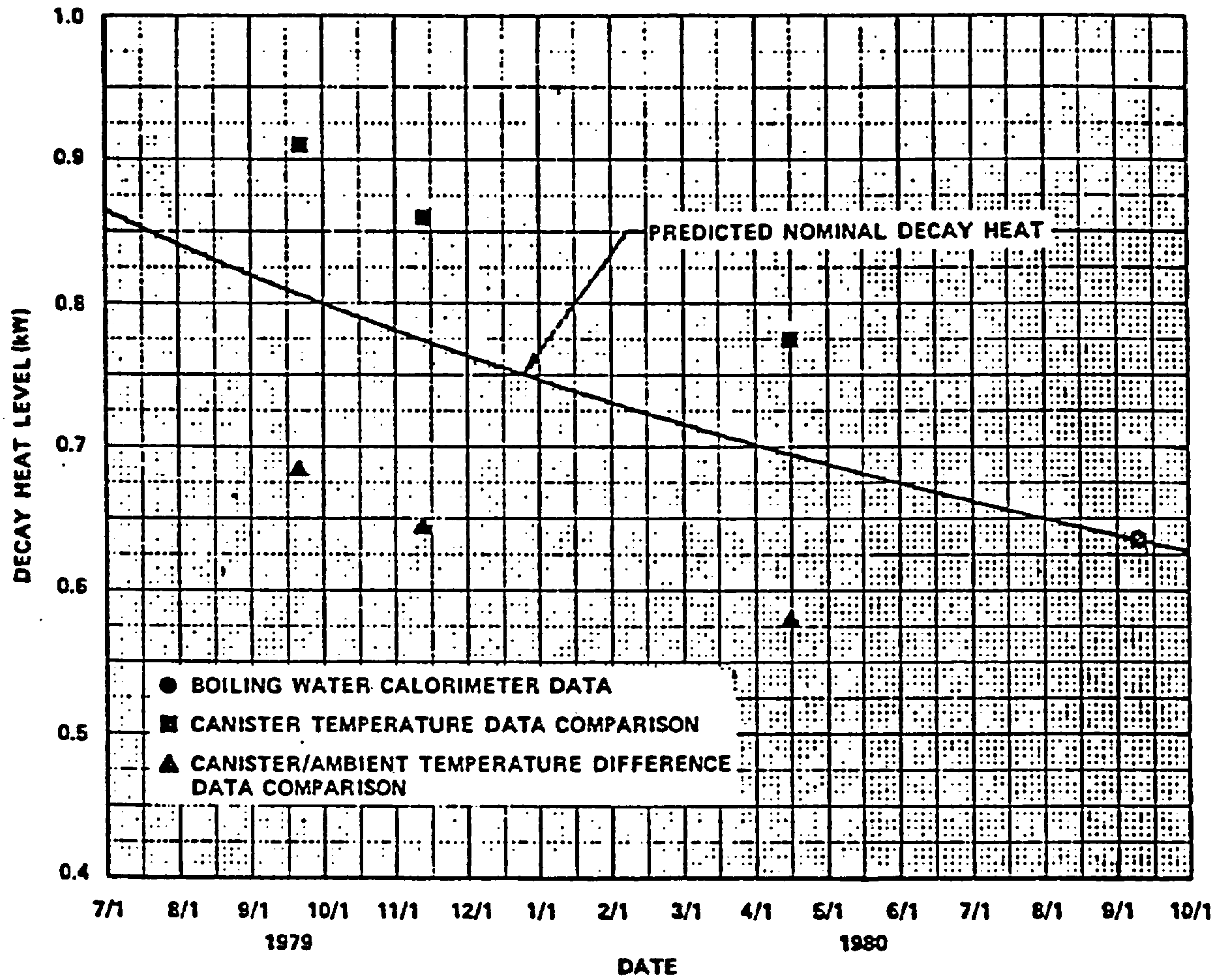

Figure 2.6-4

Comparison of Calorimetry Data with Predicted Decay Heat Curve for Fuel Assembly B43

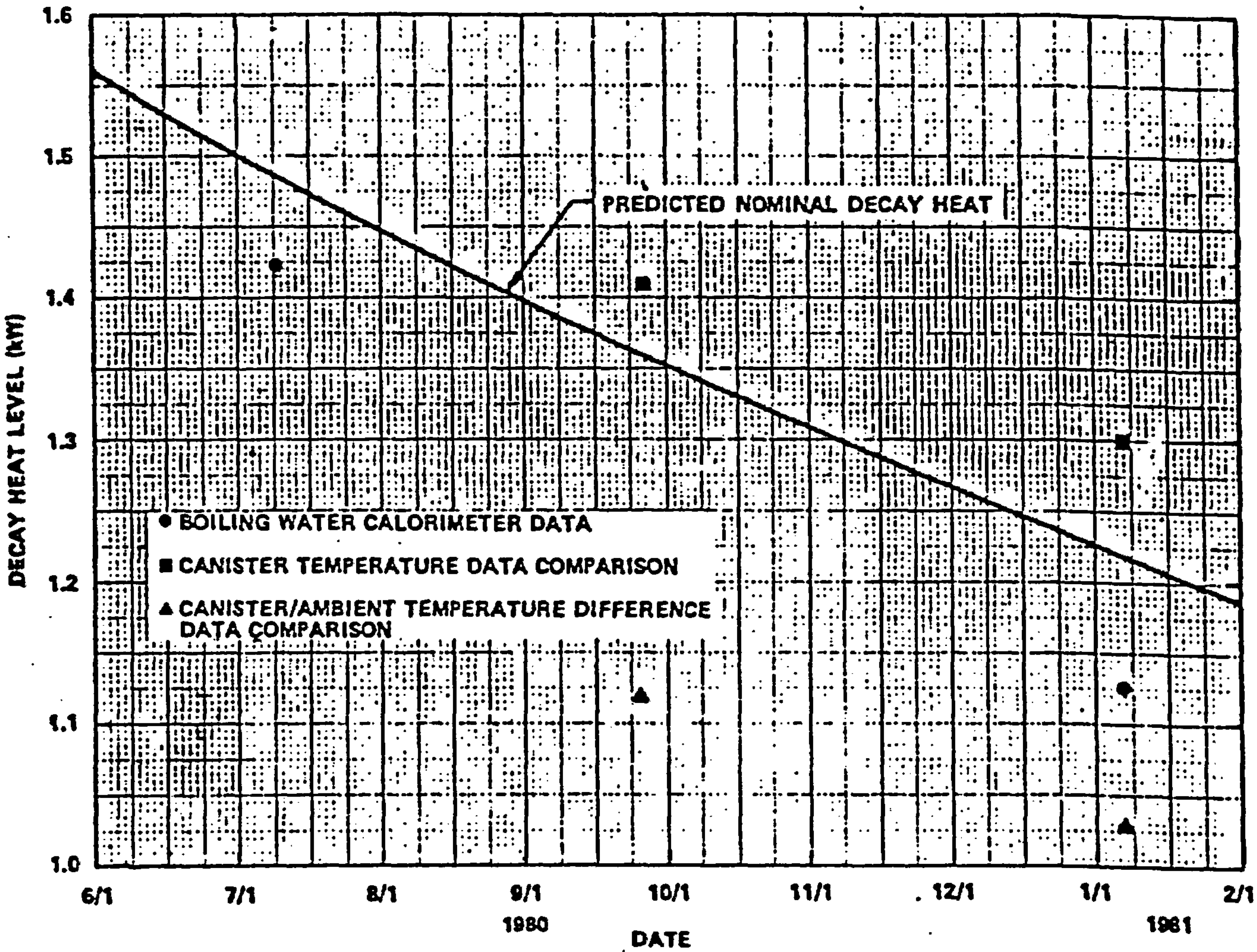

Figure 2.6-5

Comparison of Calorimetry Data with Predicted Decay Heat Curve for Fuel Assembly D15

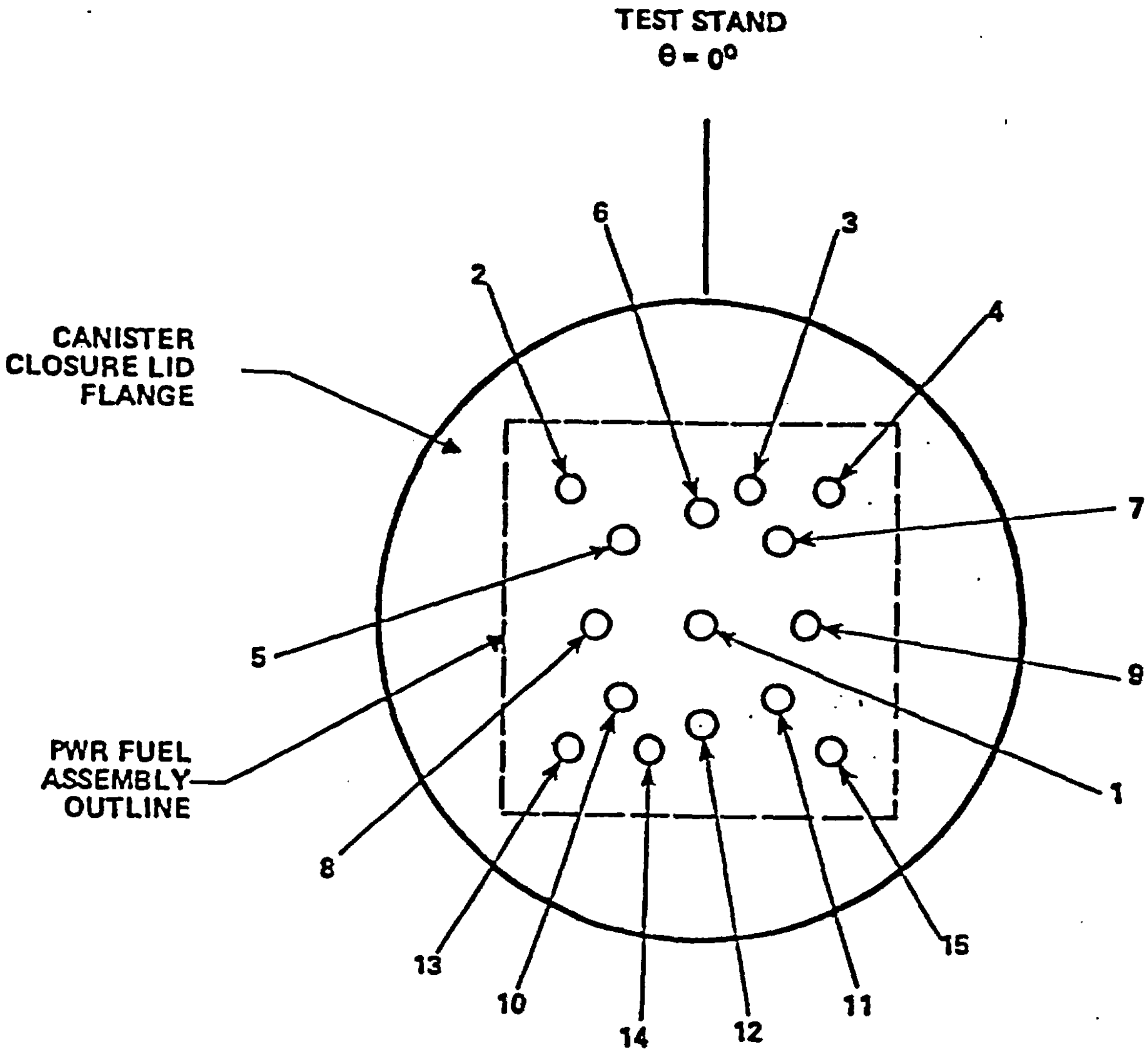

Figure 2.6-6

Canister Lid Thermowell Tube Identification
(Top View of Lid)

Table 2.6-3

Fuel Assembly Internal Temperature Measurement Test
Thermocouple Locations

Data Channel (T/C) No.	Distance Below Top of Canister (In.)	Radius (In.)	Orientation (Degrees)	Location
Data Thermocouples				
301	135.0	0	-	Canister Lid Thermowell No. 1*
302	113.0	0	-	Canister Lid Thermowell No. 1
303	86.8	0	-	Canister Lid Thermowell No. 1
304	73.0	0	-	Canister Lid Thermowell No. 1
305	53.0	0	-	Canister Lid Thermowell No. 1
306	37.0	0	-	Canister Lid Thermowell No. 1
307	25.0	0	-	Canister Lid Thermowell No. 1
308	135.0	3.97	315	Canister Lid Thermowell No. 2
309	113.0	3.97	315	Canister Lid Thermowell No. 2
310	86.8	3.97	315	Canister Lid Thermowell No. 2
311	73.0	3.97	315	Canister Lid Thermowell No. 2
312	53.0	3.97	315	Canister Lid Thermowell No. 2
313	37.0	3.97	315	Canister Lid Thermowell No. 2
314	25.0	3.97	315	Canister Lid Thermowell No. 2
315	135.0	3.03	22	Canister Lid Thermowell No. 3
316	113.0	3.03	22	Canister Lid Thermowell No. 3
317	86.8	3.03	22	Canister Lid Thermowell No. 3
318	73.0	3.03	22	Canister Lid Thermowell No. 3
319	53.0	3.03	22	Canister Lid Thermowell No. 3
320	37.0	3.03	22	Canister Lid Thermowell No. 3
321	25.0	3.03	22	Canister Lid Thermowell No. 3
322	135.0	3.97	45	Canister Lid Thermowell No. 4
323	113.0	3.97	45	Canister Lid Thermowell No. 4
324	86.8	3.97	45	Canister Lid Thermowell No. 4
325	73.0	3.97	45	Canister Lid Thermowell No. 4
326	53.0	3.97	45	Canister Lid Thermowell No. 4
327	37.0	3.97	45	Canister Lid Thermowell No. 4
328†	25.0	3.97	45	Canister Lid Thermowell No. 4
329	135.0	2.38	315	Canister Lid Thermowell No. 5
330	113.0	2.38	315	Canister Lid Thermowell No. 5
331	86.8	2.38	315	Canister Lid Thermowell No. 5
332	73.0	2.38	315	Canister Lid Thermowell No. 5
333**	53.0	2.38	315	Canister Lid Thermowell No. 5
334	37.0	2.38	315	Canister Lid Thermowell No. 5
335	25.0	2.38	315	Canister Lid Thermowell No. 5

* See Figure 2.6-6 for illustration of thermowell locations

** Connected to heater controller C21

† Electrical check showed low internal resistance - readings may be in error

Table 2.6-4

Fuel Assembly Internal Temperature Measurement Test Thermocouple Data Fuel Assembly: B43

DATE: 2/8/80 TIME: 9:00 a.m.

TEST CONDITIONS: Uniform Canister Temperature at 250°F With Vacuum

T/C No.	Temp(°F)	T/C No.	Temp(°F)	T/C No.	Temp(°F)
362	347.6	428	251.4	492	222.9
361	373.7	427	255.5	491	77.1
360	384.0	426	258.7	490	76.0
359	386.7	425	257.2	489	77.3
358	388.4	424	255.3	488	76.2
357	380.0	423	253.2	487	88.9
356	285.7	422	251.2	486	111.9
355	347.4	421	252.1	485	
354	373.6	420	247.1	484	89.6
353	382.1	419	246.2	483	115.3
352	384.1	418	244.2	482	160.4
351	385.5	417	242.7	481	146.6
350	378.5	416	236.6	480	128.7
349	303.3	415	237.5	479	114.5
348	347.6	409	234.3	478	160.7
347	373.9	408	233.9	477	232.8
346	384.5	407	215.1	476	249.5
345	386.4	406	214.6	475	227.8
344	388.6	405	292.3	474	253.4
343	381.5	404	326.7	473	228.9
342	305.9	403	348.8	472	221.7
341	350.6	402	356.8	471	190.0
340	374.9	401	359.1	470	199.9
339	384.1	400		469	204.6
338	385.3	399	354.3	468	206.0
337	387.2	398	300.8	467	196.6
336	381.2	397	338.1	466	205.9
335	304.7	396	360.8	465	206.0
334	349.9	395	368.5	464	208.0
332	383.0	394	370.5	463	204.2
331	383.7	393	372.9	462	207.2
330	385.0	392	364.4	461	206.9
329	378.6	391	293.5	460	94.2
328	292.3	390	329.6	459	197.8
327	329.8	389	348.9	458	199.2
326	349.7	388	356.8	457	204.0
325	359.1	387	358.5	456	201.3
324	361.8	386	359.9	455	201.3
323	362.5	385	350.9	454	190.8
322	356.3	384	304.3	453	180.3
321	298.2	383	345.7	451	188.1
320	339.7	382	372.4	450	193.5
319	362.4	381	382.2	449	195.7
318	371.9	380	383.8	448	191.4
317	374.0	379	385.2	447	198.3
316	375.9	378	377.8	446	200.6
315	369.4	377	299.9	445	210.3
314	292.3	376	344.0	444	221.3
313	327.3	375	372.5	443	234.7
312	348.0	374	382.1	442	224.7
311	354.9	373	383.6	441	217.3
310	357.0	372	385.9	440	228.0
309	358.4	371	379.3	437	236.8
308	354.1	370	304.9	436	239.8
307	310.8	369	346.3	435	244.3
306	357.7	368	373.0	434	255.9
305	389.4	367	382.2	433	257.7
304	400.5	366	383.0	432	261.8
303	400.6	365	383.6	431	261.4
302	402.2	364	377.1	430	252.0
301	396.1	363	300.6	429	250.2

Table 2.6-5

Fuel Assembly Internal Temperature Measurement Test
Thermocouple Data Fuel Assembly: B43

DATE: 12/6/79 TIME: 9:00 a.m.
TEST CONDITONS: Uniform Canister Temperature at 250°F With Helium

T/C No.	Temp(°F)	T/C No.	Temp(°F)	T/C No.	Temp(°F)
362	318.3	428	257.0	492	223.0
361	329.4	427	259.5	491	78.5
360	333.7	426	264.7	490	77.3
359	333.9	425	261.3	489	78.1
358	335.1	424	261.0	488	77.7
357	327.5	423	256.7	487	83.5
356	264.3	422	260.1	486	111.8
355	318.9	421	260.4	485	100.2
354	330.6	420	256.8	484	91.1
353	333.1	419	256.3	483	105.2
352	332.5	418	252.5	482	161.0
351	333.2	417	248.3	481	143.4
350	326.9	416	237.7	480	133.0
349	287.3	415	238.0	479	111.6
348	317.9	409	174.9	478	171.5
347	329.5	408	235.6	477	222.8
346	333.1	407	215.6	476	247.1
345	332.7	406	214.9	475	223.0
344	334.4	405	281.9	474	257.7
343	328.0	404	304.8	473	233.6
342	289.1	403	313.6	472	224.0
341	320.2	402	315.2	471	191.9
340	330.4	401	316.1	470	200.1
339	333.2	400	316.6	469	205.8
338	332.1	399	311.5	468	207.0
337	333.9	398	288.1	467	197.9
336	327.5	397	314.2	466	206.9
335	288.3	396	323.0	465	207.3
334	320.0	395	325.5	464	208.9
332	332.5	394	325.3	463	205.3
331	331.1	393	326.4	462	209.0
330	332.0	392	318.0	461	209.4
329	325.8	391	282.8	460	91.3
328	280.9	390	308.2	459	199.4
327	306.5	389	315.2	458	201.5
326	312.8	388	317.5	457	207.1
325	316.0	387	317.1	456	202.2
324	316.3	386	317.5	455	204.7
323	317.4	385	308.8	454	193.8
322	310.9	384	289.5	453	182.9
321	284.7	383	318.0	451	193.5
320	313.6	382	329.9	450	199.1
319	322.8	381	333.3	449	201.7
318	326.1	380	332.7	448	198.4
317	325.5	379	333.4	447	209.6
316	326.9	378	326.7	446	217.0
315	321.0	377	285.8	445	232.0
314	280.1	376	316.2	444	236.7
313	305.2	375	329.1	443	244.1
312	313.1	374	332.0	442	231.3
311	314.0	373	331.7	441	222.3
310	313.6	372	333.2	440	230.5
309	314.7	371	327.3	437	233.6
308	309.9	370	289.4	436	239.5
307	291.8	369	318.1	435	243.4
306	324.0	368	329.7	434	257.6
305	339.7	367	332.7	433	259.3
304	343.5	366	331.9	432	264.3
303	342.1	365	331.8	431	263.8
302	343.2	364	325.2	430	257.8
301	337.7	363	286.2	429	254.0

Table 2.6-6

Fuel Assembly Internal Temperature Measurement Test
Thermocouple Data Fuel Assembly: B43

DATE: 1/4/80 TIME: 1:00 p.m.
TEST CONDITIONS: Uniform Canister Temperature at 250°F With Air

T/C No.	Temp(°F)	T/C No.	Temp(°F)	T/C No.	Temp(°F)
362	363.0	428	254.1	492	234.1
361	362.6	427	258.5	491	74.4
360	369.3	426	258.7	490	73.6
359	367.8	425	257.0	489	75.0
358	363.7	424	254.9	488	74.2
357	342.1	423	254.8	487	84.3
356	317.9	422	255.9	486	113.9
355	364.8	421	256.3	485	
354	366.8	420	250.3	484	86.7
353	369.9	419	250.3	483	109.1
352	373.4	418	254.3	482	166.1
351	368.9	417	253.1	481	147.8
350	343.8	416	240.7	480	134.1
349	334.4	415	240.2	479	110.4
348	353.7	409	182.3	478	159.5
347	364.2	408	243.7	477	245.9
346	369.7	407	217.3	476	261.9
345	370.0	406	217.4	475	236.8
344	365.9	405	314.6	474	273.1
343	344.7	404	337.4	473	244.1
342	337.7	403	338.3	472	234.4
341	367.6	402	342.6	471	199.1
340	365.6	401	343.5	470	210.7
339	370.3	400	339.4	469	215.0
338	370.6	399	322.9	468	213.3
337	366.4	398	327.3	467	199.8
336	343.9	397	352.7	466	209.6
335	336.9	396	351.5	465	208.6
334	367.1	395	355.8	464	210.3
332	370.0	394	360.4	463	205.3
331	371.4	393	357.4	462	208.5
330	366.5	392	330.5	461	209.3
329	343.7	391	317.0	460	90.7
328	315.3	390	342.6	459	198.8
327	341.4	389	341.0	458	200.6
326	338.6	388	344.9	457	206.6
325	344.9	387	348.4	456	202.6
324	344.1	386	345.0	455	203.7
323	340.8	385	320.9	454	194.3
322	324.0	384	335.0	453	182.9
321	326.7	383	362.2	451	191.0
320	355.2	382	363.7	450	197.4
319	352.1	381	369.2	449	197.8
318	358.5	380	372.1	448	192.0
317	357.5	379	367.8	447	198.0
316	353.3	378	342.4	446	196.3
315	333.4	377	331.6	445	202.3
314	317.5	376	360.0	444	210.3
313	341.4	375	363.2	443	223.1
312	339.8	374	367.8	442	217.4
311	343.0	373	368.1	441	215.5
310	344.4	372	365.3	440	229.3
309	341.3	371	343.5	437	239.7
308	323.2	370	335.7	436	237.7
307	347.6	369	362.7	435	242.3
306	376.9	368	365.8	434	255.2
305	383.3	367	369.9	433	257.0
304	387.3	366	372.4	432	260.0
303	387.8	365	367.3	431	259.4
302	382.5	364	342.6	430	252.9
301	359.5	363	332.5	429	253.6

Table 2.6-7

Fuel Assembly Internal Temperature Measurement Test
Thermocouple Data Fuel Assembly: B43

DATE: 2/11/80 TIME: 9:00 a.m.
TEST CONDITIONS: Uniform Canister Temperature at 300°F With Vacuum

T/C No.	Temp(°F)	T/C No.	Temp(°F)	T/C No.	Temp(°F)
362	392.6	428	302.4	492	284.9
361	408.5	427	307.2	491	77.2
360	417.3	426	309.3	490	75.0
359	417.6	425	308.0	489	77.2
358	416.8	424	305.8	488	75.8
357	411.8	423	303.6	487	81.2
356	314.2	422	302.5	486	130.6
355	391.6	421	304.7	485	•
354	408.5	420	299.4	484	93.6
353	415.2	419	297.3	483	105.7
352	415.0	418	309.5	482	205.6
351	414.6	417	305.4	481	179.7
350	410.4	416	280.6	480	158.9
349	354.4	415	277.3	479	132.0
348	392.1	409	280.0	478	202.4
347	409.0	408	279.5	477	252.8
346	417.3	407	247.9	476	279.4
345	416.9	406	247.7	475	266.4
344	417.0	405	346.7	474	334.8
343	413.1	404	374.0	473	317.6
342	356.0	403	387.1	472	316.7
341	394.0	402	393.7	471	275.1
340	409.1	401	393.7	470	281.5
339	416.4	400		469	282.2
338	415.3	399	389.5	468	273.9
337	415.6	398	353.5	467	250.9
336	412.4	397	383.8	466	263.3
335	355.4	396	397.2	465	259.9
334	393.9	395	403.4	464	259.9
332	415.6	394	402.9	463	250.6
331	414.4	393	403.3	462	254.6
330	413.4	392	397.7	461	256.2
329	410.5	391	346.9	460	135.9
328	345.0	390	376.6	459	241.8
327	376.1	389	386.8	458	245.1
326	386.9	388	393.0	457	253.2
325	394.9	387	392.4	456	247.6
324	394.8	386	391.6	455	253.6
323	393.4	385	385.9	454	250.4
322	390.6	384	356.5	453	245.1
321	349.6	383	390.8	451	250.0
320	384.3	382	407.9	450	253.3
319	398.0	381	415.8	449	249.8
318	405.3	380	415.1	448	240.8
317	405.1	379	414.9	447	254.2
316	404.4	378	410.0	446	266.5
315	401.7	377	352.7	445	289.6
314	344.4	376	389.5	444	297.1
313	373.0	375	408.3	443	311.4
312	384.9	374	415.8	442	302.9
311	390.7	373	415.2	441	291.3
310	390.3	372	415.1	440	287.1
309	389.7	371	411.7	437	310.6
308	388.2	370	356.5	436	299.1
307	361.5	369	390.9	435	309.0
306	401.1	368	408.3	434	302.0
305	423.8	367	415.6	433	306.2
304	432.0	366	414.3	432	310.2
303	430.3	365	413.0	431	307.0
302	429.8	364	409.4	430	301.7
301	426.8	363	352.9	429	300.6

Table 2.6-8

Fuel Assembly Internal Temperature Measurement Test
Thermocouple Data Fuel Assembly: B43

DATE: 12/7/79 TIME: 8:00 a.m.
TEST CONDITIONS: Uniform Canister Temperature at 300°F With Helium

T/C No.	Temp(°F)	T/C No.	Temp(°F)	T/C No.	Temp(°F)
362	350.8	428	294.8	492	258.7
361	361.3	427	297.8	491	79.0
360	367.3	426	303.4	490	77.4
359	368.0	425	301.2	489	78.5
358	371.2	424	301.6	488	77.5
357	365.3	423	297.6	487	86.0
356	301.7	422	296.7	486	129.9
355	351.0	421	298.4	485	
354	362.5	420	294.2	484	92.8
353	366.3	419	292.6	483	106.3
352	366.3	418	297.7	482	195.6
351	369.4	417	295.5	481	175.8
350	364.9	416	273.2	480	160.3
349	324.9	415	270.8	479	132.3
348	350.7	409	209.5	478	190.5
347	361.4	408	270.8	477	215.8
346	366.8	407	242.4	476	234.9
345	367.0	406	242.0	475	240.4
344	370.7	405	319.8	474	309.7
343	366.1	404	337.4	473	299.4
342	326.6	403	346.9	472	302.8
341	352.7	402	350.3	471	260.4
340	362.2	401	351.0	470	264.9
339	366.6	400	353.3	469	263.8
338	366.4	399	350.5	468	257.8
337	370.2	398	324.7	467	241.1
336	365.4	397	346.1	466	251.9
335	325.8	396	355.4	465	250.4
334	352.3	395	359.2	464	252.9
332	365.8	394	359.1	463	249.1
331	365.2	393	362.7	462	257.6
330	368.3	392	356.5	461	261.3
329	363.8	391	320.4	460	142.1
328	319.5	390	340.8	459	249.4
327	339.9	389	348.1	458	249.8
326	345.6	388	351.7	457	257.4
325	351.0	387	351.3	456	250.8
324	351.9	386	354.6	455	248.3
323	355.0	385	347.7	454	234.3
322	349.9	384	326.1	453	221.8
321	322.8	383	349.9	451	249.4
320	346.6	382	362.0	450	252.1
319	355.0	381	366.8	449	246.2
318	360.0	380	366.4	448	236.6
317	360.3	379	369.4	447	246.4
316	363.7	378	364.7	446	252.8
315	359.3	377	323.0	445	271.0
314	318.9	376	348.4	444	284.9
313	338.3	375	361.1	443	304.8
312	345.6	374	365.7	442	296.4
311	348.5	373	365.6	441	283.4
310	348.5	372	369.3	440	279.3
309	352.7	371	365.5	437	292.7
308	348.6	370	326.0	436	287.9
307	328.7	369	350.0	435	295.8
306	356.0	368	361.7	434	298.8
305	371.1	367	366.0	433	300.9
304	376.3	366	365.6	432	305.7
303	375.5	365	367.8	431	305.3
302	378.4	364	363.2	430	296.9
301	375.1	363	323.4	429	292.6

Table 2.6-9

Fuel Assembly Internal Temperature Measurement Test
Thermocouple Data Fuel Assembly: B43

DATE: 1/14/80 TIME: 10:30 a.m.
TEST CONDITIONS: Uniform Canister Temperature at 300°F With Air

T/C No.	Temp(°F)	T/C No.	Temp(°F)	T/C No.	Temp(°F)
362	393.5	428	297.6	492	237.4
361	395.9	427	302.2	491	73.5
360	402.7	426	302.9	490	72.2
359	401.5	425	301.6	489	74.6
358	399.6	424	299.4	488	73.1
357	384.3	423	298.1	487	83.6
356	337.2	422	295.8	486	124.6
355	394.6	421	297.7	485	
354	398.4	420	291.7	484	86.9
353	403.2	419	290.0	483	108.5
352	405.4	418	309.8	482	195.4
351	402.0	417	303.6	481	177.9
350	384.7	416	276.6	480	156.3
349	362.4	415	272.8	479	130.4
348	392.6	409	277.5	478	186.1
347	396.3	408	279.3	477	241.5
346	402.4	407	242.4	476	256.1
345	402.1	406	242.7	475	222.0
344	400.0	405	350.0	474	257.8
343	385.2	404	371.8	473	267.4
342	365.3	403	374.4	472	300.0
341	395.4	402	379.4	471	276.1
340	396.4	401	379.5	470	280.9
339	402.3	400	376.0	469	276.5
338	401.6	399	364.8	468	264.4
337	399.1	398	361.2	467	247.6
336	383.4	397	384.8	466	259.6
335	365.6	396	386.0	465	255.3
334	396.1	395	391.4	464	250.5
332	402.5	394	393.7	463	244.1
331	402.9	393	391.6	462	244.9
330	399.2	392	372.4	461	247.7
329	383.5	391	353.0	460	125.5
328	347.1	390	376.4	459	236.4
327	372.6	389	375.8	458	239.9
326	372.9	388	381.0	457	246.3
325	379.9	387	382.8	456	240.3
324	378.9	386	379.6	455	248.6
323	376.0	385	362.2	454	251.3
322	364.5	384	366.3	453	246.2
321	355.8	383	393.2	451	236.3
320	383.2	382	397.2	450	241.3
319	384.1	381	403.5	449	239.3
318	390.9	380	404.7	448	230.5
317	389.6	379	401.8	447	240.6
316	386.5	378	384.0	446	246.0
315	372.8	377	361.8	445	263.4
314	350.4	376	391.0	444	281.8
313	372.2	375	396.8	443	306.9
312	372.7	374	402.2	442	299.4
311	377.5	373	401.5	441	285.2
310	377.6	372	400.4	440	281.5
309	374.7	371	385.5	437	286.6
308	363.2	370	366.7	436	287.5
307	374.3	369	393.5	435	294.7
306	405.0	368	398.2	434	294.8
305	413.7	367	403.7	433	298.1
304	419.0	366	404.9	432	300.2
303	418.0	365	400.9	431	297.7
302	415.3	364	383.8	430	296.4
301	400.0	363	361.3	429	296.9

Table 2.6-10

Fuel Assembly Internal Temperature Measurement Test
Thermocouple Data Fuel Assembly: B43

DATE: 1/30/80 TIME: 6:30 a.m.
TEST CONDITIONS: Uniform Canister Temperature at 400°F With Vacuum

T/C No.	Temp(°F)	T/C No.	Temp(°F)	T/C No.	Temp(°F)
362	465.1	428	395.2	492	382.4
361	480.8	427	401.3	491	79.0
360	490.5	426	403.6	490	76.4
359	489.3	425	402.6	489	79.4
358	487.6	424	400.1	488	76.9
357	484.4	423	397.7	487	87.4
356	389.8	422	398.0	486	161.9
355	463.7	421	402.2	485	
354	480.9	420	397.2	484	103.0
353	487.6	419	394.0	483	117.5
352	485.8	418	400.9	482	275.9
351	484.9	417	398.9	481	246.4
350	483.2	416	402.1	480	219.4
349	433.3	415	399.0	479	175.6
348	465.1	409	394.9	478	271.3
347	481.3	408	393.7	477	324.5
346	490.6	407	364.9	476	342.4
345	483.5	406	366.0	475	322.2
344	488.0	405	426.3	474	401.3
343	486.0	404	449.0	473	386.3
342	434.8	403	464.1	472	396.7
341	466.5	402	471.8	471	357.1
340	481.5	401	469.4	470	366.8
339	489.5	400		469	375.5
338	487.0	399	466.5	468	369.2
337	486.8	398	431.3	467	348.4
336	485.3	397	456.8	466	369.5
335	434.1	396	471.6	465	368.6
334	466.3	395	478.5	464	368.1
332	488.3	394	476.0	463	360.6
331	485.8	393	475.6	462	368.5
330	484.6	392	472.7	461	359.5
329	483.3	391	426.6	460	220.4
328	426.1	390	451.5	459	331.3
327	452.2	389	463.1	458	335.0
326	463.4	388	469.9	457	343.1
325	472.9	387	467.0	456	336.4
324	470.6	386	465.7	455	348.9
323	468.8	385	462.8	454	360.7
322	467.7	384	433.9	453	360.1
321	429.7	383	462.8	451	354.0
320	458.7	382	480.4	450	359.5
319	472.3	381	488.7	449	358.7
318	480.8	380	486.6	448	352.3
317	478.9	379	485.0	447	369.1
316	477.8	378	482.9	446	366.4
315	476.7	377	431.1	445	374.3
314	425.5	376	461.8	444	375.4
313	448.5	375	480.7	443	395.0
312	461.4	374	489.1	442	391.2
311	468.0	373	486.9	441	392.3
310	465.8	372	485.8	440	402.4
309	464.9	371	484.6	437	392.6
308	465.1	370	434.1	436	386.1
307	438.8	369	462.9	435	398.4
306	471.6	368	480.6	434	394.9
305	493.4	367	488.1	433	400.6
304	502.1	366	485.4	432	405.7
303	499.3	365	483.4	431	402.3
302	497.6	364	482.2	430	393.5
301	498.9	363	431.4	429	392.6

Table 2.6-11

Fuel Assembly Internal Temperature Measurement Test
Thermocouple Data Fuel Assembly: B43

DATE: 12/11/79 TIME: 12:00 noon
TEST CONDITIONS: Uniform Canister Temperature at 400°F With Helium

T/C No.	Temp(°F)	T/C No.	Temp(°F)	T/C No.	Temp(°F)
362	454.2	428	407.9	492	
361	459.7	427	412.1	491	81.9
360	468.7	426	415.4	490	79.2
359	465.4	425	413.4	489	82.1
358	459.9	424	412.6	488	78.9
357	459.7	423	409.4	487	92.1
356	385.8	422	407.0	486	163.4
355	453.2	421	409.7	485	
354	460.2	420	406.5	484	107.3
353	466.5	419	404.0	483	126.6
352	462.3	418	415.4	482	283.3
351	457.6	417	413.0	481	254.9
350	459.3	416	417.1	480	222.1
349	433.7	415	417.0	479	183.4
348	454.0	409	347.7	478	286.2
347	459.8	408	408.2	477	334.0
346	468.4	407	379.8	476	354.0
345	463.8	406	380.1	475	338.5
344	459.4	405	429.6	474	414.3
343	460.6	404	442.6	473	402.4
342	434.9	403	448.5	472	414.5
341	455.3	402	456.6	471	377.6
340	460.2	401	451.6	470	388.2
339	467.5	400	444.7	469	392.1
338	462.6	399	448.5	468	380.4
337	458.6	398	433.0	467	357.0
336	459.6	397	449.0	466	378.4
335	434.4	396	454.3	465	374.6
334	455.1	395	461.8	464	370.9
332	466.5	394	456.9	463	365.5
331	461.7	393	452.6	462	373.7
330	456.6	392	452.7	461	367.1
329	458.3	391	429.6	460	223.8
328	429.4	390	445.5	459	342.4
327	445.6	389	448.3	458	345.1
326	446.7	388	455.7	457	353.5
325	456.3	387	450.7	456	280.6
324	451.7	386	445.4	455	362.2
323	446.1	385	445.3	454	380.8
322	447.1	384	434.4	453	383.1
321	431.9	383	452.5	451	360.1
320	450.6	382	460.1	450	361.4
319	454.0	381	468.3	449	361.3
318	462.3	380	463.5	448	361.6
317	458.0	379	458.4	447	386.8
316	452.9	378	459.6	446	382.9
315	454.4	377	432.4	445	390.1
314	428.5	376	451.5	444	391.4
313	442.6	375	459.8	443	411.7
312	446.0	374	467.8	442	408.7
311	452.0	373	463.6	441	409.6
310	448.0	372	458.5	440	419.9
309	442.6	371	460.5	437	406.2
308	445.6	370	434.2	436	397.0
307	437.0	369	452.4	435	410.1
306	457.8	368	459.6	434	400.2
305	467.7	367	467.0	433	405.3
304	475.7	366	462.3	432	409.8
303	470.8	365	456.7	431	406.1
302	465.8	364	458.0	430	407.1
301	468.1	363	432.7	429	405.0

Table 2.6-12

Fuel Assembly Internal Temperature Measurement Test
Thermocouple Data Fuel Assembly: B43

DATE: 1/17/80 TIME: 3:52 p.m.
TEST CONDITIONS: Uniform Canister Temperature at 400°F With Air

T/C No.	Temp(°F)	T/C No.	Temp(°F)	T/C No.	Temp(°F)
362	472.3	428	392.8	492	392.6
361	477.4	427	399.0	491	77.2
360	482.7	426	400.3	490	75.3
359	481.0	425	399.7	489	78.2
358	480.1	424	396.8	488	75.1
357	472.8	423	394.7	487	88.3
356	398.0	422	397.5	486	156.5
355	470.7	421	400.4	485	
354	477.5	420	396.1	484	101.4
353	481.3	419	394.1	483	121.7
352	479.6	418	408.1	482	275.4
351	478.2	417	404.7	481	247.7
350	471.2	416	409.2	480	212.3
349	443.2	415	408.2	479	171.4
348	472.0	409	402.3	478	279.2
347	477.7	408	401.3	477	327.1
346	482.6	407	371.3	476	342.2
345	480.3	406	372.1	475	329.0
344	480.2	405	435.1	474	406.8
343	473.8	404	455.0	473	392.9
342	444.6	403	400.4	472	407.4
341	473.2	402	464.3	471	367.1
340	477.4	401	462.3	470	376.9
339	481.8	400	458.8	469	381.2
338	478.9	399	455.6	468	370.8
337	478.5	398	440.8	467	348.1
336	472.2	397	463.3	466	368.1
335	444.0	396	487.7	465	366.4
334	473.1	395	471.8	464	365.6
332	481.3	394	470.3	463	357.7
331	478.8	393	469.2	462	364.3
330	477.1	392	461.0	461	356.2
329	471.0	391	435.2	460	215.8
328	434.4	390	457.4	459	329.4
327	458.1	389	459.7	458	332.7
326	459.5	388	463.6	457	341.2
325	464.7	387	461.3	456	334.8
324	462.2	386	459.0	455	346.4
323	460.6	385	451.6	454	360.2
322	456.1	384	444.2	453	358.9
321	438.7	383	469.8	451	341.9
320	465.0	382	476.9	450	349.6
319	468.2	381	482.0	449	352.5
318	472.8	380	480.3	448	352.6
317	470.1	379	478.5	447	375.6
316	468.4	378	471.3	446	369.6
315	463.6	377	441.4	445	373.3
314	433.7	376	469.0	444	376.0
313	454.3	375	477.5	443	398.4
312	457.8	374	481.8	442	398.7
311	461.0	373	479.5	441	401.9
310	458.4	372	479.1	440	413.9
309	456.9	371	473.3	437	394.8
308	453.4	370	444.2	436	385.6
307	449.9	369	469.8	435	396.8
306	479.4	368	477.2	434	392.1
305	490.5	367	481.8	433	397.8
304	495.0	366	479.5	432	401.9
303	492.3	365	477.0	431	398.0
302	490.8	364	470.4	430	390.5
301	485.2	363	441.7	429	390.6

Table 2.6-13

Fuel Assembly Internal Temperature Measurement Test
Thermocouple Data Fuel Assembly: B43

DATE: 12/20/79 TIME: 2:38 p.m.
TEST CONDITIONS: Uniform Canister Temperature at 500°F With Vacuum

T/C No.	Temp(°F)	T/C No.	Temp(°F)	T/C No.	Temp(°F)
362	548.0	428	488.0	492	573.4
361	554.8	427	494.4	491	84.9
360	561.7	426	497.0	490	80.9
359	559.1	425	496.0	489	85.8
358	558.4	424	493.8	488	81.5
357	560.1	423	491.2	487	92.6
356	459.0	422	494.4	486	196.8
355	545.9	421	498.7	485	
354	554.5	420	494.8	484	115.2
353	558.4	419	492.3	483	126.6
352	555.3	418	503.8	482	355.8
351	556.0	417	500.8	481	328.4
350	558.8	416	501.5	480	272.9
349	524.0	415	497.2	479	228.8
348	547.7	409	432.1	478	351.4
347	555.0	408	493.4	477	347.6
346	561.5	407	471.0	476	373.5
345	558.0	406	476.9	475	375.4
344	558.9	405	519.4	474	466.8
343	561.3	404	535.1	473	461.2
342	525.2	403	542.2	472	486.5
341	548.8	402	547.8	471	456.5
340	555.1	401	543.5	470	466.8
339	560.1	400	541.0	469	486.5
338	556.3	399	546.9	468	486.2
337	557.7	398	522.8	467	461.0
336	560.3	397	540.9	466	477.1
335	524.4	396	547.5	465	479.0
334	548.6	395	552.3	464	477.5
332	559.0	394	548.2	463	464.1
331	555.2	393	549.3	462	465.3
330	555.8	392	551.1	461	461.1
329	558.6	391	519.1	460	325.7
328	519.0	390	537.3	459	435.1
327	538.1	389	540.9	458	435.3
326	540.9	388	545.6	457	444.5
325	547.9	387	540.8	456	428.9
324	544.0	386	541.3	455	443.2
323	543.6	385	543.2	454	464.2
322	547.1	384	524.6	453	466.1
321	521.5	383	545.5	451	447.8
320	543.1	382	554.5	450	457.3
319	547.8	381	560.4	449	463.6
318	554.0	380	556.8	448	460.0
317	550.3	379	556.4	447	482.1
316	550.7	378	558.9	446	476.8
315	553.9	377	522.6	445	483.7
314	518.2	376	544.9	444	480.3
313	534.4	375	554.8	443	500.9
312	539.3	374	560.7	442	499.6
311	542.9	373	557.1	441	502.3
310	539.2	372	557.1	440	511.8
309	539.8	371	560.4	437	483.2
308	544.5	370	524.4	436	486.9
307	527.9	369	545.3	435	500.7
306	552.5	368	554.4	434	491.5
305	564.3	367	559.3	433	497.9
304	570.3	366	555.3	432	503.0
303	566.1	365	555.0	431	498.5
302	566.1	364	558.2	430	486.4
301	569.5	363	522.7	429	485.1

Table 2.6-14

Fuel Assembly Internal Temperature Measurement Test
Thermocouple Data Fuel Assembly: B43

DATE: 12/17/79 TIME: 1:30 p.m.
TEST CONDITIONS: Uniform Canister Temperature at 500°F With Helium

T/C No.	Temp(°F)	T/C No.	Temp(°F)	T/C No.	Temp(°F)
362	535.5	428	485.6	492	
361	538.9	427	491.4	491	83.3
360	544.6	426	495.4	490	79.7
359	538.8	425	493.8	489	85.6
358	538.0	424	492.7	488	80.9
357	543.6	423	488.8	487	90.0
356	441.3	422	494.4	486	193.8
355	533.5	421	498.8	485	
354	538.7	420	495.9	484	120.9
353	541.2	419	493.3	483	122.2
352	534.8	418	499.7	482	353.7
351	535.8	417	496.8	481	325.6
350	542.5	416	495.5	480	275.0
349	515.9	415	491.9	479	224.7
348	535.3	409	426.3	478	348.4
347	538.9	408	487.8	477	343.0
346	544.1	407	464.1	476	374.4
345	537.1	406	469.4	475	371.0
344	538.1	405	512.8	474	462.7
343	544.2	404	525.1	473	454.0
342	516.7	403	529.6	472	477.3
341	536.0	402	534.1	471	450.3
340	539.0	401	526.6	470	463.9
339	542.7	400	524.3	469	484.0
338	535.6	399	534.1	468	483.6
337	537.4	398	515.1	467	462.4
336	543.4	397	530.0	466	481.6
335	516.0	396	533.7	465	480.3
334	535.9	395	537.4	464	474.9
332	541.4	394	530.0	463	464.2
331	534.5	393	531.4	462	469.8
330	535.4	392	537.2	461	455.4
329	542.0	391	511.9	460	304.1
328	512.4	390	527.3	459	423.4
327	528.1	389	528.7	458	425.3
326	527.9	388	531.9	457	434.5
325	533.7	387	524.1	456	412.2
324	526.4	386	524.9	455	442.3
323	526.5	385	530.8	454	461.5
322	533.1	384	516.5	453	460.2
321	514.2	383	533.3	451	449.8
320	532.1	382	538.8	450	459.6
319	533.8	381	543.5	449	465.5
318	538.4	380	536.6	448	458.7
317	531.8	379	536.5	447	482.3
316	532.2	378	543.0	446	476.7
315	539.0	377	514.8	445	485.7
314	510.9	376	532.7	444	478.7
313	524.6	375	539.0	443	498.1
312	526.5	374	543.6	442	493.9
311	528.7	373	537.0	441	495.9
310	522.0	372	536.9	440	505.0
309	523.1	371	544.1	437	477.8
308	530.9	370	516.1	436	485.4
307	519.0	369	533.0	435	497.9
306	538.0	368	538.4	434	489.6
305	546.1	367	541.9	433	496.6
304	550.4	366	535.0	432	502.0
303	543.4	365	535.0	431	497.7
302	542.9	364	542.0	430	484.4
301	550.6	363	515.0	429	482.0

Table 2.6-15

Fuel Assembly Internal Temperature Measurement Test
Thermocouple Data Fuel Assembly: B43

DATE: 1/24/80 TIME: 8:30 a.m.
TEST CONDITIONS: Uniform Canister Temperature at 500°F With Air

T/C No.	Temp(°F)	T/C No.	Temp(°F)	T/C No.	Temp(°F)
362	552.9	428	488.3	492	571.7
361	559.4	427	496.3	491	75.4
360	566.0	426	499.2	490	73.7
359	563.8	425	498.8	489	77.6
358	565.2	424	495.9	488	75.1
357	561.0	423	492.7	487	82.4
356	444.7	422	493.5	486	190.3
355	549.8	421	499.7	485	
354	558.5	420	496.2	484	116.8
353	562.5	419	492.2	483	112.5
352	560.2	418	503.2	482	352.0
351	562.4	417	499.3	481	324.0
350	558.9	416	498.8	480	278.5
349	527.3	415	493.9	479	223.6
348	552.3	409	492.7	478	356.4
347	559.5	408	491.9	477	335.0
346	565.7	407	467.6	476	361.5
345	562.8	406	472.9	475	358.3
344	565.3	405	522.5	474	455.1
343	562.2	404	539.2	473	449.2
342	527.9	403	546.0	472	474.9
341	552.8	402	551.4	471	446.8
340	559.3	401	548.1	470	459.5
339	564.1	400	547.4	469	483.1
338	560.9	399	547.4	468	487.8
337	563.6	398	525.7	467	465.2
336	561.1	397	544.7	466	480.3
335	527.0	396	551.1	465	483.1
334	552.5	395	555.6	464	482.9
332	563.1	394	552.5	463	472.0
331	560.1	393	555.4	462	477.2
330	562.0	392	551.1	461	469.3
329	559.4	391	521.0	460	332.0
328	521.2	390	540.2	459	437.8
327	541.4	389	543.9	458	439.5
326	544.9	388	548.4	457	449.5
325	551.4	387	544.8	456	439.5
324	548.1	386	546.8	455	448.8
323	549.4	385	543.1	454	463.8
322	548.0	384	528.2	453	459.5
321	523.8	383	550.2	451	455.9
320	546.3	382	558.7	450	464.5
319	551.7	381	564.4	449	466.6
318	557.1	380	561.5	448	455.6
317	554.1	379	563.1	447	479.3
316	555.5	378	559.7	446	472.5
315	554.3	377	526.3	445	483.4
314	519.0	376	549.8	444	475.7
313	536.5	375	559.4	443	499.6
312	542.1	374	564.9	442	496.4
311	546.0	373	561.9	441	500.2
310	543.1	372	564.1	440	509.3
309	545.6	371	561.5	437	473.7
308	544.9	370	527.5	436	485.1
307	532.1	369	549.6	435	496.6
306	557.6	368	558.5	434	495.6
305	569.8	367	563.4	433	502.9
304	575.1	366	560.2	432	507.5
303	571.7	365	561.5	431	503.5
302	573.2	364	558.6	430	485.7
301	571.0	363	526.4	429	485.0

Table 2.6-16

Fuel Assembly Internal Temperature Measurement Test
Thermocouple Data Fuel Assembly: D15

DATE: 10/8/80 TIME: 8:00 a.m.
TEST CONDITIONS: Uniform Canister Temperature at 350°F With Air

T/C No.	Temp(°F)	T/C No.	Temp(°F)	T/C No.	Temp(°F)
362	501.5	428	352.1	492	318.2
361	503.2	427	359.8	491	88.2
360	510.3	426	362.8	490	86.8
359	511.6	425	362.4	489	88.4
358	511.2	424	356.5	488	87.0
357	487.0	423	353.8	487	100.0
356	429.4	422	355.6	486	150.0
355	496.3	421	359.5	485	139.2
354	499.0	420	352.7	484	106.6
353	504.8	419	349.8	483	132.2
352	508.6	418	353.1	482	231.2
351	507.1	417	343.4	481	206.4
350	487.1	416	304.0	480	178.6
349	456.3	415	297.6	479	146.9
348	499.9	409	311.8	478	189.4
347	501.8	408	312.5	477	299.2
346	509.3	407	272.6	476	316.1
345	511.2	406	271.9	475	295.2
344	510.2	405	434.5	474	359.2
343	488.9	404	470.1	473	343.4
342	456.9	403	472.2	472	349.5
341	500.7	402	475.4	471	296.4
340	499.7	401	476.8	470	297.9
339	507.2	400	475.2	469	301.2
338	508.8	399	459.1	468	299.4
337	507.9	398	447.3	467	281.3
336	489.4	397	485.1	466	296.0
335	454.2	396	484.8	465	295.2
334	499.4	395	488.7	464	296.7
332	505.9	394	490.7	463	288.0
331	507.7	393	491.2	462	294.4
330	506.1	392	468.7	461	294.5
329	488.0	391	432.7	460	193.0
328	432.9	390	469.7	459	279.0
327	470.7	389	468.1	458	280.9
326	468.9	388	473.5	457	289.1
325	477.4	387	476.3	456	283.1
324	478.8	386	475.8	455	285.4
323	477.5	385	456.1	454	268.3
322	460.8	384	457.4	453	250.8
321	444.0	383	498.2	451	264.0
320	485.0	382	501.9	450	274.8
319	482.9	381	505.4	449	278.3
318	492.3	380	507.1	448	271.7
317	493.8	379	505.7	447	286.2
316	492.0	378	484.8	446	296.1
315	474.2	377	453.2	445	316.1
314	426.7	376	497.7	444	314.5
313	462.4	375	503.2	443	322.6
312	463.9	374	507.3	442	304.2
311	471.3	373	507.3	441	290.4
310	473.6	372	507.9	440	295.0
309	473.9	371	487.4	437	340.0
308	459.7	370	456.1	436	339.1
307	471.3	369	497.0	435	345.9
306	515.7	368	501.3	434	359.0
305	524.0	367	505.6	433	362.6
304	529.3	366	507.5	432	367.3
303	529.9	365	505.1	431	365.9
302	527.5	364	486.5	430	350.0
301	507.9	363	454.5	429	350.5

Table 2.6-17

Fuel Assembly Internal Temperature Measurement Test
Thermocouple Data Fuel Assembly: D15

DATE: 10/27/80 TIME: 8:00 a.m.
TEST CONDITIONS: Uniform Canister Temperature at 400°F With Helium

T/C No.	Temp(°F)	T/C No.	Temp(°F)	T/C No.	Temp(°F)
362	495.1	428	390.3	492	418.4
361	497.9	427	395.6	491	91.4
360	499.7	426	402.3	490	88.7
359	498.1	425	398.6	489	90.9
358	500.9	424	398.1	488	88.3
357	497.7	423	393.3	487	100.4
356	418.2	422	401.0	486	163.2
355	494.1	421	402.0	485	154.4
354	499.9	420	396.4	484	113.1
353	498.7	419	396.0	483	138.1
352	497.6	418	403.7	482	268.6
351	499.9	417	401.0	481	239.0
350	498.2	416	366.2	480	201.9
349	456.8	415	362.2	479	166.3
348	495.5	409	366.4	478	229.8
347	498.2	408	365.9	477	339.5
346	499.7	407	339.4	476	363.9
345	497.8	406	339.9	475	335.0
344	501.5	405	446.5	474	405.5
343	498.6	404	473.9	473	401.3
342	458.8	403	475.5	472	420.6
341	497.6	402	473.6	471	359.3
340	499.5	401	472.7	470	348.6
339	499.7	400	474.2	469	354.9
338	497.9	399	476.5	468	354.3
337	501.8	398	453.8	467	328.7
336	500.3	397	486.0	466	344.1
335	456.8	396	487.8	465	340.6
334	497.5	395	487.2	464	339.5
332	499.1	394	485.4	463	327.7
331	496.5	393	488.8	462	333.7
330	499.3	392	486.1	461	333.8
329	498.1	391	445.9	460	236.9
328	447.2	390	478.3	459	317.2
327	478.4	389	477.2	458	319.2
326	474.6	388	476.7	457	328.8
325	476.2	387	474.9	456	323.2
324	475.5	386	477.0	455	327.1
323	478.2	385	474.2	454	314.1
322	477.4	384	456.7	453	296.3
321	453.2	383	492.6	451	318.4
320	488.7	382	497.8	450	326.9
319	488.2	381	497.5	449	326.0
318	489.8	380	495.7	448	321.8
317	488.7	379	498.1	447	344.5
316	491.7	378	496.7	446	368.6
315	489.4	377	452.3	445	401.0
314	445.6	376	491.3	444	396.1
313	476.4	375	497.7	443	399.7
312	475.8	374	497.1	442	380.1
311	474.1	373	494.8	441	366.2
310	473.1	372	498.1	440	367.3
309	476.5	371	497.5	437	400.2
308	476.6	370	456.1	436	390.0
307	462.4	369	492.9	435	401.8
306	503.6	368	498.8	434	395.8
305	513.4	367	498.0	433	400.4
304	514.0	366	496.0	432	407.1
303	510.8	365	497.2	431	404.6
302	512.8	364	497.3	430	392.3
301	512.4	363	453.5	429	386.5

Table 2.6-18

Fuel Assembly Internal Temperature Measurement Test
Thermocouple Data Fuel Assembly: D15

DATE: 10/10/80 TIME: 4:00 p.m.
TEST CONDITIONS: Uniform Canister Temperature at 400°F.With Air

T/C No.	Temp(°F)	T/C No.	Temp(°F)	T/C No.	Temp(°F)
362	529.6	428	393.3	492	418.2
361	531.5	427	400.8	491	91.7
360	536.2	426	402.0	490	89.4
359	534.5	425	400.0	489	92.4
358	535.2	424	396.4	488	90.5
357	522.5	423	395.1	487	98.9
356	443.0	422	402.8	486	165.0
355	531.3	421	404.6	485	148.7
354	536.6	420	396.6	484	117.5
353	537.6	419	395.7	483	132.4
352	539.3	418	407.6	482	272.6
351	539.1	417	399.1	481	238.9
350	525.0	416	369.6	480	204.7
349	485.9	415	364.2	479	165.5
348	529.3	409	371.5	478	237.7
347	532.2	408	374.3	477	329.8
346	536.6	407	340.4	476	352.4
345	536.4	406	342.5	475	329.2
344	537.3	405	468.4	474	404.4
343	525.1	404	500.9	473	399.8
342	489.0	403	503.5	472	416.5
341	532.2	402	505.5	471	362.5
340	533.3	401	504.9	470	355.0
339	536.6	400	504.4	469	364.7
338	536.6	399	497.3	468	364.1
337	537.7	398	482.3	467	336.0
336	526.1	397	518.1	466	348.2
335	489.4	396	518.8	465	343.7
334	533.8	395	520.8	464	340.5
332	537.5	394	522.1	463	329.9
331	537.5	393	523.6	462	335.8
330	537.2	392	507.1	461	337.4
329	525.3	391	471.7	460	322.3
328	465.5	390	507.3	459	316.2
327	502.1	389	506.5	458	320.0
326	501.8	388	508.2	457	330.3
325	507.1	387	509.4	456	323.4
324	506.3	386	509.6	455	327.7
323	506.6	385	495.1	454	
322	498.2	384	489.3	453	303.1
321	477.1	383	529.0	451	323.2
320	516.9	382	533.6	450	334.6
319	517.0	381	535.7	449	332.3
318	522.1	380	536.5	448	322.8
317	522.3	379	536.7	447	340.3
316	522.3	378	522.4	446	351.8
315	511.5	377	483.5	445	375.3
314	469.4	376	526.7	444	375.0
313	503.1	375	532.7	443	386.3
312	503.4	374	535.1	442	376.3
311	505.4	373	533.4	441	368.2
310	506.2	372	535.5	440	370.9
309	506.3	371	524.1	437	398.8
308	497.7	370	490.0	436	390.6
307	500.5	369	530.2	435	401.0
306	545.5	368	536.2	434	398.9
305	554.7	367	537.5	433	403.8
304	557.4	366	537.9	432	408.3
303	556.3	365	536.9	431	404.5
302	555.9	364	524.2	430	391.6
301	544.0	363	483.4	429	392.1

Table 2.6-19

Fuel Assembly Internal Temperature Measurement Test
Thermocouple Data Fuel Assembly: D15

DATE: 11/5/80 **TIME:** 8:00 a.m.
TEST CONDITIONS: Uniform Canister Temperature at 450°F With Helium

T/C No.	Temp(°F)	T/C No.	Temp(°F)	T/C No.	Temp(°F)
362	525.9	428	437.6	492	519.1
361	528.5	427	444.2	491	90.9
360	530.2	426	451.6	490	87.8
359	531.2	425	448.4	489	90.4
358	534.3	424	447.5	488	87.2
357	533.1	423	442.1	487	99.3
356	446.0	422	445.1	486	178.3
355	525.0	421	446.8	485	169.6
354	530.3	420	442.4	484	118.1
353	528.9	419	440.9	483	137.7
352	529.9	418	453.0	482	309.9
351	533.0	417	450.7	481	276.4
350	533.6	416	443.0	480	232.7
349	492.9	415	440.3	479	186.6
348	526.1	409	440.3	478	268.1
347	528.7	408	440.0	477	363.5
346	530.1	407	431.3	476	384.6
345	530.4	406	436.3	475	373.1
344	534.6	405	483.9	474	466.4
343	533.8	404	506.8	473	456.0
342	494.5	403	509.1	472	471.2
341	527.9	402	507.6	471	402.9
340	529.7	401	509.0	470	391.4
339	529.6	400	510.5	469	409.0
338	530.3	399	514.8	468	416.0
337	534.6	398	490.3	467	384.8
336	535.1	397	517.5	466	398.5
335	493.0	396	519.7	465	398.6
334	527.9	395	519.0	464	401.5
332	528.9	394	519.5	463	385.4
331	528.7	393	523.3	462	389.8
330	532.2	392	523.0	461	388.7
329	533.1	391	484.0	460	279.1
328	484.7	390	510.9	459	376.9
327	511.1	389	510.4	458	378.8
326	507.9	388	509.5	457	389.6
325	509.4	387	509.8	456	382.5
324	511.2	386	512.7	455	393.6
323	514.2	385	512.3	454	376.9
322	515.4	384	492.9	453	348.0
321	489.6	383	523.5	451	367.5
320	520.1	382	528.6	450	377.7
319	519.8	381	528.3	449	376.5
318	521.0	380	528.7	448	380.1
317	522.4	379	531.5	447	411.0
316	525.9	378	532.3	446	414.5
315	525.8	377	489.3	445	427.4
314	483.2	376	522.3	444	426.8
313	508.8	375	528.5	443	445.3
312	508.7	374	528.0	442	436.8
311	506.5	373	528.1	441	434.3
310	508.2	372	531.7	440	445.4
309	512.1	371	533.0	437	451.9
308	514.3	370	492.7	436	438.3
307	498.2	369	523.7	435	451.3
306	533.1	368	529.3	434	443.7
305	542.0	367	528.2	433	449.4
304	542.5	366	528.5	432	456.3
303	541.6	365	530.4	431	452.5
302	544.2	364	532.6	430	439.3
301	545.9	363	490.2	429	433.1

Table 2.6-20

Fuel Assembly Internal Temperature Measurement Test
Thermocouple Data Fuel Assembly: D15

DATE: 11/7/80 TIME: 8:00 a.m.

TEST CONDITIONS: Uniform Canister Temperature at 450°F With Air

T/C No.	Temp(°F)	T/C No.	Temp(°F)	T/C No.	Temp(°F)
362	562.2	428	436.8	492	517.4
361	564.8	427	446.6	491	90.6
360	566.1	426	449.9	490	87.6
359	568.1	425	449.4	489	90.1
358	571.2	424	444.8	488	87.0
357	559.5	423	441.8	487	99.0
356	473.6	422	447.8	486	179.7
355	558.9	421	450.1	485	171.0
354	564.8	420	444.2	484	116.8
353	565.8	419	443.0	483	137.2
352	568.3	418	453.7	482	312.1
351	569.1	417	451.4	481	278.8
350	559.0	416	447.1	480	230.6
349	519.9	415	443.6	479	183.2
348	562.5	409	445.5	478	266.6
347	565.6	408	445.5	477	360.0
346	567.6	407	431.6	476	380.1
345	569.0	406	436.9	475	369.6
344	571.9	405	503.5	474	462.8
343	561.2	404	535.2	473	452.7
342	521.9	403	538.4	472	469.2
341	563.9	402	537.4	471	410.5
340	566.1	401	539.6	470	405.4
339	567.8	400	540.9	469	417.4
338	568.1	399	535.3	468	414.6
337	570.6	398	512.8	467	383.5
336	561.8	397	547.5	466	399.9
335	519.9	396	549.3	465	401.0
334	563.0	395	550.2	464	404.1
332	567.0	394	551.9	463	387.1
331	567.5	393	555.1	462	391.0
330	568.7	392	543.5	461	392.1
329	559.8	391	502.8	460	284.2
328	504.3	390	536.8	459	383.2
327	540.1	389	537.5	458	386.3
326	538.6	388	538.2	457	397.3
325	540.6	387	540.2	456	389.2
324	542.4	386	541.7	455	401.3
323	544.6	385	531.9	454	374.6
322	536.9	384	519.4	453	335.3
321	512.9	383	557.9	451	361.0
320	551.9	382	563.1	450	380.7
319	552.1	381	564.3	449	388.1
318	555.0	380	565.7	448	384.9
317	555.9	379	567.6	447	405.5
316	557.5	378	557.5	446	402.5
315	548.7	377	515.4	445	411.6
314	502.7	376	557.6	444	412.1
313	535.2	375	564.4	443	433.6
312	537.1	374	564.5	442	433.6
311	537.7	373	564.9	441	438.6
310	538.9	372	568.8	440	451.1
309	541.0	371	559.6	437	451.7
308	535.0	370	519.1	436	437.2
307	529.9	369	558.0	435	449.7
306	573.7	368	564.4	434	444.0
305	583.4	367	565.4	433	449.9
304	585.1	366	566.4	432	456.4
303	585.2	365	566.7	431	452.5
302	586.1	364	558.5	430	435.3
301	577.2	363	516.9	429	433.6

Table 2.6-21

Fuel Assembly Internal Temperature Measurement Test
Thermocouple Data Fuel Assembly: D15

DATE: 10/20/80 TIME: 8:00 a.m.
TEST CONDITIONS: Uniform Canister Temperature at 500°F With Vacuum

T/C No.	Temp(°F)	T/C No.	Temp(°F)	T/C No.	Temp(°F)
362	546.2	428	495.5	492	614.1
361	609.2	427	503.2	491	94.6
360	617.3	426	505.1	490	90.8
359	615.3	425	503.9	489	94.0
358	610.2	424	500.8	488	90.1
357	606.0	423	499.2	487	101.9
356	496.9	422	496.3	486	202.5
355	594.5	421	499.8	485	188.9
354	610.0	420	493.9	484	127.9
353	614.9	419	491.2	483	140.1
352	613.3	418	501.7	482	352.0
351	609.1	417	499.3	481	316.8
350	606.4	416	495.8	480	270.4
349	553.1	415	490.9	479	223.0
348	596.9	409	493.5	478	301.2
347	609.9	408	493.8	477	369.7
346	618.0	407	496.3	476	394.1
345	615.2	406	505.2	475	389.1
344	611.4	405	541.1	474	486.9
343	607.9	404	573.2	473	480.8
342	554.8	403	585.2	472	506.3
341	598.4	402	591.6	471	471.9
340	610.5	401	589.2	470	481.9
339	616.8	400	582.5	469	480.9
338	614.3	399	583.5	468	454.2
337	610.6	398	548.4	467	416.9
336	608.9	397	584.1	466	441.6
335	553.5	396	595.7	465	451.6
334	598.4	395	601.7	464	459.9
332	616.1	394	599.2	463	442.4
331	613.2	393	596.1	462	436.9
330	608.8	392	592.1	461	434.2
329	606.8	391	541.1	460	319.3
328	541.7	390	576.2	459	419.6
327	577.5	389	584.6	458	423.2
326	584.8	388	590.7	457	432.0
325	593.8	387	588.3	456	421.0
324	591.4	386	583.9	455	444.6
323	585.6	385	580.5	454	449.5
322	584.5	384	552.8	453	436.4
321	547.8	383	593.0	451	438.2
320	587.7	382	608.3	450	438.9
319	597.3	381	614.5	449	433.7
318	605.2	380	612.2	448	435.0
317	603.5	379	607.8	447	467.1
316	598.6	378	605.1	446	465.1
315	596.3	377	546.8	445	473.6
314	540.6	376	592.2	444	471.0
313	574.2	375	608.8	443	492.3
312	583.7	374	615.4	442	488.8
311	589.4	373	612.3	441	490.3
310	587.7	372	608.6	440	501.6
309	582.9	371	606.8	437	500.7
308	583.0	370	552.9	436	488.0
307	560.5	369	593.7	435	507.2
306	606.8	368	609.6	434	493.0
305	626.3	367	615.0	433	499.6
304	633.1	366	612.1	432	503.5
303	629.6	365	607.0	431	498.5
302	624.6	364	606.0	430	493.7
301	623.7	363	549.5	429	492.2

Table 2.6-22

Fuel Assembly Internal Temperature Measurement Test
Thermocouple Data Fuel Assembly: D15

DATE: 10/22/80 TIME: 8:00 a.m.
TEST CONDITIONS: Uniform Canister Temperature at 500°F With Helium

T/C No.	Temp(°F)	T/C No.	Temp(°F)	T/C No.	Temp(°F)
362	570.3	428	482.4	492	615.9
361	572.9	427	489.5	491	95.2
360	575.1	426	495.1	490	91.5
359	574.2	425	492.3	489	94.9
358	574.6	424	490.9	488	90.8
357	573.5	423	486.2	487	102.6
356	481.4	422	490.3	486	196.7
355	568.9	421	492.7	485	188.9
354	574.1	420	488.3	484	131.2
353	573.0	419	486.5	483	141.9
352	572.4	418	500.1	482	348.0
351	573.2	417	497.7	481	314.5
350	573.9	416	495.5	480	261.1
349	537.8	415	491.2	479	214.7
348	570.6	409	492.7	478	298.9
347	573.0	408	492.8	477	373.9
346	574.9	407	496.0	476	399.0
345	573.5	406	504.8	475	393.7
344	575.1	405	528.8	474	493.2
343	574.5	404	551.7	473	485.0
342	539.3	403	554.1	472	508.6
341	572.2	402	553.4	471	467.6
340	573.8	401	552.8	470	471.4
339	574.2	400	551.5	469	474.9
338	573.0	399	555.7	468	453.2
337	575.0	398	534.9	467	418.2
336	575.5	397	561.6	466	439.8
335	538.0	396	563.5	465	444.9
334	572.1	395	563.5	464	450.3
332	573.3	394	562.3	463	434.6
331	571.6	393	563.8	462	437.2
330	572.6	392	563.3	461	431.5
329	573.7	391	528.6	460	316.3
328	529.4	390	555.3	459	415.9
327	555.9	389	554.6	458	418.1
326	552.6	388	554.3	457	427.9
325	554.9	387	552.9	456	419.5
324	554.4	386	553.3	455	437.9
323	554.8	385	552.9	454	431.0
322	556.0	384	537.8	453	408.1
321	534.4	383	567.7	451	415.9
320	564.4	382	572.6	450	425.1
319	563.9	381	573.0	449	428.1
318	565.6	380	571.8	448	432.5
317	565.1	379	572.2	447	465.4
316	566.0	378	573.0	446	463.4
315	566.0	377	534.3	445	472.3
314	528.0	376	566.7	444	470.1
313	553.2	375	572.8	443	491.7
312	552.9	374	573.0	442	488.2
311	551.3	373	571.3	441	489.8
310	551.1	372	572.5	440	501.3
309	552.4	371	573.8	437	498.2
308	554.7	370	537.5	436	484.2
307	543.2	369	568.0	435	499.7
306	577.6	368	573.3	434	485.7
305	586.2	367	572.8	433	492.1
304	587.1	366	571.4	432	498.5
303	584.7	365	571.0	431	493.8
302	585.0	364	573.2	430	482.9
301	586.7	363	535.2	429	477.8

Table 2.6-23

Fuel Assembly Internal Temperature Measurement Test
Thermocouple Data Fuel Assembly: D15

DATE: 10/17/80 TIME: 8:00 a.m.
TEST CONDITIONS: Uniform Canister Temperature at 500°F With Air

T/C No.	Temp(°F)	T/C No.	Temp(°F)	T/C No.	Temp(°F)
362	600.9	428	492.5	492	610.4
361	606.8	427	500.3	491	93.9
360	612.7	426	501.7	490	90.5
359	609.0	425	500.6	489	93.7
358	607.8	424	496.6	488	89.8
357	601.5	423	495.0	487	101.8
356	505.0	422	498.1	486	202.1
355	599.2	421	501.6	485	191.9
354	603.1	420	495.2	484	126.6
353	611.4	419	492.6	483	139.8
352	608.9	418	505.5	482	355.1
351	607.0	417	500.5	481	322.4
350	601.4	416	497.1	480	272.2
349	559.9	415	491.9	479	224.6
348	601.1	409	496.0	478	303.1
347	607.2	408	496.9	477	366.6
346	612.7	407	496.9	476	390.1
345	609.0	406	506.1	475	385.9
344	608.9	405	546.4	474	483.6
343	603.0	404	576.7	473	478.2
342	561.6	403	583.2	472	503.7
341	602.5	402	587.5	471	472.2
340	607.6	401	583.9	470	483.5
339	611.6	400	580.1	469	482.3
338	608.0	399	579.7	468	455.6
337	607.8	398	555.2	467	425.6
336	603.3	397	588.5	466	451.8
335	560.6	396	593.7	465	461.2
334	602.8	395	598.2	464	467.8
332	611.7	394	595.1	463	447.2
331	607.9	393	593.8	462	444.7
330	606.4	392	587.2	461	436.6
329	601.8	391	546.7	460	320.3
328	546.2	390	579.7	459	413.5
327	580.2	389	582.9	458	415.8
326	581.9	388	587.5	457	424.8
325	588.4	387	584.2	456	411.8
324	584.5	386	581.6	455	432.3
323	583.0	385	576.3	454	442.6
322	580.1	384	560.5	453	437.9
321	553.3	383	597.8	451	437.9
320	591.0	382	606.4	450	439.7
319	594.0	381	610.9	449	435.1
318	599.6	380	607.8	448	436.2
317	596.4	379	605.5	447	467.5
316	595.0	378	600.4	446	460.6
315	590.8	377	556.3	445	465.5
314	545.5	376	597.0	444	465.8
313	577.1	375	607.0	443	491.4
312	581.3	374	611.3	442	489.7
311	585.0	373	606.9	441	491.2
310	581.9	372	606.4	440	502.4
309	580.0	371	602.4	437	498.1
308	578.5	370	560.4	436	489.3
307	569.1	369	598.3	435	503.6
306	612.2	368	508.0	434	495.0
305	624.6	367	611.6	433	502.1
304	629.0	366	608.0	432	508.3
303	624.6	365	605.0	431	502.5
302	622.7	364	601.2	430	489.7
301	618.5	363	557.1	429	489.5

Table 2.6-24

Fuel Assembly Internal Temperature Measurement Test
Thermocouple Data Fuel Assembly: D15

DATE: 11/14/80 TIME: 12:00 noon

TEST CONDITIONS: Uniform Canister Temperature at 550°F With Vacuum

T/C No.	Temp(°F)	T/C No.	Temp(°F)	T/C No.	Temp(°F)
362	637.8	428	537.9	492	590.4
361	643.7	427	548.0	491	87.2
360	649.3	426	551.0	490	82.0
359	647.9	425	550.3	489	87.9
358	643.9	424	546.7	488	84.2
357	646.5	423	544.0	487	86.9
356	509.7	422	543.0	486	204.1
355	635.7	421	547.6	485	183.9
354	644.2	420	543.5	484	126.4
353	646.5	419	541.1	483	117.2
352	645.1	418	552.9	482	386.7
351	642.5	417	549.9	481	354.9
350	646.3	416	539.6	480	292.3
349	598.7	415	531.8	479	234.3
348	638.2	409	537.8	478	349.2
347	644.3	408	538.0	477	342.2
346	649.7	407	536.7	476	363.0
345	647.3	406	546.4	475	366.7
344	645.0	405	589.0	474	467.3
343	647.6	404	617.3	473	464.0
342	600.1	403	622.3	472	490.8
341	639.3	402	626.5	471	476.8
340	644.5	401	624.1	470	497.0
339	648.3	400	617.9	469	517.4
338	645.9	399	627.1	468	516.7
337	644.3	398	594.8	467	502.7
336	648.3	397	626.6	466	527.3
335	598.6	396	631.0	465	529.3
334	639.3	395	634.9	464	519.6
332	647.4	394	632.5	463	491.9
331	644.9	393	630.4	462	488.3
330	642.3	392	634.3	461	481.6
329	646.7	391	588.3	460	368.4
328	589.2	390	619.8	459	470.3
327	621.5	389	621.2	458	471.0
326	621.7	388	624.6	457	480.8
325	628.1	387	622.3	456	473.6
324	625.6	386	619.0	455	491.9
323	621.6	385	624.2	454	502.1
322	627.5	384	598.5	453	488.6
321	594.1	383	634.5	451	479.1
320	630.0	382	642.5	450	485.1
319	632.5	381	646.8	449	488.7
318	637.7	380	644.5	448	490.9
317	636.3	379	641.1	447	531.2
316	633.4	378	645.4	446	530.1
315	637.4	377	595.0	445	543.4
314	587.4	376	634.0	444	527.5
313	617.7	375	643.5	443	546.2
312	620.4	374	647.7	442	538.0
311	622.8	373	645.0	441	539.5
310	621.7	372	642.0	440	548.4
309	618.6	371	646.8	437	506.5
308	625.3	370	598.3	436	533.2
307	604.9	369	634.7	435	547.7
306	646.8	368	643.6	434	538.5
305	659.1	367	646.7	433	547.1
304	663.6	366	644.0	432	554.4
303	660.2	365	640.3	431	549.6
302	656.9	364	646.1	430	536.1
301	660.9	363	595.8	429	534.0

Table 2.6-25

Fuel Assembly Internal Temperature Measurement Test
Thermocouple Data Fuel Assembly: D15

DATE: 11/17/80 TIME: 8:00 a.m.
TEST CONDITIONS: Uniform Canister Temperature at 550°F With Helium

T/C No.	Temp(°F)	T/C No.	Temp(°F)	T/C No.	Temp(°F)
362	614.7	428	544.3	492	606.0
361	618.5	427	551.6	491	94.5
360	626.4	426	555.7	490	90.3
359	623.7	425	553.4	489	93.7
358	617.6	424	551.9	488	88.0
357	625.5	423	548.3	487	97.2
356	515.5	422	544.7	486	213.6
355	613.3	421	548.8	485	211.4
354	619.8	420	544.6	484	131.1
353	624.3	419	542.2	483	133.0
352	621.0	418	554.0	482	392.9
351	616.4	417	551.3	481	368.2
350	625.3	416	546.9	480	296.4
349	585.2	415	539.5	479	249.6
348	615.0	409	544.1	478	332.1
347	618.9	408	544.3	477	359.9
346	626.5	407	544.6	476	385.5
345	622.2	406	554.7	475	380.5
344	618.3	405	577.3	474	479.1
343	625.9	404	597.8	473	473.5
342	586.5	403	602.2	472	501.5
341	616.4	402	608.4	471	472.6
340	619.5	401	604.6	470	491.2
339	625.4	400	595.7	469	518.4
338	621.5	399	610.1	468	529.6
337	618.2	398	582.4	467	508.9
336	626.8	397	606.5	466	523.5
335	585.2	396	610.4	465	531.7
334	616.3	395	616.2	464	532.6
332	624.4	394	612.2	463	500.7
331	620.2	393	607.5	462	487.2
330	615.9	392	616.5	461	475.6
329	625.0	391	576.9	460	361.1
328	577.9	390	601.0	459	469.7
327	601.8	389	602.2	458	470.5
326	600.6	388	608.0	457	478.6
325	609.4	387	603.6	456	472.2
324	605.6	386	597.7	455	497.8
323	599.3	385	607.5	454	512.6
322	610.2	384	585.0	453	498.8
321	582.1	383	612.1	451	479.7
320	609.3	382	618.6	450	489.2
319	610.4	381	624.8	449	494.6
318	618.0	380	620.7	448	494.5
317	614.6	379	615.2	447	523.6
316	609.7	378	624.6	446	518.1
315	618.4	377	582.1	445	526.7
314	576.3	376	611.4	444	523.2
313	598.7	375	618.7	443	548.6
312	600.5	374	624.9	442	545.3
311	605.1	373	621.0	441	546.7
310	602.2	372	615.5	440	556.6
309	596.8	371	625.5	437	507.3
308	608.7	370	584.9	436	534.2
307	590.0	369	612.2	435	547.1
306	621.0	368	618.9	434	541.2
305	630.6	367	624.2	433	549.3
304	636.8	366	620.0	432	556.6
303	632.1	365	614.1	431	551.1
302	626.8	364	624.8	430	543.5
301	636.4	363	582.9	429	539.3

Table 2.6-26

Fuel Assembly Internal Temperature Measurement Test
Thermocouple Data Fuel Assembly: D15

DATE: 11/12/80 TIME: 8:00 a.m.
TEST CONDITIONS: Uniform Canister Temperature at 550°F With Air.

T/C No.	Temp(°F)	T/C No.	Temp(°F)	T/C No.	Temp(°F)
362	645.9	428	540.7	492	607.3
361	644.6	427	549.6	491	92.1
360	646.8	426	551.4	490	87.6
359	644.3	425	550.6	489	91.5
358	641.7	424	546.9	488	87.6
357	640.9	423	544.9	487	95.0
356	535.4	422	549.2	486	213.6
355	642.5	421	551.7	485	197.9
354	644.9	420	547.5	484	134.7
353	644.5	419	546.4	483	129.4
352	642.7	418	557.9	482	394.6
351	640.4	417	553.3	481	365.3
350	639.9	416	542.2	480	293.7
349	608.1	415	535.0	479	238.2
348	645.8	409	541.9	478	350.0
347	645.1	408	542.4	477	360.4
346	647.3	407	538.3	476	386.9
345	644.0	406	547.8	475	383.4
344	642.6	405	598.3	474	482.6
343	642.1	404	625.5	473	477.5
342	609.0	403	623.4	472	505.6
341	646.4	402	624.0	471	483.3
340	645.2	401	621.5	470	504.3
339	646.4	400	615.7	469	525.6
338	642.8	399	621.7	468	527.9
337	641.6	398	604.1	467	508.3
336	642.4	397	634.0	466	527.9
335	607.0	396	631.6	465	528.6
334	646.0	395	632.7	464	521.4
332	645.5	394	630.2	463	493.3
331	642.2	393	627.9	462	489.9
330	640.0	392	628.0	461	481.9
329	640.6	391	596.0	460	367.8
328	597.3	390	626.5	459	470.2
327	628.9	389	622.4	458	471.1
326	622.8	388	622.8	457	479.8
325	625.8	387	620.5	456	472.5
324	622.4	386	616.8	455	492.0
323	619.1	385	618.1	454	505.1
322	622.2	384	608.4	453	493.0
321	602.5	383	642.3	451	473.8
320	637.1	382	643.2	450	482.0
319	633.5	381	644.5	449	490.1
318	635.9	380	641.9	448	499.5
317	632.9	379	638.8	447	541.1
316	630.2	378	639.4	446	542.5
315	631.7	377	605.0	445	554.0
314	594.2	376	642.2	444	532.9
313	624.0	375	644.5	443	544.5
312	621.8	374	645.4	442	536.8
311	621.3	373	641.8	441	538.9
310	619.2	372	639.8	440	549.0
309	616.2	371	641.2	437	513.3
308	619.4	370	607.5	436	536.8
307	615.0	369	641.9	435	550.0
306	654.4	368	644.4	434	538.4
305	660.1	367	644.7	433	540.6
304	661.3	366	641.7	432	554.0
303	657.4	365	638.2	431	549.6
302	654.6	364	639.9	430	537.7
301	655.3	363	605.7	429	536.9

Table 2.6-27

Fuel Assembly Internal Temperature Measurement Test
Thermocouple Data Fuel Assembly: D15

DATE: 11/20/80 TIME: 8:00 a.m.
TEST CONDITIONS: Uniform Canister Temperature at 600°F With Helium

T/C No.	Temp(°F)	T/C No.	Temp(°F)	T/C No.	Temp(°F)
362	666.2	428	592.9	492	607.3
361	667.1	427	601.3	491	94.2
360	670.9	426	605.2	490	89.8
359	667.6	425	603.1	489	93.4
358	665.6	424	601.6	488	86.9
357	676.9	423	598.3	487	95.6
356	557.0	422	600.4	486	235.9
355	664.1	421	605.1	485	237.0
354	667.9	420	601.6	484	144.5
353	668.1	419	599.7	483	130.6
352	664.9	418	604.1	482	440.7
351	664.3	417	601.2	481	422.3
350	676.7	416	582.9	480	332.7
349	636.0	415	574.1	479	282.8
348	666.5	409	581.8	478	360.1
347	667.3	408	582.1	477	357.5
346	670.7	407	582.5	476	383.5
345	666.3	406	592.5	475	379.7
344	666.2	405	629.7	474	481.1
343	677.0	404	650.9	473	475.9
342	637.0	403	652.5	472	510.6
341	667.5	402	654.3	471	500.7
340	667.7	401	650.0	470	537.8
339	669.5	400	645.5	469	580.7
338	665.5	399	663.3	468	606.2
337	666.1	398	633.8	467	589.6
336	678.1	397	658.2	466	597.7
335	635.4	396	659.2	465	596.6
334	667.3	395	660.8	464	583.2
332	668.3	394	656.6	463	558.1
331	664.2	393	656.4	462	551.1
330	663.8	392	669.4	461	542.4
329	676.3	391	628.5	460	429.1
328	629.8	390	653.4	459	534.6
327	654.8	389	651.9	458	532.6
326	650.9	388	653.1	457	541.3
325	655.2	387	648.5	456	532.3
324	650.8	386	647.4	455	554.1
323	648.5	385	661.3	454	563.1
322	662.8	384	635.9	453	543.1
321	633.1	383	663.4	451	543.2
320	661.2	382	666.9	450	553.3
319	659.5	381	669.0	449	558.2
318	662.8	380	664.7	448	557.7
317	659.1	379	663.4	447	589.2
316	658.2	378	676.2	446	584.9
315	670.0	377	633.0	445	594.7
314	627.4	376	662.9	444	582.5
313	651.1	375	667.3	443	603.1
312	650.4	374	669.4	442	589.3
311	650.6	373	665.0	441	582.9
310	647.2	372	663.7	440	590.7
309	646.4	371	677.0	437	529.8
308	661.4	370	635.4	436	592.5
307	640.0	369	663.2	435	606.1
306	671.5	368	667.1	434	596.7
305	678.2	367	668.2	433	605.0
304	680.2	366	664.0	432	611.2
303	675.3	365	662.2	431	604.4
302	673.9	364	676.8	430	592.5
301	686.7	363	633.7	429	587.8

2.7 Hypothetical Calculation of Canister Temperature Distribution Subsequent to Being Filled with a Hot Glass Waste Form

Problem Description. Under some heat transfer conditions, large temperature gradients can exist. These temperature gradients can impose large internal loads on the structure due to the structure's inherent constraint of the accompanying thermal expansion. The design and performance assessment of canisters into which molten glass waste is poured must be analyzed to determine the temperature distribution. The temperature distribution will subsequently be used to evaluate the stress distribution. Since the heat transfer process is a transient one, its response will need to be monitored at various discrete values of time so that it is likely that approximately the worst stress conditions will be monitored. A sketch of the waste canister into which the molten glass is assumed to be poured is shown in Figure 2.7-1.

Objectives. The objectives of this problem solution are to obtain the temperature distribution in a canister for various times subsequent to the thermal shock of being filled with a molten glass waste form. The temperature distribution conditions will be used to analyze corresponding thermal stress distributions.

Analytical Solution. This is a hypothetical problem for which computer program modeling will be conducted and the simulated response obtained. It is expected that ANSYS will be used. An analytical solution other than that from the computer program model will not be determined.

Assumptions.

- The molten waste form is poured instantaneously into the canister at time zero.
- The thickness of the canister walls is 0.5 cm.
- The atmosphere is at a fixed temperature.

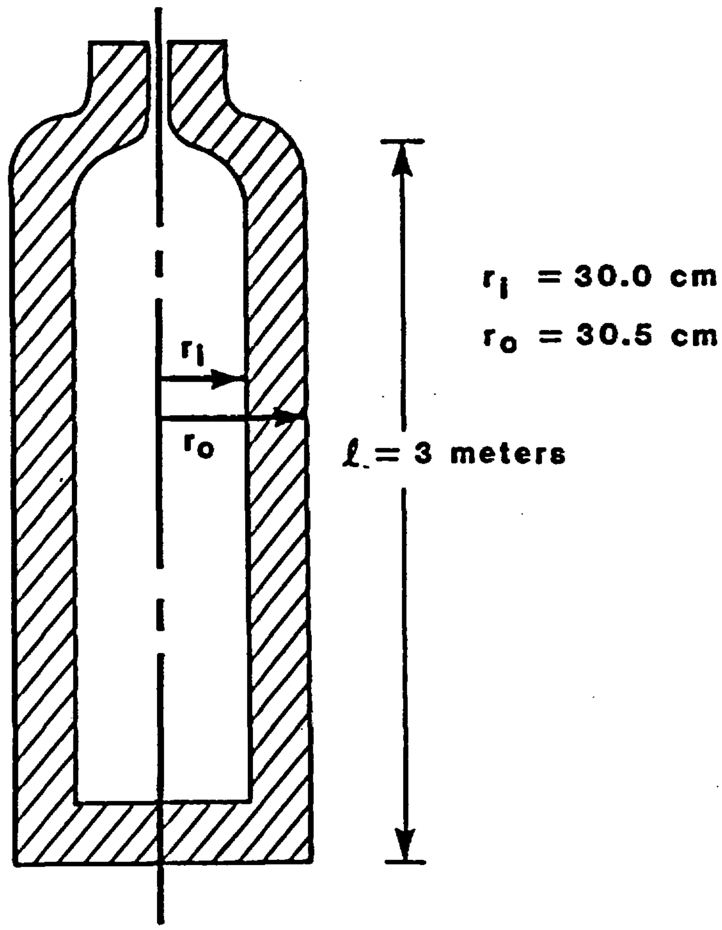

Figure 2.7-1

Canister into Which Molten Glass Waste Form Is Poured

- The nuclear decay heat generation can be neglected because the glass is very hot and only the early part of the transient is of interest.

Input Specifications. The canister material is 304 stainless steel. The dimensions are:

ℓ = length = 300.0 (cm)

r_i = inside radius = 30.0 (cm)

r_o = outside radius = 30.5 (cm)

The molten glass assumed to be poured into the canister instantaneously at the beginning of the transient (at time equals zero) has a temperature of 1000°C. The canister is initially at 800°C. The outside surface of the canister loses heat to the atmosphere which is at a fixed temperature of 300°C according to

$$q = h(T_o - T_a)$$

where

q = heat transfer rate per unit area (w/m^2)

h = heat transfer coefficient between canister and atmosphere ($w/m^2{}^oC$)

T_o = outside temperature of canister (°C)

T_a = fixed temperature of atmosphere which serves as a heat sink = 300.0 (°C)

The free convection heat transfer coefficient between the outside surface of the canister and the atmosphere is given by

$$h = 0.25(T_o - T_a)^{0.25}$$

The following glass properties will be used:

T (°C)	k (watts/m°C)	(kg/m^3)	c_p (watt-hr/kg°C)	a (m^2/hr)
20	0.872	2750	0.228	0.00139
100	0.972	2743	0.276	0.00128
200	1.097	2735	0.315	0.00127
300	1.222	2726	0.344	0.00130
400	1.347	2718	0.365	0.00136
500	1.472	2713	0.381	0.00142
600	1.598	2672	0.393	0.00152

The following 304 stainless steel conduction properties will be used:

T (°C)	k (w/m°C)	(kg/m^3)	c_p (w-hr/kg°C)	a (m^2/hr)
21.1	14.49	8030	0.130	0.0139
37.8	14.53	8030	0.130	0.0139
65.6	15.00	8012	0.132	0.0142
93.3	15.39	8001	0.134	0.0144
121.1	15.77	7990	0.135	0.0146
148.9	16.17	7978	0.136	0.0148
176.7	16.53	7966	0.139	0.0149
204.4	16.95	7955	0.141	0.0151
232.2	17.30	7943	0.143	0.0152
260.0	17.64	7931	0.144	0.0154
287.8	18.16	7919	0.146	0.0157
315.6	18.51	7907	0.147	0.0159
343.3	18.85	7894	0.149	0.0160
371.1	19.20	7882	0.150	0.0162
398.9	19.72	7869	0.153	0.0164
426.7	20.06	7856	0.155	0.0165
454.4	20.41	7844	0.156	0.0167
482.2	20.75	7831	0.158	0.0168
510.0	21.10	7818	0.159	0.0170
537.8	21.45	7805	0.160	0.0172

Output Specifications. The analyst must monitor the temperature distributions at various times and choose those that are most severe as the thermal load cases for the subsequent stress analyses.

3.0 MECHANICAL ANALYSIS PROBLEMS

Problems included in this section have been selected to test the mechanical or stress aspects of waste package codes against analytical solutions or hypothetical problems. Specific processes that must be tested in waste package performance assessment codes include:

- Linear-elastic displacements
- Elastic-plastic displacements
- Creep
- Thermal-induced stresses
- Dynamic displacements due to handling accidents or normal transportation loads
- Geometric instability (buckling)
- Creep buckling

Not all of the above processes can necessarily be analyzed using one code. The testing of the code may therefore involve analyzing two or three of the problems developed for relatively simple codes or up to six or seven for the more complex codes.

3.1 Radial and Tangential Stress Components at the Inner and Outer Surfaces of a Thick-Walled Cylinder with a Radial Temperature Profile

Problem Statement. This problem concerns the radial and tangential stress components at the inner and outer surfaces of a hollow cylinder ($r_i \leq r \leq r_o$), which suppports a radial temperature distribution

$$T(r) = T_o + \frac{q''' r_w^2}{2k} \ \ln (r_o/r) \tag{42}$$

as given in thermal problem 2.1. In this equation

r = radial position $r_i \leq r \leq r_o$ [ℓ]

r_i = inside radius of hollow cylinder [ℓ]

r_o = outside radius of hollow cylinder [ℓ]

r_w = outside radius of solid cylindrical region in which volumetric heat generation q''' applies $r_i \leq r_w$ [ℓ]

k = thermal conductivity of hollow cylinder material (assumed constant) [e/tℓθ]

q''' = uniform volumetric heat generation rate in solid cylindrical region of outer region r_w [e/tℓ³]

T_o = temperature of outer surface of hollow cylinder at $r = r_o$ [θ]

Objectives. The solution to this problem can be used to verify the accuracy of the WAPPA and ANSYS structural analysis models. The verification is directed to the treatment of the radial temperature distribution and the structural response, in terms of the radial and circumferential stress components that it causes.

Analytical Solution. The general solution given by Timoshenko (TI-56) for the radial stress component at any position $r_i \leq r \leq r_o$ where the radial stress is zero on the inside and outside surfaces is

$$\sigma_r = \frac{E}{1-\nu}\left[-\frac{1}{r^2}\int_{r_i}^{r} \alpha T(r)rdr + \frac{r^2 - r_i^2}{r^2(r_o^2 - r_i^2)} \int_{r_i}^{r_o} \alpha T(r)rdr\right] \tag{43}$$

and the circumferential stress component is given by

$$\sigma_t = \frac{E}{1-\nu}\left[\frac{1}{r^2}\int_{r_i}^{r} \alpha T(r) r dr + \frac{r^2 + r_i^2}{r^2(r_o^2 - r_i^2)}\int_{r_i}^{r_o} \alpha T(r) r dr - \alpha T(r)\right]$$

(44)

where

E = material's elastic modulus [f/ℓ^2]

ν = material's Poisson's ratio [ ]

α = material's coefficient of thermal expansion [$1/\theta$]

r = general radial position in the range $r_i \le r \le r_o$ [ℓ]

r_i = inside radius of hollow cylinder [ℓ]

r_o = outside radius of hollow cylinder [ℓ]

σ_r = radial stress component [f/ℓ^2]

σ_t = circumferential stress component [f/ℓ^2]

$T(r)$ = temperature at position r ($r_i \le r \le r_o$) in the hollow cylinder [θ]

Figure 3.1-1 shows the solid cylinder configuration in which the heat is generated and the larger concentric hollow cylinder for which the radial and tangential thermal stress components will be analyzed.

Using Equation 42 for the temperature distribution

$$T(r) = T_o + \frac{q''' r_w^2}{2k} \ln(r_o/r)$$

(42)

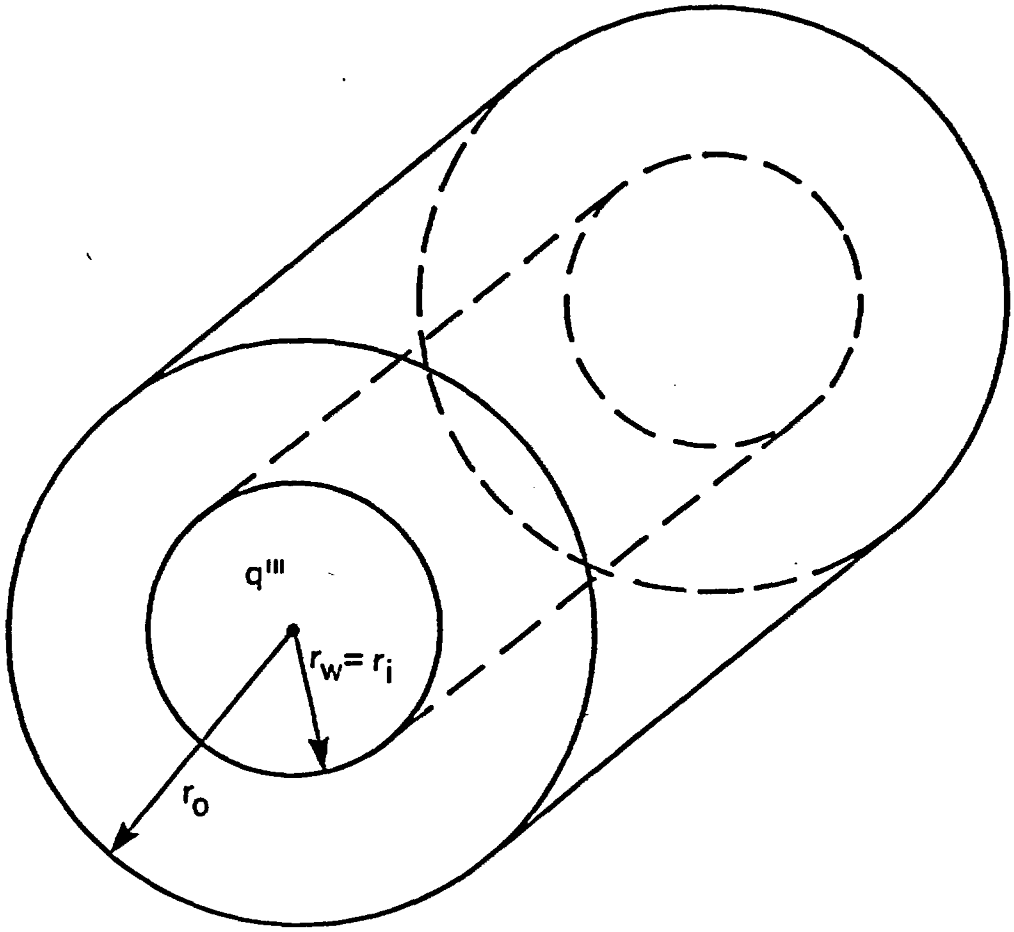

Figure 3.1-1

Hollow Cylinder $r_i<r<r_o$ with Steady-State Radial Temperature Distribution for Which Radial and Tangential Stress Components Will Be Analyzed

and for k = constant, the integrals are

$$\int_{r_i}^{r} T(r)rdr = \frac{T_o}{2}(r^2 - r_i^2) + \frac{q'''r_w^2}{2k}\left[\frac{r^2}{2}\left(\ln\frac{r_o}{r} + \frac{1}{2}\right) - \frac{r_i^2}{2}\left(\ln\frac{r_o}{r_i} + \frac{1}{2}\right)\right] \tag{45}$$

and

$$\int_{r_i}^{r_o} T(r)rdr = \frac{T_o}{2}(r_o^2 - r_i^2) + \frac{q'''r_w^2}{2k}\left[\frac{r_o^2 - r_i^2}{4} - \frac{r_i^2}{2}\ln\frac{r_o}{r_i}\right] \tag{46}$$

Thus, Equations 43 and 44 can be evaluated to give the radial and tangential stress components for any radial position r for the temperature distribution given by Equation 42.

Equations 43 and 44 can be written as

$$\sigma_r = \frac{E}{1-\nu}\left[\frac{\left(1 - r_i^2/r^2\right)B}{\left(r_o^2 - r_i^2\right)} - \frac{A(r)}{r^2}\right] \tag{47}$$

and

$$\sigma_t = \frac{E}{1-\nu}\left[\frac{1 + (r_i/r)^2 B}{\left(r_o^2 - r_i^2\right)} + \frac{A(r)}{r^2} - \alpha T(r)\right] \tag{48}$$

where

$$B = \frac{\alpha T_o}{2}(r_o^2 - r_i^2) + \frac{q''' r_w^2 \alpha}{2k}\left[\left(\frac{r_o^2 - r_i^2}{4}\right) - \frac{r_i^2}{2}\ln\frac{r_o}{r_i}\right] \tag{49}$$

and

$$A(r) = \frac{\alpha T_o}{2}(r^2 - r_i^2) + \frac{q''' r_w^2 \alpha}{4k}\left\{r^2\left[\ln\left(\frac{r_o}{r_i}\right) + 1/2\right] - r_i^2\left[\ln(r_o/r_i) + 1/2\right]\right\} \tag{50}$$

Equations 47, 48, 49, and 50 can be evaluated to predict analytically the radial distribution of the radially and tangentially directed stress components.

Assumptions.

- The thermal conductivity of the hollow cylinder material is constant.
- The coefficient of thermal expansion of the hollow cylinder is constant.
- The material is isotropic

Input Specifications.

- Geometry
  - waste region radius, r_w = 30.5 (cm)
  - hollow cylinder inside radius, r_i = 30.5 (cm)
  - hollow cylinder outside radius, r_o = 67.5 (cm)
- Material properties
  - thermal conductivity; k = 0.5 (w/cm°C)
  - coefficient of thermal expansion , $\alpha = 11 \times 10^{-6}$ (1/°C)
  - Poisson's ratio; ν = 0.25 ( )
  - elastic modulus; $E = 16.2 \times 10^4$ (MPa)
- Thermal conditions
  - hollow cylinder outside temperature; T_o = 200(°C)
  - volumetric heat generation rate; q''' = 0.001291 (w/cm^3)

Equations 47, 48, 49 and 50 have been evaluated at eight radial positions as shown in Table 3.1-1 to determine the radial and tangential stress components at eight values of radius in the range ($r_i \leq r \leq r_o$).

Output Specifications. The solution to this problem will determine the stress components at the radial positions indicated in Table 3.1-1 using WAPPA and ANSYS.

Table 3.1-1

Calculated Values of Radial and Tangential Stress Components

r (cm)	T (^oC)	A (cm^2)	σ_r (MPa)	σ_t (MPa)
30.5	200.954	0.0	0.00	-1.422
35.0	200.789	0.3256	-0.146	-0.883
40.0	200.628	0.7396	-0.209	-0.433
45.0	200.487	1.2083	-0.215	-0.0969
50.0	200.360	1.7320	-0.189	0.179
55.0	200.246	2.310	-0.145	0.406
60.0	200.141	2.943	-0.0908	0.601
67.5	200.000	3.996	0.000	0.845

3.2 Horizontal Simply Supported Beam Subjected to Vertical Motion at Both Supports as Defined by a Particular Acceleration Response Spectrum

Problem Statement. This problem is intended to determine the maximum displacement relative to the supports and the maximum bending stress for the beam shown in Figure 3.2-1. The response spectrum is given in Figure 3.2-2 (Reference BI-64).

Objectives. This sample problem will be used to verify the response spectrum analysis capabilities of structural codes.

Analytical Solution. The fundamental natural frequency of a beam with a uniform mass distribution is given by

$$f = \frac{\pi}{2\ell^2}\sqrt{\frac{EI}{m}} \tag{51}$$

where

f = vibrational frequency [1/t]

ℓ = beam length [ℓ]

E = beam material's elastic modulus [f/ℓ^2]

I = beam moment of inertia for in plane bending (Figure 3.2-1) [ℓ^4]

m = beam mass per unit length [m/ℓ]

Only the first mode given by

$$\phi_1(x) = \text{Sin}\,\frac{\pi x}{\ell} \tag{52}$$

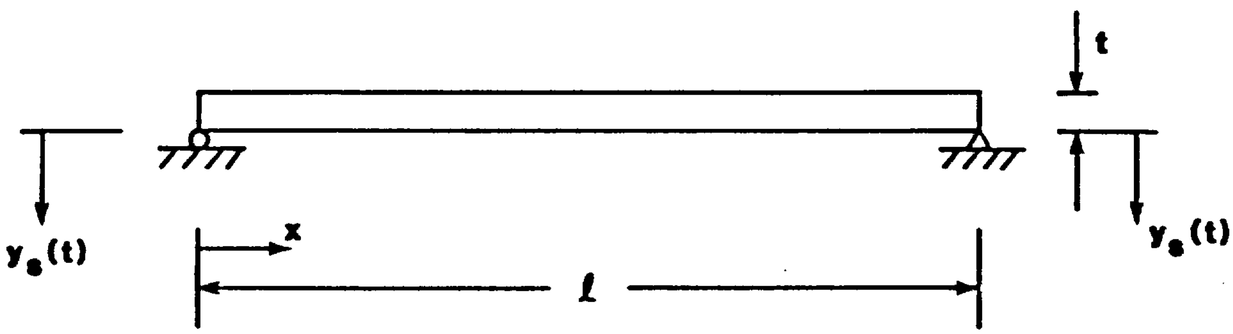

ℓ = 240 in

t = 14 in

m = 0.2 $lb_f\ sec^2/in$

EI = 10^{10} lb_f-in^2

Figure 3.2-1

Simply Supported Beam with Support Motion $y_S(t)$

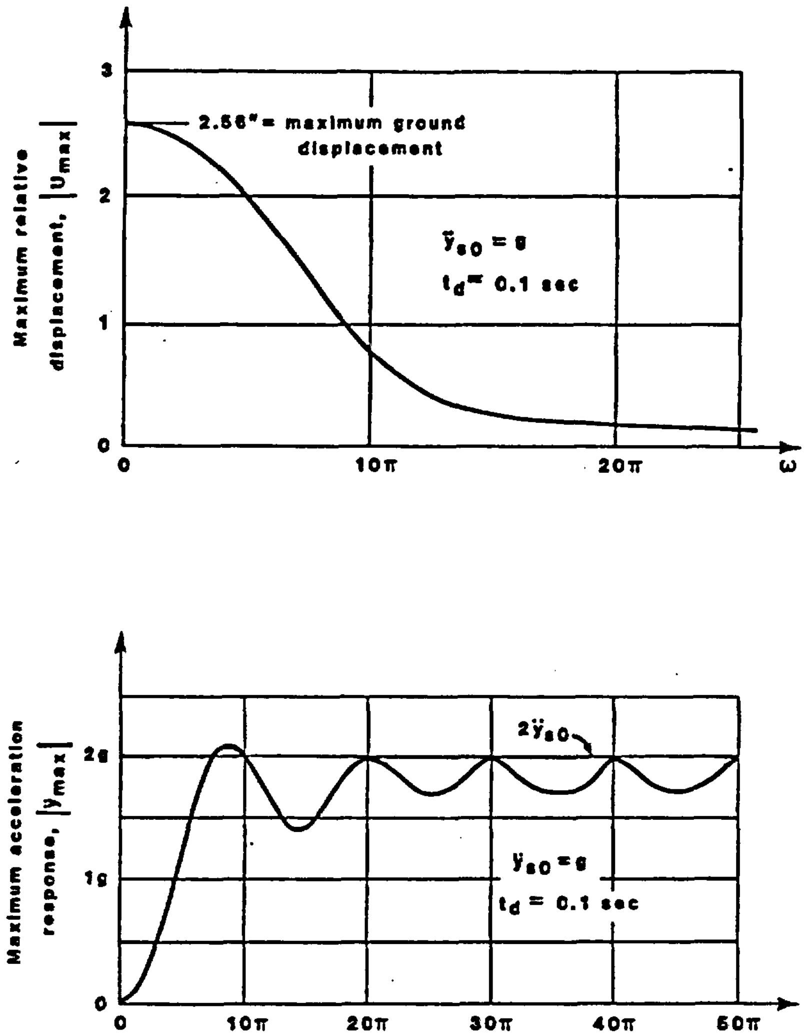

Figure 3.2-2

Maximum Relative Displacement and Maximum Vertical Acceleration Plotted as Response Spectra for Beam Supports Motion will be considered where

$\phi_1(x)$ = mode shape [ ]

The participation factor of that mode in the total motion is given by

$$\Gamma_1 = \frac{\int_0^{\ell} m\phi_1(x)dx}{\int_0^{\ell} m[\phi_1(x)]^2 dx} \tag{53}$$

where

Γ_1 = modal participation factor for the fundamental mode [ ]

m = beam mass [m]

The modal displacement is given by

$$A_1(t) = \Gamma_1 U_1(t) \tag{54}$$

where

$A_1(t)$ = modal displacement for the fundamental mode [ℓ]

Γ_1 = participation factor of the fundamental mode [ ]

$U_1(t)$ = response of the single degree of freedom system [ℓ]

The modal displacement of the distributed mass is

$$U(t) = \Gamma_1 U_1(t)\ \phi_1(x) \tag{55}$$

or using Equations 52 and 54

$$U_1(t) = A_1(t)\ \text{Sin}\ \frac{\pi x}{\ell} \tag{56}$$

The maximum bending moment in the beam is given by

$$M = -EI\ \frac{\partial^2 u}{\partial x^2} \tag{57}$$

and the maximum bending stress is given by

$$\sigma = \frac{Mc}{I} \tag{58}$$

where

σ = bending stress $[f/\ell^2]$

M = internal moment by beam cross section at the midspan $[f\text{-}\ell]$

c = beam half thickness in vertical direction $[\ell]$

I = cross section's moment of inertia $[\ell^4]$

These equations allow for the determination of the dynamic response when used in conjunction with the spectra of Figure 3.2-2.

Assumptions. It is assumed that the fundamental mode predominates and the contribution of higher harmonics is negligible.

Input Specifications. As shown in Figure 3.2-1, the beam dimensions and properties are:

ℓ = length = 240 (in)

t = height of cross section = 14 (in)

m = mass of unit length of beam = 0.2 (lb_f -sec^2/in^2)

EI = product of beam elastic modulus and moment of inertia = 10^{10} (lb_f-in^2)

For this particular case, Equation 51 gives

$$f = \frac{\pi}{2\ell^2}\sqrt{\frac{EI}{m}} = \frac{\pi^2}{2(240)^2}\sqrt{\frac{10^{10}}{0.2}}$$

$$f = 6.1 \text{ (cps)} \tag{59}$$

At a circular frequency of

$$\omega = 2\pi f = 2(6.1)\pi = 12.2\pi \tag{60}$$

the maximum relative displacement U_{max} from Figure 3.2-2 is

$$U_1 = 0.44 \text{ (in)} \tag{61}$$

Substituting Equation 52 in Equation 53 and integrating, the participation factor for the fundamental mode becomes

$$\Gamma_1 = 4/\pi \tag{62}$$

and from Equation 54

$$A_{max} = \frac{4}{\pi}(0.44) = 0.56 \text{ (in)} \tag{63}$$

The displacement is then given by Equation 55

$$u(t) = 0.56 \operatorname{Sin} \frac{\pi x}{\ell} \tag{64}$$

The maximum bonding moment occurs at the midspan and is given by

$$M_{max} = \frac{EI\pi^2}{\ell^2} A_{max}$$

$$M_{max} = \frac{10^{10}\pi^2(0.56)}{(240)^2}$$

$$M_{max} = 9.6 \times 10^5 \text{ (in-lb)} \tag{65}$$

The maximum bending stress in the outer fiber at $x = \ell/2$ is given by Equation 58

$$\sigma = \frac{Mc}{I} = \frac{EI\pi^2 c}{\ell^2 I} A_{max}$$

$$\sigma = \frac{(30 \times 10^6)\pi^2(7)\ (0.56)}{(240)^2}$$

$$\sigma = 20{,}100\ (lb/in^2)$$

(66)

Output Specification. The output should determine the natural frequencies and the maximum displacement at the center of the span in terms of the internal moment and the bonding stress using a finite element structural analysis program which offers modal summation analysis capabilities.

3.3 A Mass Supported by a Thin Rod and Subjected to a Step Load Causing Tension in the Rod and Plastic Deformation

Problem Statement. A mass supported by a thin rod is subjected to a step load which imposes a tensile load in the rod and causes it to experience elastic strain followed by plastic tensile strain. Figure 3.3-1 shows a mechanical model of the structure and the loading history.

Objectives. The objective of this analysis is to determine the displacement transient of the mass and the time when the displacement is at its maximum.

Analytical Solution. The ramp portion of the response when the rod is strained elastically as represented by the spring elongation is regarded

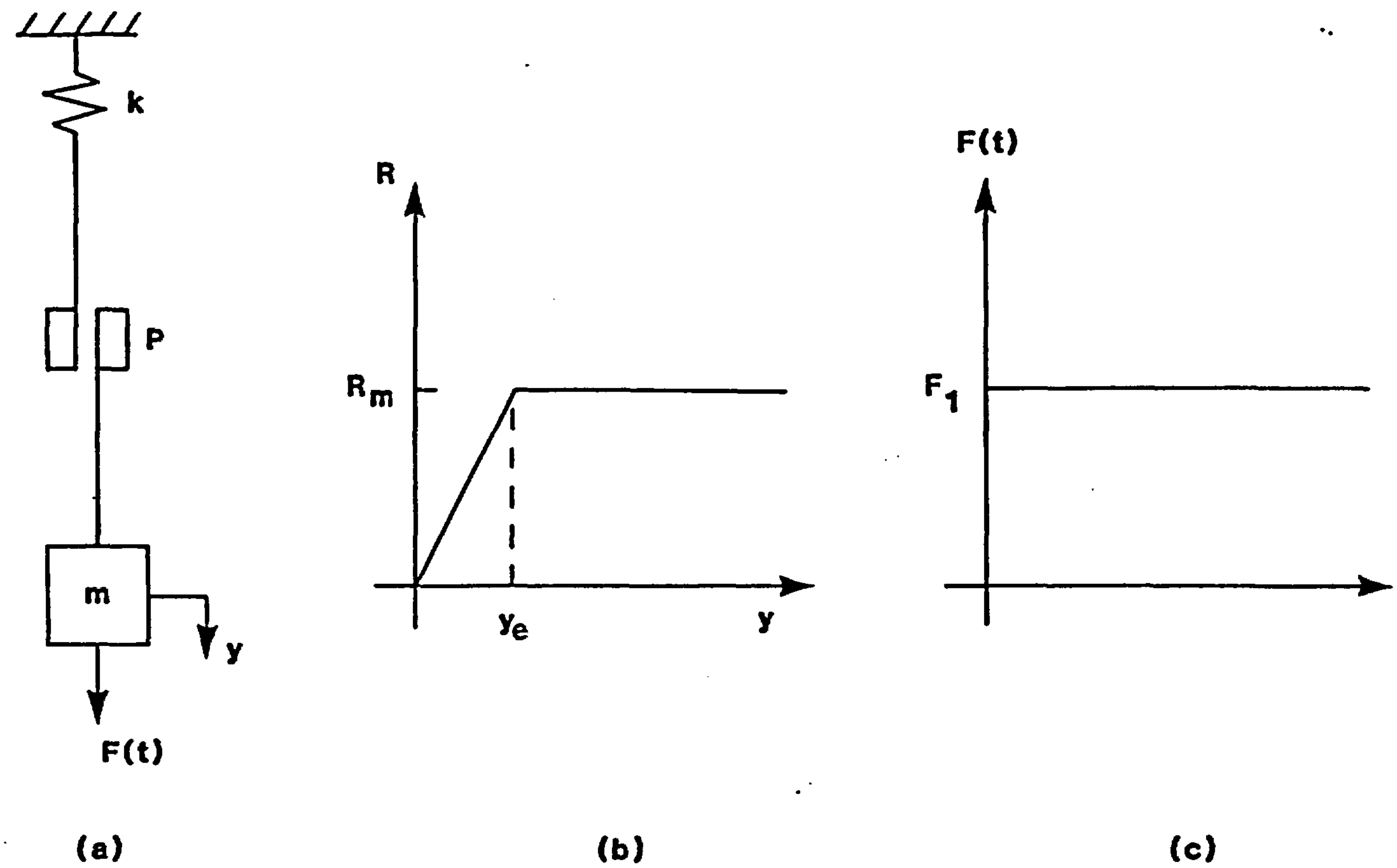

Figure 3.3-1

(a) Mechanical Model and (b) Force Versus Deflection (y) Response Characteristic of the Rod and c) the Load History (f) Versus Time (t). In (a) the Friction Joint p Slips When the Load Reaches R_m Representing Plastic Yielding of the Rod as the first stage. In this stage, there is no slipping at the joint p. The differential equation of motion and the boundary conditions are:

$$m\ddot{y} + ky = F_1 \tag{67}$$

$$t = 0, \; y = 0 \tag{68}$$

$$t = 0, \; \dot{y} = 0 \tag{69}$$

where the differential Equation 67 is based on Newton's second law and the initial conditions state that the initial deflection is equal to the steady downward force of F_1 divided by the spring stiffness and that the initial velocity of the mass is zero. The solution to the differential equation is

$$y = y_{st} + C_1 \text{ Sin } \omega t + C_2 \text{ Cos } \omega t \tag{70}$$

where $y_{st} = F_1/k$. Upon applying the boundary conditions, it is determined that

$$C_1 = 0 \tag{71}$$

$$C_2 = -y_{st} \tag{72}$$

So the solution can be written as

$$y = y_{st}\ (1\text{-Cos}\ \omega t) \tag{73}$$

In Equations 70 and 73, ω is the circular frequency defined as

$$\omega = \sqrt{\frac{k}{m}} \tag{74}$$

The second stage begins at time $t = t_e$ when the first stage is completed. Time range for the second stage which begins at zero when $t = t_e$ is established by defining a time variable t_i for the second stage according to

$$t_i = t - t_e \tag{75}$$

The differential equation for the second stage is

$$m\ddot{y} + R_m = F_1 \tag{76}$$

and the boundary conditions are

$$t_1 = 0, \quad y = y_e \tag{77}$$

$$t_1 = 0, \quad \dot{y} = y_{st}\ \omega\ \text{Sin}\ \omega t_e \tag{78}$$

The general solution to Equation 76 is

$$y = \left(\frac{F_1 - R_m}{2m}\right) t_1^{\,2} + C_1 t_1 + C_2$$

(79)

Equation 73, which is the dynamic response of the mass during the first stage, can be used to solve for the time t_e at which the transition between the two stages occurs:

$$t_e = \frac{1}{\omega} \; \mathrm{Cos}^{-1} \left(1 - \frac{y_e}{y_{st}}\right)$$

(80)

Applying the boundary conditions of Equations 77 and 78 to the general solution of Equation 79 gives

$$y = \frac{1}{2m} (F_1 - R_m)\; t_1^{\,2} + (y_{st}\; \omega \;\mathrm{Sin}\; \omega t_e)\; t_1 + y_e$$

(81)

where $y_{st} = F_1/k$ is given in Equation 68.

By setting the first derivative of Equation 81 with respect to t_1 to zero, the time at which the displacement of the mass reaches a maximum is found to be

$$t_1\Big|_{y_{max}} = \frac{m y_{st}\; \omega \;\mathrm{Sin}\; \omega t_e}{(R_m - F_1)}$$

(82)

and the time from the beginning of the transient from Equations 75 and 80 is

$$t\Big|_{y_{max}} = \frac{1}{\omega} \cos^{-1}\left(1 - \frac{y_e}{y_{st}}\right) + \frac{m y_{st}\, \omega \sin \omega t_e}{(R_m - F_1)} \tag{83}$$

which is more convenient.

Assumptions. In the analysis, it is assumed that the rod material displays linear elastic response followed by perfectly plastic force versus displacement response.

Input Specifications. The problem is completely specified in terms of four parameters R_m, y_e, m, and F_1 which allow quantification of k and the other parameters such as ω.

R_m = force necessary to cause yielding in the rod (f) = 500,000 (lb_f)

y_e = axial elongation of the rod when plastic deformation begins (ℓ) = 0.1666 (in)

k = spring stiffness effort of the rod when deformation is in the elastic range (f/ℓ) = R_m/y_e = 3.0×10^6 (lb/in)

m = mass attached to the rod = 30,000 (lb_f-sec^2/in)

F_1 = magnitude of uniform tensile force applied to the mass = 3,000,000 (lb_f)

For these values, Equation 74 gives

ω = 10 (1/sec)

and Equation 80 gives

$$t_e = 0.230 \text{ (sec)}$$

and Equation 82 gives

$$t_1 = 0.1118 \text{ (sec)}$$

so that Equation 75 gives

$$t|_{max} = t_e + t_1$$
$$t|_{max} = 0.3418 \text{ (sec)}$$

Output Specifications. The output should be the time of maximum deflection of the mass determined by using a structural analysis computer program that will stimulate elastic and plastic material behavior for this structure and its loading.

3.4 Displacement and Velocity of Mass When a Package Is Dropped on a Rigid Floor and the Subsequent Maximum Displacement of the Mass and Maximum Spring Force

Problem Statement. A mass m represents the contents of a package; the contents are attached to the package with a linear spring of stiffness k. The spring connecting the mass to the package acts in the vertical direction, and all motion of the mass and the package occurs in the vertical direction as shown in Figure 3.4-1.

Objectives. The quantities to be determined are the displacement and velocity of the mass when the container reaches the floor and the subsequent maximum force transmitted to the mass and the required "rattle space" as indicated by the maximum deflection.

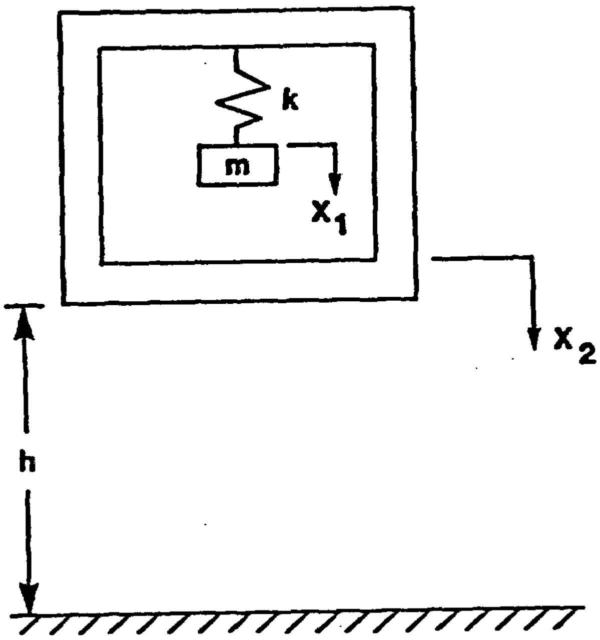

Figure 3.4-1

Package System Used to Drop Dynamics Analytical Simulation

<u>Analytical Solution</u>. The dynamics of the package contents are described in Reference TH-65 as

$$m(\ddot{x}_1 + \ddot{x}_2) + kx_1 = 0 \tag{84}$$

where

m = mass of contents [m]

x_1 = position of the mass relative to the container measured vertically [ℓ]

x_2 = position of container measured vertically [ℓ]

k = linear spring force to displacement ratio [f/ℓ]

$\ddot{x} = \dfrac{d^2x}{dt^2}$ [ℓ/t²]

t = time measured through the dynamic transient [θ]

The initial conditions applicable to the first phase of the transient (pre-container impact) are:

$$t = 0,\ x_1 = 0 \tag{85}$$

$$t = 0,\ \dot{x}_1 = 0 \tag{86}$$

$$t = 0,\ x_2 = 0 \tag{87}$$

$$t = 0,\ \dot{x}_2 = 0 \tag{88}$$

which state that the initial displacement of the mass and the container are zero as are their initial velocities in the vertical (downward) direction. All rotation and translation, orthogonal to the vertical, are constrained to zero.

The Laplace transform of the differential Equation 84 for the given initial conditions 2, 3, 4, and 5 is

$$\bar{x}_1(s) = [x_1(0) + x_2(0)] \frac{s}{s^2 + \omega_n^2} + [\dot{x}_1(0) + \dot{x}_2(0)] \frac{1}{s^2 + \omega_n^2} - \frac{s^2\bar{x}_2(s)}{s^2 + \omega_n^2} \tag{89}$$

where

$\omega_n = \sqrt{\frac{k}{m}}$ = natural frequency of the contents mass, m, and its attachment spring k to the box [1/θ]

s = transformed variable replacing time [1/θ]

$\bar{x}_1(s)$ = Laplace transform of $x_1(t)$

$\bar{x}_2(s)$ = Laplace transform of $x_2(t)$

The inverse of Equation 89 can be written as

$$x_1(t) = [x_1(0) + x_2(0)] \operatorname{Cos} \omega_n t + \frac{1}{\omega_n} [\dot{x}_1(0) + \dot{x}_2(0)] \operatorname{Sin} \omega_n t - \mathcal{L}^{-1} \frac{s^2\bar{x}_2(s)}{s^2 + \omega_n^2} \tag{90}$$

The motion of the container is

$$x_2(t) = \frac{1}{2} gt^2 \tag{91}$$

and its transform is

$$\bar{x}_2(s) = g/s^3 \tag{92}$$

which when substituted into Equation 89 gives

$$\bar{x}_1(s) = - \frac{g}{s(s^2 + \omega_n^2)} \tag{93}$$

for the initial conditions of Equations 85, 86, 87, and 88 and the inverse is

$$x(t) = - \frac{g}{\omega_n^2} (1 - \text{Cos } \omega_n t) \tag{94}$$

Using Equation 91, the time to fall from the initial height h supporting the container to the floor is

$$t_o = \sqrt{2h/g} \tag{95}$$

The displacement and velocity of the mass m relative to the container when the container impacts the floor are

$$x_1(t_o) = -\frac{g}{\omega^2}(1-\cos\omega_n t_o) \tag{96}$$

$$\dot{x}_1(t_o) = -\frac{g}{\omega_n}\sin\omega_n t_o \tag{97}$$

These expressions can be evaluated to give the initial conditions for the second phase of the problem subsequent to the container's impact with the floor.

Redefining a new time variable t_1, which is zero at the instant the container impacts the floor

$$t_1 = t - t_o \tag{98}$$

This time variable, t_1, will be used during the second, post-container impact phase of the problem. The initial conditions for the second phase are

$$t_1 = 0,\ x_1 = -g/\omega_n^2\,(1-\cos\omega_n t_o) \tag{99}$$

$$t_1 = 0,\ x_2 = L \tag{100}$$

$$t_1 = 0, \ \dot{x}_1 = g/\omega_n \ \text{Sin} \ \omega_n t_o \tag{101}$$

$$t_1 = 0, \ \ddot{x}_2 = g t_o \tag{102}$$

From Equation 90, the displacement after impact for the initial conditions of Equations 99, 100, 101, and 102 becomes

$$x_1(t) = \left[h - \frac{g}{\omega_n^2}(1 - \text{Cos} \ \omega_n t_o)\right] \text{Cos} \ \omega_n t + \frac{1}{\omega_n}\left[g t_o - \frac{g}{\omega_n} \ \text{Sin} \ \omega_n t_o\right] \text{Sin} \ \omega_n t - h \ \text{Cos} \ \omega_n t \tag{103}$$

The first and last terms cancel, and this equation can be rewritten using a trigonometric identity as

$$x_1(t) = \frac{g}{\omega_n^2}\sqrt{(1 - \text{Cos} \ \omega_n t_o)^2 + [\omega_n t_o - \text{Sin} \ \omega_n t_o]^2} \ \text{Sin} \ (\omega_n t_1 - \phi) \tag{104}$$

where

where

$$\phi = \mathrm{Tan}^{-1}\left[\frac{(1-\mathrm{Cos}\ \omega_n t_o)}{(\omega_n t_o - \mathrm{Sin}\ \omega_n t_o)}\right] \tag{105}$$

The maximum amplitude of the mass m is

$$A = x_1\Big|_{max} = \frac{g}{\omega_n^2}\sqrt{(1-\mathrm{Cos}\ \omega_n t_o)^2 + (\omega_n t_o - \mathrm{Sin}\ \omega_n t_o)^2} \tag{106}$$

and the maximum occurs at a time consistent with

$$\omega_n t_1 - \phi = \frac{\pi}{2} \tag{107}$$

or

$$t_1 = \frac{1}{\omega_n}\left(\frac{\pi}{2} - \phi\right) \tag{108}$$

Using Equation 98, the time from the beginning of the first phase of the transient until the maximum displacement of the mass is reached is

$$t = t_o + \frac{1}{\omega_n}\left(\frac{\pi}{2} - \phi\right) \tag{109}$$

The maximum spring force is given by

$$F_{max} = kA$$

where

k = spring stiffness [f/ℓ]

A = maximum amplitude of the mass m [ℓ] (see Equation 106)

Assumptions.

- The mass m is supported within the box by a linear spring of stiffness k.
- The mass of the container is large compared to that of the contents, m, so that the free fall of the container is not influenced by the force associated with the relative motion of the mass, m.
- Upon striking the floor, the container remains in contact with the floor.

Input Specifications. For an initial height of the box above the plane of

$$h = 10(\text{in})$$

the time at which it reaches the plane is given by Equation 95 as

$$t_0 = 0.2275 \text{ (sec)}$$

If the spring stiffness is

$$k = 39.48 \text{ (lb/in)}$$

and the mass of the contents is

$$m = 0.12 \text{ slugs} = 3.864 \text{ lb}_m$$

then the circular natural frequency is

$$\omega_n = \sqrt{\frac{k}{m}} = 20\pi \frac{1}{\text{sec}}$$

and the vibrational natural frequency is

$$f_n = \omega_n/2\pi = 10 \text{ (1/sec)}$$

Equation 106 can be evaluated for

$$\omega_n t_o = 20 \text{ (0.2275)} = 14.29$$

to give

$$A = 1.306 \text{(in)}$$

This is the required rattle space in terms of amplitude.

Output Specifications. The output should simulate the dynamics of this problem with a time history transient analysis program and determine the maximum displacement of the mass after the container strikes the plane and the time at which the maximum amplitude is reached.

3.5 Determine the Natural Frequencies and Normal Modes of an Elastic Discrete Mass System

Problem Statement. This problem concerns the normal modes and natural frequencies of the system shown in Figure 3.5-1, where the two masses each have one translational degree of freedom (in the x direction) and are of equal magnitude as are the three linear spring stiffness values.

Objectives. This analytical solution will provide for numerical testing of all of the frequency extraction and normal mode vector calculation procedures in modal summation type dynamic analysis programs.

Analytical Solution. For the system shown in Figure 3.5-1, the differential equations describing the motion are

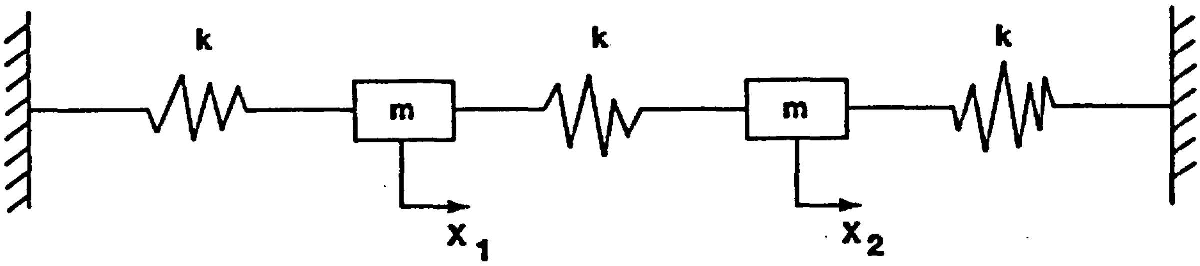

Figure 3.5-1

Two Degree of Freedom System for Which the Natural Frequencies and Mode Shapes Will Be Determined

$$m\ddot{x}_1 + 2kx_1 - kx_2 = 0 \tag{110}$$

$$m\ddot{x}_2 + 2kx_2 - kx_1 = 0 \tag{111}$$

Assume that the motion of each mass is periodic and composed of harmonic motions of various amplitudes and frequencies. Let one of these components be

$$x_1 = A \text{ Sin } (\omega t + \phi) \tag{112}$$

$$x_2 = B \text{ Sin } (\omega t + \phi) \tag{113}$$

Substituting Equations 112 and 113 into 110 and 111 gives

$$(2k-m\omega^2)A-kB=0 \tag{114}$$

$$-kA + (2k-m\omega^2)B = 0 \tag{115}$$

which are homogeneous linear algebraic equations for the undetermined magnitudes A and B. The trivial solution A = B = 0 is real and represents the static equilibrium position of the masses. The natural frequencies and mode shapes result from

$$\begin{bmatrix} (2k-m\omega^2) & -k \\ -k & (2k-m\omega^2) \end{bmatrix} \begin{bmatrix} A \\ B \end{bmatrix} = \begin{bmatrix} 0 \\ 0 \end{bmatrix} \tag{116}$$

solving for the values of ω which allows the coefficient matrix of Equation 116 to have a determinant equal to zero. The fourth order equation in the circular vibrational frequency of the system is

$$\omega^4 - \frac{4k}{m}\,\omega^2 + \frac{3k^2}{m^2} = 0 \tag{117}$$

The roots of this equation are

$$\omega_1 = \sqrt{k/m} \tag{118a}$$

$$\omega_2 = \sqrt{3k/m} \tag{118b}$$

$$\omega_3 = -\sqrt{k/m} \tag{118c}$$

$$\omega_4 = -\sqrt{3k/m} \tag{118d}$$

The natural frequencies must be real and positive and are given by Equations 118a and 118b.

By substituting Equation 118a into Equations 114 and 115, the mass displacement amplitude ratio for mode 1 is determined

$$\frac{A_1}{B_1} = \frac{k}{2k - m\omega_1^{\ 2}} = \frac{2k - m\omega_1^{\ 2}}{k}$$

$$\frac{A_1}{B_1} = 1$$

(119)

Similarly, by substituting Equation 118b into Equations 114 and 115

$$\frac{A_2}{B_2} = \frac{k}{2k - m\omega_2^{\ 2}} = \frac{2k - m\omega_2^{\ 2}}{k}$$

$$\frac{A_2}{B_2} = -1$$

(120)

In this way, the amplitude ratios are determined. The mode shapes can't be solved for explicitly but are determined on a relative basis from the amplitude ratios by assuming the displacement amplitude of one of the masses to be unity. Thus, the mode shapes are

$$\begin{bmatrix} A_1 \\ \\ B_1 \end{bmatrix} \begin{matrix} = \\ \\ = \end{matrix} \begin{bmatrix} 1 \\ \\ 1 \end{bmatrix}$$

(121)

which correspond to the first natural frequency

$$A_2 = 1$$

$$B_2 = -1 \tag{122}$$

which occurs along with the second natural frequency. The mode shapes are drawn in Figure 3.5-2.

Assumptions. It is assumed that the motion of each mass is periodic and composed of harmonic motion of various amplitudes and frequencies. The mode shapes are determined by assuming unit displacement in the positive direction for the mass on the left in Figure 3.5-1.

Input Specifications. The natural frequencies are given by Equations 118a and 118b. For

$$k = 1.0 \text{ lb/in}$$

$$m = 1.0 \text{ lb}_m$$

$$\omega_1 = \sqrt{\frac{K}{m}} = \sqrt{\frac{32.2\ (12)}{1}}$$

$$\omega_1 = 19.657 \text{ (1/sec)}$$

$$\omega_2 = \sqrt{\frac{3k}{m}} = \sqrt{\frac{3(32.2)\ (12)}{1}}$$

$$\omega_2 = 34.047 \text{ (1/sec)}$$

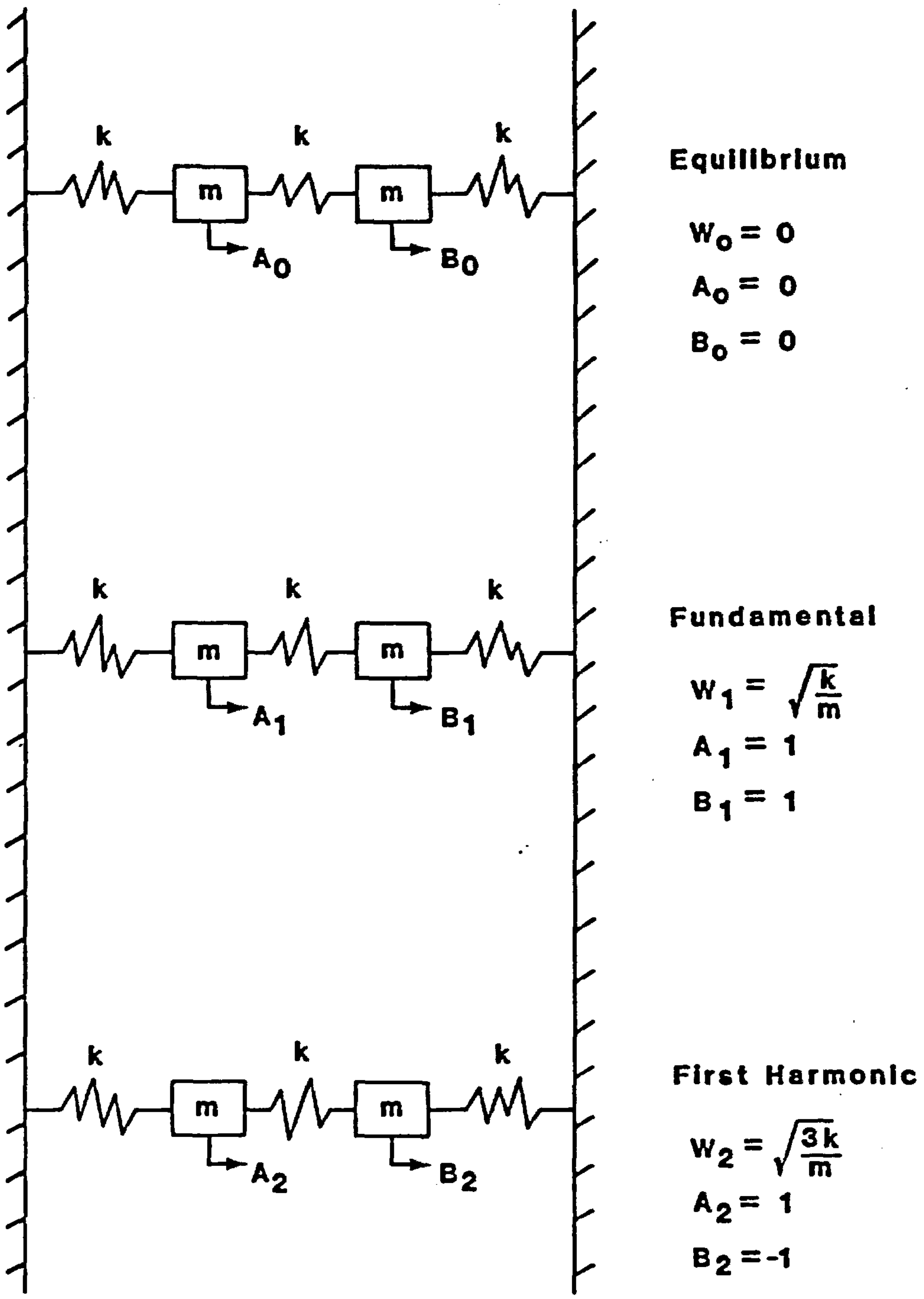

Figure 3.5-2

Equilibrium Position, Fundamental Frequency and First Mode Shape and Second Natural Frequency and Mode Shape for Two Degree of Freedom Violating System

For A_1 = 1.0, B_1 = 1.0 from Equation 119; similarly, from Equation 120 for A_2 = 1.0, it is determined that B_2 = -1.0.

Output Specifications. In solving this problem, the dynamics of the mass and elasticity are simulated by a finite element computer model such as ANSYS. The output determines how accurately the model predicts the natural frequencies and mode shapes.

3.6 Determine the Stress in a Pretensioned Body Which Experiences Stress Relaxation Due to Creep

Problem Statement. The ends of a bolt are held a fixed distance apart for a long period of time. Initially, the bolt is tightened producing an initial stress of σ_0. The bolt material is 0.30% carbon steel, which is assumed to have a creep rate given by

$$\dot{\varepsilon}^c = k \ ^n \tag{123}$$

where

$\dot{\varepsilon}^c$ = creep rate (1/hr)

k = creep constant (1/hr)

σ = axial stress component in bolt (lb/in^2)

n = creep exponent of stress ( )

The creep causes the elastic strain to decrease while the creep strain increases such that the sum of the two is always equal to a constant. The constant is the amount of elastic strain initially induced in the bolt by the initial stress σ_0 (see Figure 3.6-1 for a schematic of the bolt).

Objectives. The objective is to calculate the bolt stress as a function of time.

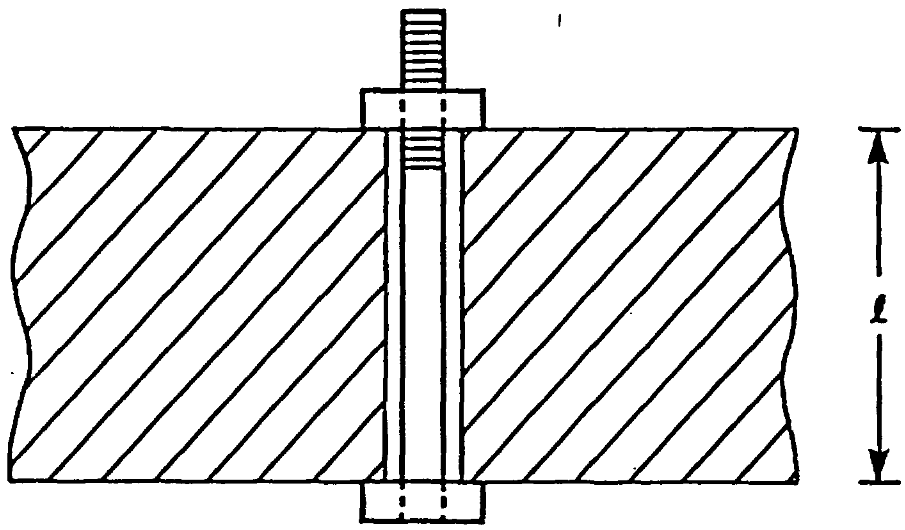

Figure 3.6-1

Bolt of Length 1 in Unloaded State Which Is Inititally Stressed to σ_o = 10,000 psi and Allowed to Stress Relax Due to Creep

Analytical Solution. It is assumed that the initial stress causes only elastic strain on an instantaneous basis and that the total strain in the bolt remains constant.

$$\varepsilon_o^{\,e} = \varepsilon^e + \varepsilon^c \tag{124}$$

where

ε_o^e = initial elastic strain ( )

ε^e = elastic strain at any time ( )

ε^c = creep strain at any time (initially zero) ( )

The elastic strain is related to the stress by Hook's law

$$\varepsilon_o^{\,e} = \frac{\sigma_o}{E} \tag{125a}$$

$$\varepsilon^e = \frac{\sigma}{E} \tag{125b}$$

where

E = elastic modulus of bolt material (psi)

σ_o = initial axial stress component in bolt (psi)

σ = axial stress component in bolt at any time (psi)

Substitution of Equation 125 into Equation 124 gives

$$\frac{\sigma_o}{E} = \frac{\sigma}{E} + \varepsilon^c \tag{126}$$

and the differentiating Equation 126 with respect to time gives

$$\frac{d\varepsilon^c}{dt} = -\frac{1}{E}\frac{d\sigma}{dt} \tag{127}$$

where the terms on the left side are the material creep rate. Combining Equations 123 and 127 eliminates the creep rate and gives the first order non-linear differential equation

$$-\frac{1}{kE}\ \sigma^{-n}\ d\sigma = dt \tag{128}$$

The initial condition is

$$t = 0 \qquad \sigma = \sigma_o \tag{129}$$

and the solution is of the form

$$\sigma = \sigma_o \left[kE(n-1)\sigma_o^{\,n-1}\ \ t + 1 \right]^{-1/n} \tag{130}$$

Assumptions. It is assumed that initially upon loading, the bolt strain is in the elastic range.

Input Specifications. For the following values of the parameters

$k = 4.78 \times 10^{-37}$ (1/hr)

$n = 6.9$ ( )

$E = 30 \times 10^{6}$ (psi)

$\sigma_0 = 10{,}000$ (psi)

Equation 130 becomes

$$\sigma = 10{,}000 \left[3.368 \times 10^{-5}\ t + 1\right]^{-0.1695} \tag{131}$$

which can be evaluated to give:

time (years)	time (hours)	σ (psi)
0	0	10,000
1	8,760	9,571
2	17,520	9,244
3	26,280	8,981
4	35,040	8,762
10	87,600	7,922
50	438,000	6,267
100	876,000	5,603
200	1,752,000	4,996
500	4,380,000	4,284
1000	8,760,000	3,812

Output Specifications. The output indicates the stress in the bolt as a function of time using the creep strain features of a finite element analysis program.

3.7 Elastic Stability of a Thin Tube of Infinite Length with External Pressure Loading

Problem Statement. The solution of this problem determines the magnitude of the external pressure loading that will cause a long, thin-walled, cylindrical tube to reach elastic instability. The cylinder configuration and pressure loading are shown in Figure 3.7-1.

Objectives. This problem will test the elastic stability prediction capability of structural analysis programs.

Analytical Solution. The solution given by Roary (Reference RO-65) for the external pressure load limit based on elastic stability is

$$p = \frac{1}{4}\frac{E}{1-\nu^2}\left(\frac{t}{r}\right)^3 \tag{132}$$

where

p = limit external pressure load [f/ℓ^2]

E = elastic modules of tube material [f/ℓ^2]

ν = Poisson's ratio of tube material [ ]

t = tube wall thickness [ℓ]

r = tube radius [ℓ]

The buckling solution should apply providing that the structure does not fail due to yielding (see Figure 3.7-2). According to the Tresca criterion, yielding will not occur providing that

$$\sigma_i < \sigma_t = \frac{pr}{t} < \sigma_{cy} \tag{133}$$

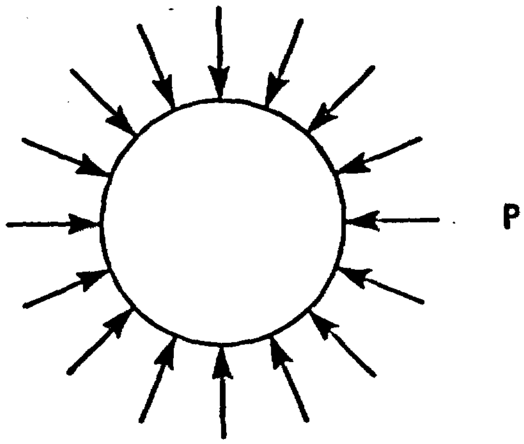

Figure 3.7-1

Long, Thin-Walled Circular Cylinder Loaded with External Pressure

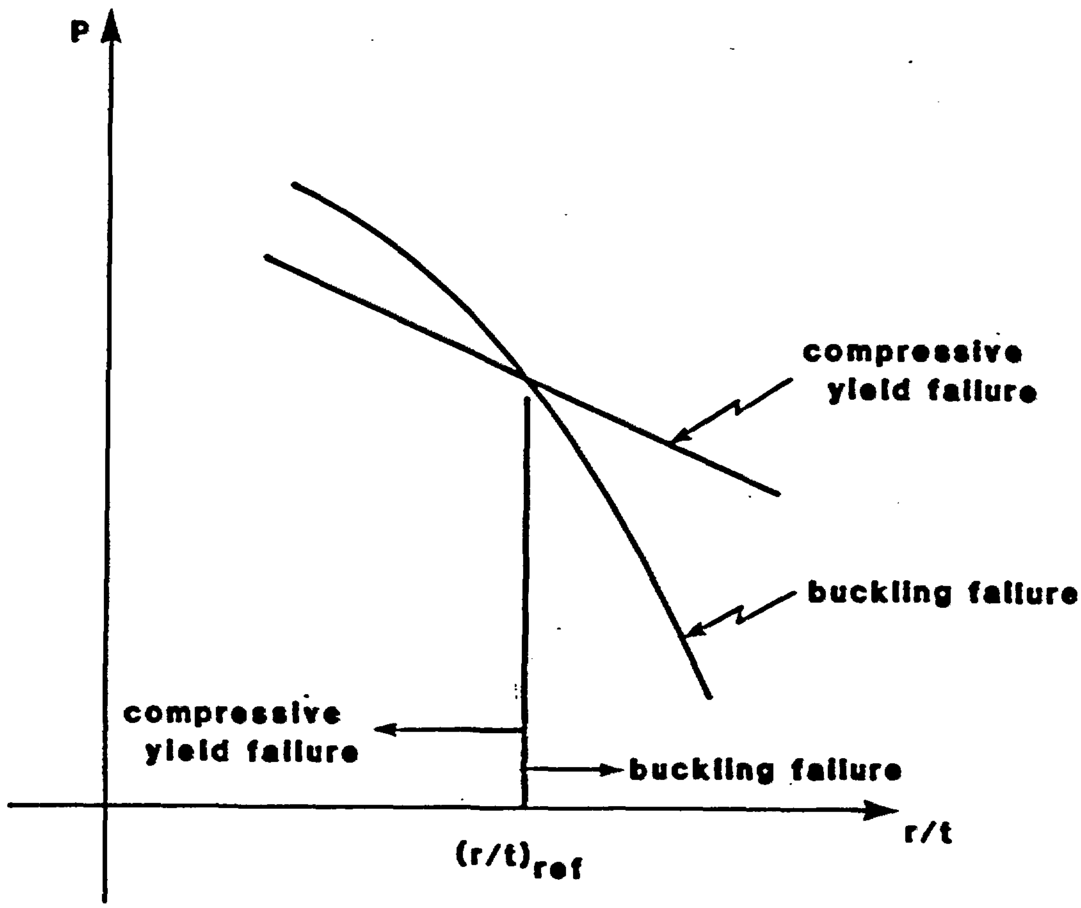

Figure 3.7-2

Compressive Yield and Buckling Failure Required for a Long Cylinder. External Pressure Is Plotted Against Cylinder Geometric Feature (r/t) where*

σ_i = Tresca stress intensity $[f/\ell^2]$

σ_t = compressive hoop stress component $[f/\ell^2]$

σ_{cy} = material yield stress in compression $[f/\ell^2]$

Equation 132 can be rewritten in terms of the hoop stress σ_t at which the cylinder becomes elastically unstable σ_{EU} as

$$\sigma_{EU} = \frac{1}{4} \frac{E}{1-\nu^2} \left(\frac{t}{r}\right)^2 \tag{134}$$

The tube should then have a stress σ_t such that $\sigma_t < \sigma_{EU}$ and $\sigma_t < \sigma_{cy}$. The limiting pressure becomes

$$p = \min \left\{ \begin{array}{l} \sigma_{cy}\,(t/r) = p_{cy} \\ \frac{1}{4} \frac{E}{1-\nu^2} (t/r)^3 = p_{EU} \end{array} \right\} \tag{135}$$

based on Equations 133 and 132 with $\sigma_t = \sigma_{cy}$. To obtain buckling failure

$$p_{EU} < p_{cy} \tag{136}$$

*In this problem, it is convenient to consider compressive stresses and the compressive yield stress σ_{cy} as positive quantities. This sign convention will apply to this problem.

from Equation 135. Substituting Equation 135 into Equation 136 gives

$$\frac{r}{t} > \sqrt{\frac{E}{4(1-\nu^2)\ \sigma_{cy}}} = \left(\frac{r}{t}\right)_{ref} \tag{137}$$

to assure buckling failure. Thus, when $r/t > (r/t)_{ref}$, buckling failure is expected, and when $r/t < (r/t)_{ref}$, compressive yield failure is expected.

If $E = 3 \times 10^6$ (psi) and $\nu = 0.3$ as is typical for some steels, the $(r/t)_{ref}$ for various values of σ_{cy} is given in Table 3.7-1.

Assumptions. It is assumed that the cylinder is round and of uniform thickness and that the deformed shape is oval. The material properties are assumed to be isotropic.

Input Specifications. The following material properties must be defined:

- Elastic modulus = $E = 30 \times 10^6$ (psi)
- Poisson's ratio = $\nu = 0.30$ ( )
- Compressive yield strength = $\sigma_{cy} = 30{,}000$ (psi)
- Cylindrical tube mean radius = $r = 20$ (in)
- Cylindrical tube wall thickness = $t = 1$ (in)

The external pressure loading that will cause buckling is determined by

$r/t = 20$

Table 3.7-1

Values of $(r/t)_{ref}$ at Which Failure Mode Changes Versus Compressive Yield Strength, σ_{cy}, for Steel Type Materials Where $E=30x10^6$ and $\nu = 0.3$

σ_{cy} (psi)	$(r/t)_{ref}$ ( )
20,000	20.3
24,000	18.5
27,000	17.5
30,000	16.6
32,000	16.0
36,000	15.1
40,000	14.4

and for σ_{cy} = 30,000 psi; $(r/t)_{ref}$ = 16.6. Since $r/t > (r/t)_{ref}$, buckling failure should occur.

For this case, Equations 132 and 134 give

$$p = 1030 \text{ (psi)}$$

$$\sigma_{EU} = 20{,}600 \text{ (psi)}$$

and the latter is clearly less than the σ_{cy}. Equation 133 allows a 1500 psi pressure because buckling is more limiting when $r/t > (r/t)_{ref}$.

Output Specifications. The output should include:

- Dimensions
- Material properties
- Allowable external pressure based on elastic instability (check against Equation 132 value)
- Elastic instability hoop stress σ_{EU} (check against Equation 134 value)

3.8 Creep Deformation of a Finite Length, Hollow Elastic Cylinder Due to External Pressure

Problem Statement. A hollow cylinder of finite length is subjected to external pressure loading (see Figure 3.8-1). The pressure acts both radially and axially.

Objectives. The objective of this problem is to compare the COVE program's creep deformation predictions with analytical and experimental observations. Typically, poor agreement is achieved between analytical predictions of collapse and experiments. A specific objective is to determine whether COVE results are conservative relative to experimental determinations of when collapse occurs.

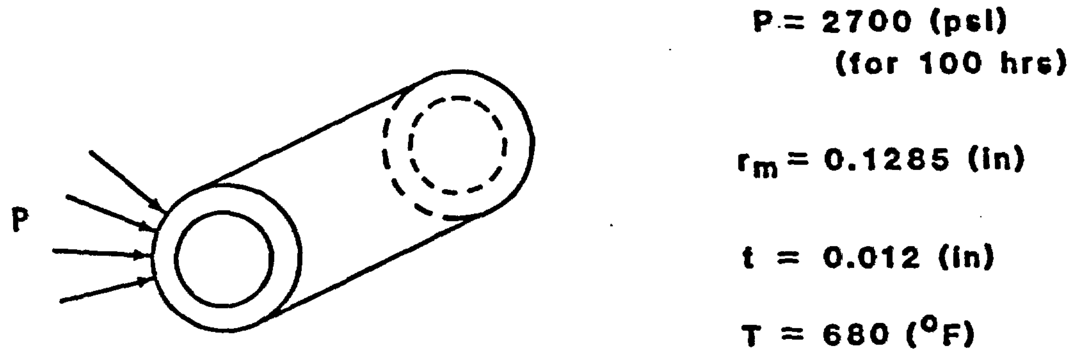

Figure 3.8-1

Finite Length Hollow cylinder Subjected to External Pressure Loading

Analytical Solution. Griffin (GR-67) has proposed a simplified theory of creep collapse which is analogous to instantaneous elastic-inelastic creep collapse. It uses isochronous stress strain curves instead of instantaneous stress strain curves. The isochronous stress-strain curves give the stress as a function of strain after having the load applied for a fixed time.

The collapse is predicted using

$$\sigma_\theta = -pr/t \tag{138}$$

$$\sigma_x = -\frac{pr}{2t} \tag{139}$$

$$\tau_{x\theta} = 0 \tag{140}$$

The von Mises stress intensity for these stress components is

$$\sigma_i = \frac{\sqrt{3}}{2}\,\frac{pr}{t} \tag{141}$$

The critical or buckling stress is calculated from

$$\sigma_\theta\big|_b = \frac{\eta E_s\, t^2}{4(1-\nu^2)\, r^2} \tag{142}$$

$$\eta = 1 - \frac{(1 - E_t/E_s)}{1 + (1-4\nu^2)\ Et/3E_s} \qquad (143)$$

where

η = correction factor which takes into account nonlinear nature of the isochronous stress-strain curve [ ]

E_t = tangent of the isochronous stress-strain curve at the point describing the state of stress σ_i [psi]

E_s = ratio of stress to strain at the point describing the state of stress σ_i [psi]

ν = Poisson's ratio of the material [ ]

t = cylinder radial wall thickness [in]

r = mean radius of the cylinder wall [in]

$\sigma_\theta\big|_b$ = value of hoop stress at which buckling is predicted to occur [psi]

In Equations 142 and 143, the moduli E_t and E_s correspond to a state of stress as represented by the von Mises stress intensity given by Equation 141.

Figure 3.8-2 gives the generalized stress versus strain curve for various values of the Larson-Miller parameter (LMP) given by

$$LMP = (T + 460)\ (20 + \log_{10} \tau) \qquad (144)$$

where

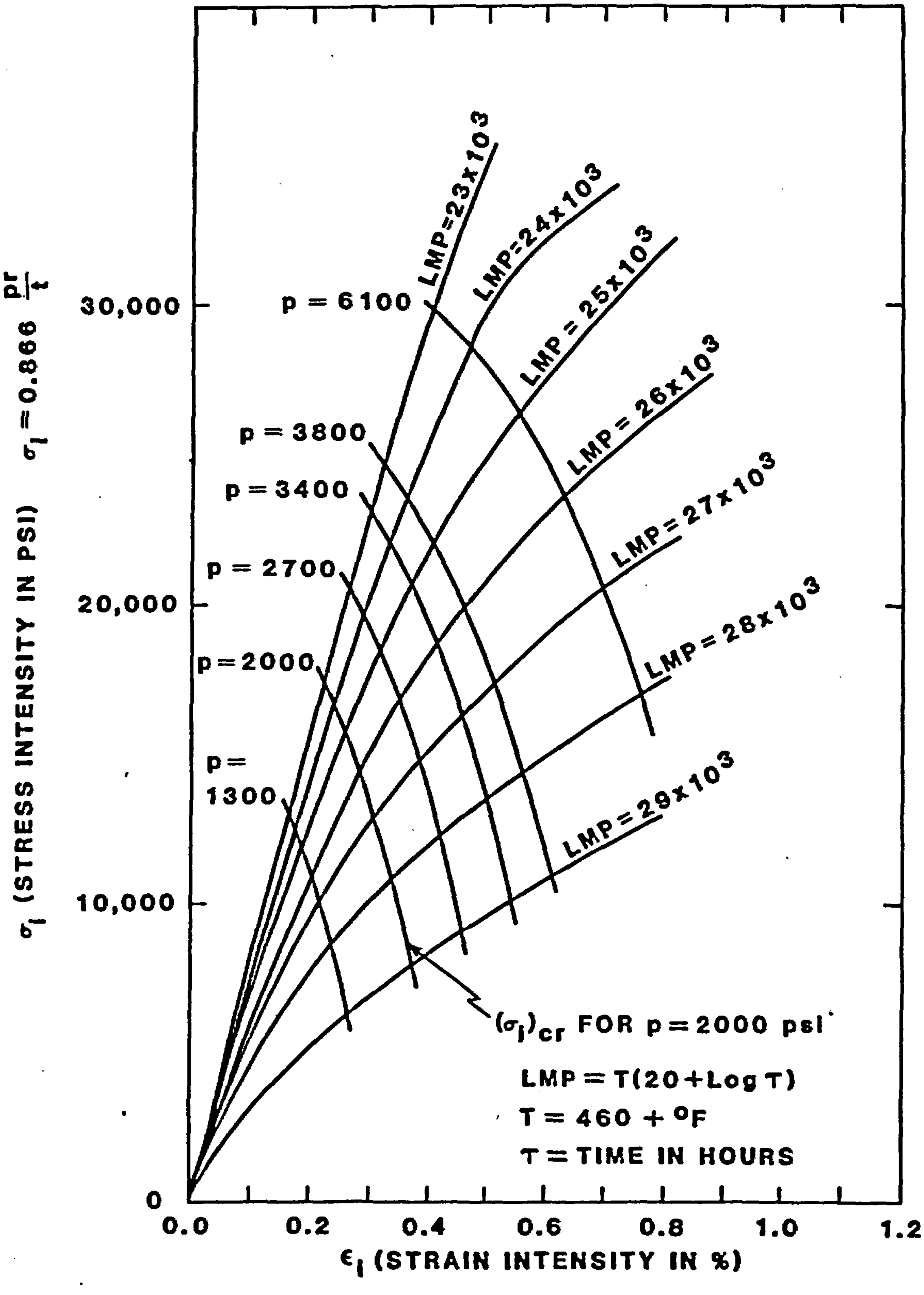

Figure 3.8-2

Iso-LMP Stress-Strain Curves for 15% Cold Worked Zircaloy in the 550 to 750°F Temperature Range

T = temperature of material [^{o}F]

= duration of loading [hrs]

LMP = combined time and temperature parameter used in correlating creep strain effects [ ]

These curves shown in Figure 3.8-2 are used as isochronous stress-strain curves.

Assumptions. In the analysis, the cylinder is assumed to have an initial ovality which is typical of the tolerance on roundness as described by diametral dimensions:

$$U = U_0 \cos 2\theta$$

Input Specifications. For 15% cold-worked Zircaloy tubing material, the following conditions define the geometry of the cylinder, its loading and the atmospheric conditions:

p = external pressure = 2700 (psi)

T = material temperature = 680 (^{o}F)

t = cylinder wall thickness = 0.013 (in)

U_0 = initial ovality = .0005

r = cylinder mean radius = 0.1285 (in)

LMP = Larson-Miller parameter (from Equation 144) = 23,940 ( )

L = tube length = 144 (in)

ν = Poisson's ratio = 0.25 ( )

E_t = tangent modulus (see Figure 3.8-2 for values) [psi]

E_s = secant modulus (see Figure 3.8-2 for values) [psi]]

Griffin (Reference GR-67) has analyzed this case using Equations 142 and 143 along with Figure 3.8-2. Collapse in less than 10 hours was predicted.

He also reports limited test data in which collapse occurred before the first observation, which was made after 72 hours of loading.

Output Specifications. The output indicates whether substantial magnification of ovality approaching the equivalent of collapse is predicted with the COVE program to have occurred within 10 hours. If it is predicted, this would be an indication that COVE is likely to be conservative.

Collapse often depends on individual properties of specimens and loading conditions beyond those described by average properties. Analytical prediction methods are generally not very precise.

3.9 Hypothetical Prediction of Deformation Including Progressive Creep for a Waste Package

Problem Statement. The waste package must function for a very long time. External loads due to groundwater pressure or rock forces could act during most or all of the waste package service life. The cumulative effects of these loads of long duration are much greater than the effects of shorter duration. Therefore, creep strain must be considered because its contribution to total strain may be much greater than the instantaneous strain. Creep strain causes additional ductility to be consumed which must be accounted for in the structural integrity assessment.

This problem considers a long cylindrical overpack reinforcement as shown in Figure 3.9-1. The waste package is proportioned so that the reinforcement is relied on to resist the entire external load.

Objectives. The objectives of this analysis are

- To demonstrate a method for estimating creep strain in a waste package structure
- To estimate the creep strains for a particular waste package

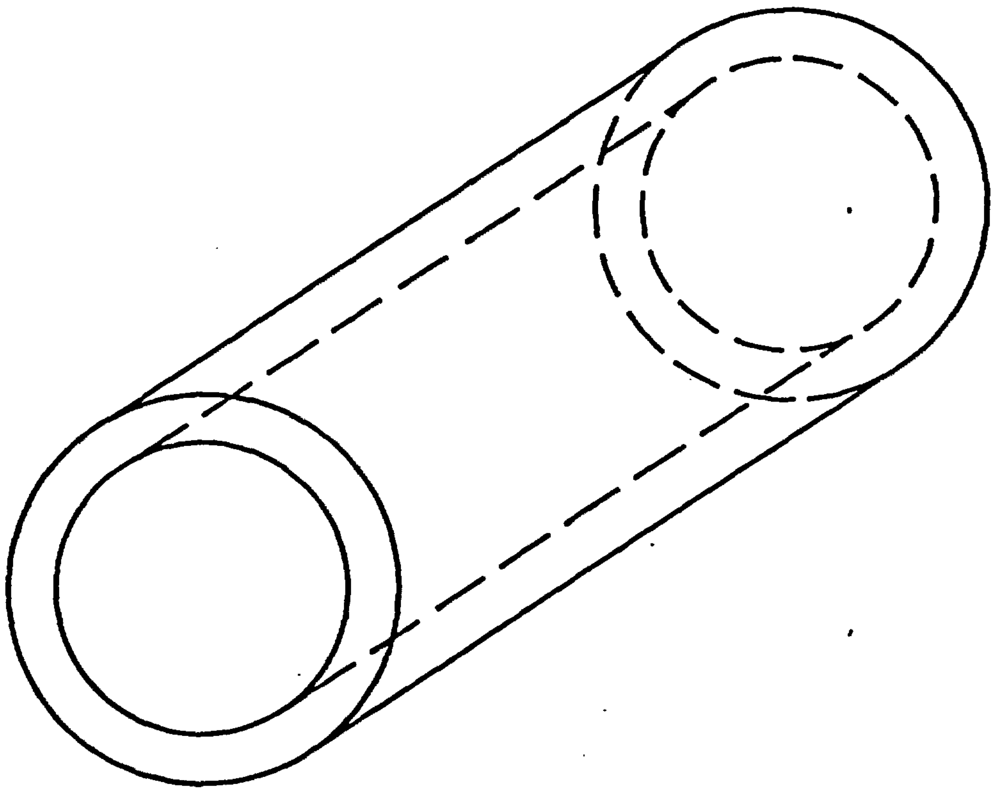

Figure 3.9-1

Hollow Cylindrical Overpack Reinforcement Structure for a Waste Package for Carrying External Pressure Loading

Analytical Solution. This is a hypothetical problem. An analytical solution will not be presented for comparison with the computer program solution.

Assumptions. In posing the problem, it is assumed that the overpack reinforcement carries all of the externally applied structural load. This is consistent with the assumptions made during the conceptual design process for waste packages to be emplaced in tuff.

It will be assumed that the carbon steel maintains a secondary creep rate during the entire loading duration.

Input Specifications. The configuration for the waste package (Reference ON-83, p. 15) is:

$D_O = 55$ (cm)

$t = 2.5$ (cm)

$\ell = 4.1$ (m)

The loading is a uniform external pressure on the cylinder

$p = 2250$ (psi)

t = duration of loading = 1,000 (years)

$T = 400$ (^oC)

The creep rate is taken to be of the form

$$\varepsilon^c \frac{d\varepsilon^c}{dt} = k\sigma^n \tag{145}$$

where

$k = 48 \times 10^{-38}$ [1/hr]

$n = 6.9$ [ ]

giving a creep strain rate of

$$\dot{\varepsilon}^c = 9.93 \times 10^{-7} \left[\frac{1}{hr}\right]$$

for the stress of

$$\sigma = \frac{pr}{t} = 2250\ (55/2)\ (1/2.5)$$

$$\sigma = 24{,}750\ [psi]$$

The overpack and overpack reinforcement are fabricated from carbon steel. The material properties are

E = elastic modulus = 27.4×10^6 (psi)

ν = Poisson's ratio = 0.30 ( )

Output Specifications. The solution compares the creep strain and the ratio of total strain to instantaneous strain and the ratio of creep strain to instantaneous strain after several loading intervals such as 10, 100, 300, and 1,000 years.

3.10 Hypothetical Calculation of Stress Resulting from a Steady-State Temperature Distribution in a Waste Package

Problem Statement. This problem is designed to determine the hoop stress component distribution in a series of n concentric hollow cylinders (annular sections). The stress distribution is the result of a radial temperature distribution in the hollow cylinders.

The n concentric hollow cylinders (annular sections) surround a solid cylinder acted on by a spatially uniform heat generation representative of the waste acts. The concentric hollow cylinders each have a predetermined temperature distribution. This results from the solution of Problem 2.5. The purpose of this problem is to impose those temperatures along with sufficient mechanical properties so the state of stress can be determined at the inside and outside radius of each of the annuli. The concentric cylinders are shown in Figure 3.10-1.

Objectives. This problem is useful in representing a waste package region such as a thick self-shielding canister. The annular regions are arbitrarily defined in that they are subregions of a larger continuous wall of the canister. Because different physical properties are present in the different regions, it is not convenient to obtain an analytical solution. Solution comparisons between WAPPA and ANSYS are intended.

Analytical Solution. This problem does not have an analytical solution that can be readily obtained (without the linear equations solution capabilities of structural programs). Modeling will be done on as nearly an equivalent basis as possible with the WAPPA and ANSYS programs, and the resulting solution in terms of stress values will be compared.

Assumptions. It is assumed that the mechanical properties are uniform and constant in each region.

Input Specifications (see Reference ON-83). The radial temperature distribution will be as determined in the solution to Problem 2.5.

- Geometry (See Figure 3.10-1)
  - radii

    $r_o^7 = 65$ (cm)

    $r_o^6 = r_i^7 = 60$ (cm)

    $r_o^5 = r_i^6 = 55$ (cm)

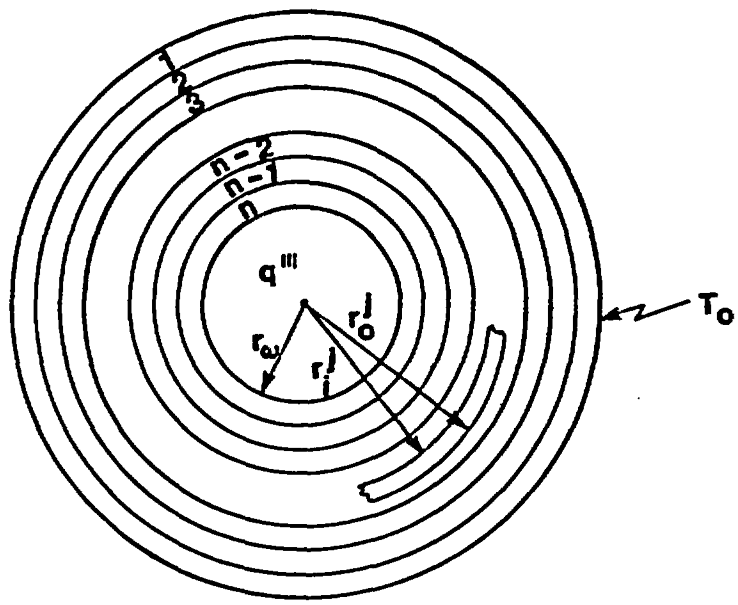

Figure 3.10-1

n Concentric Cylindrical Annuli with Known Outside Temperature T_O, Surrounding a Waste Region of Radius r_W in Which a Known Volumetric Heat Generation Rate q''' Exists. Each Region Can Have Its Unique Set of Mechanical Properties

$r_o^4 = r_i^5 = 50$ (cm)

$r_o^3 = r_i^4 = 45$ (cm)

$r_o^2 = r_i^3 = 40$ (cm)

$r_o^1 = r_i^2 = 35$ (cm)

$r_i^1 = r_o^w = 30.5$ (cm)

$r_i^w = 0$

Material Properties.

- Elastic modulus

  $E^7 = 27.4 \times 10^6$ (psi)

  $E^6 = 27.0 \times 10^6$ (psi)

  $E^5 = 26.6 \times 10^6$ (psi)

  $E^4 = 26.2 \times 10^6$ (psi)

  $E^3 = 25.8 \times 10^6$ (psi)

  $E^2 = 25.4 \times 10^6$ (psi)

  $E^1 = 25.0 \times 10^6$ (psi)

  $E^w = 10.0 \times 10^6$ (psi)

- Poisson's ratio

  $\nu^7 = 0.30$

  $\nu^6 = 0.30$

  $\nu^5 = 0.30$

  $\nu^4 = 0.30$

  $\nu^3 = 0.30$

  $\nu^2 = 0.30$

  $\nu^1 = 0.30$

  $\nu^w = 0.20$

- Temperature coefficient of thermal expansion

  $\alpha^7 = 6.52 \times 10^{-6}$ (1/°F)

  $\alpha^6 = 6.55 \times 10^{-6}$ (1/°F)

  $\alpha^5 = 6.58 \times 10^{-6}$ (1/°F)

  $\alpha^4 = 6.61 \times 10^{-6}$ (1/°F)

  $\alpha^3 = 6.64 \times 10^{-6}$ (1/°F)

  $\alpha^2 = 6.67 \times 10^{-6}$ (1/°F)

  $\alpha^1 = 6.70 \times 10^{-6}$ (1/°F)

  $\alpha^W = 6.78 \times 10^{-6}$ (1/°F)

Output Specifications. The output will be the stresses at the inside and outside radii of each of the annular sections which make up the waste package.

3.11 Hypothetical Analyses of Canister Stresses Subsequent to Being Filled with a Hot Glass Waste Form

Problem Statement. Some thermal conditions produce large internal forces and moments and hence stress values because different portions of the structure are at different temperatures. Since these different portions of the structure are connected, they constrain each other from the independent, free expansion necessary to receive internal forces, moments, and thermal stresses. The performance assessment of canisters into which molten glass waste forms are poured should be analyzed to determine the stress values resulting from the temperature distribution which exists at various times subsequent to filling. The temperature distributions are determined in Problem 2.7. Figure 3.11-1 shows the canister before filling.

Objectives. The objective of this problem is to solve for the structural response caused by severe temperature gradients in a canister. The

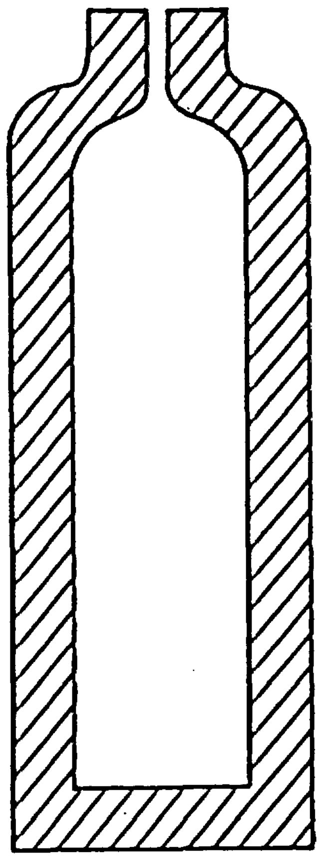

Figure 3.11-1

Canister into Which Molten Glass Waste Is Poured quantities of interest will be the stress values throughout the structure. The known temperature distributions at various times in the transient will be the loading conditions.

Analytical Solution. This is a hypothetical problem. A computer program model will be developed and structural response simulated. It is anticipated that the ANSYS computer program will be used. An independent analytical solution will not be determined.

Assumptions. It is assumed that the molten waste form is poured instantaneously into the canister at time zero.

Input Specifications. The structural analysis will be for the configuration and heat transfer conditions given in Table 3.11-1. The mechanical properties (in English units) as a function of temperature for 304 stainless steel are

T (^oF)	E (MPa)	ν (-)	G (10^6 psi)	λ (10^6 psi)	K (10^6 psi)	α ($10^6/^oF$)
70	28.3	.29	10.97	15.15	22.46	9.11
100	-					9.16
150	-					9.25
200	27.7					9.34
250	-					9.41
300	27.1					9.47
350	-					9.53
400	26.6					9.59
450	-					9.65
500	26.1					9.70
550	-					9.76
600	25.4					9.82
650	-					9.87
700	24.8					9.93
750	-					9.99
800	24.1					10.05

Legend

E - Elastic Modulus
ν - Poisson's Ratio
G - Shear Modulus (Lame's Constant μ)
λ - Lame's Constant
K - Bulk Modulus
α - Mean Coefficient of Thermal Expansion from
70^oF to the Indicated Temperature

Table 3.11-1

In Development

Similarly, the glass mechanical properties (in metric units) are:

T (^{o}C)	E (MPa)	ν (-)	G (MPa)	λ (MPa)	K (MPa)	α ($10^{-6}/^{o}C$)
25	6.9×10^4	0.20	2.9×10^4	1.9×10^4	3.8×10^4	10.0

Legend

E - Elastic Modulus
ν - Poisson's Ratio
G - Shear Modulus (Lame's Constant μ)
λ - Lame's Constant
K - Bulk Modulus
α - Coefficient of Thermal Expansion

Output Specifications. Generalized stress intensity values will be monitored at various node locations throughout the canister wall thickness and examined for reasonableness.

3.12 Hypothetical Calculation of Stress Due to Uniform External Pressures on a Waste Package

Problem Statement. A waste package structure is loaded by uniform external pressure. Only instantaneous structural response to the loading is to be considered. Material deformation is in the elastic range. The loading is substantial but not large enough to cause instantaneous plastic deformation.

A sketch of the structure is shown in Figure 3.12-1. The inside and outside radius of the structure's cylindrical annulus cross section are denoted by r_i and r_o. Intermediate positions are denoted by r_a, r_b, and r_c as shown in Figure 3.12-1.

Objectives. The objectives of this problem are to compare structural responses predicted by WAPPA to those obtained from a finite element program. The ANSYS finite element program will be used to generate

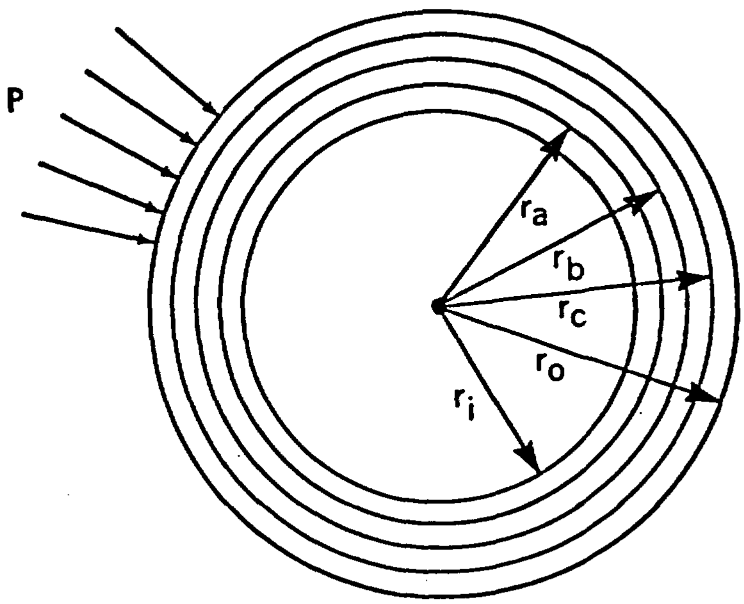

Figure 3.12-1

Waste Package Structure with Uniform External Pressure Loading comparative responses. Stress components in the tangential direction at various radial positions will be the principal quantity of interest.

<u>Analytical Solution</u>. This is a hypothetical problem in which WAPPA and ANSYS are to be compared. The thick-walled cylinder solution for the stress component in the circumferential direction as a function of radial position, inside and outside radius, and external pressure can readily be used to obtain an additional check. The tangential stress component is given by

$$\sigma_t = - \frac{p_o \, r_o^2}{r_o^2 - r_i^2} \left(1 + \frac{r_i^2}{r^2}\right) \tag{146}$$

where

p_o = uniform external pressure acting at radius r_o $[f/\ell^2]$

r_o = outside radius $[\ell]$

r_i = inside radius $[\ell]$

r = particular position of interest in the range $r_i \leq r \leq r_o$ $[\ell]$

σ_t = tangential stress quantity at radius r $[f/\ell^2]$

<u>Assumptions</u>. It is assumed that pressure is not applied to the ends of the cylinder.

<u>Input Specifications</u>. A static pressure loading of 5 MPa will be applied to the following carbon steel overpack structure:

Outside radius = r_o = 32.25 (cm)

Inside radius = r_i = 29.75 (cm)

The intermediate radial positions are at:

r_a = 30.375 (cm)
r_b = 31.000 (cm)
r_c = 31.625 (cm)

Output Specifications. The tangential stress component at radii r_i, r_a, r_b, r_c, and r_o are to be evaluated. Using Equation 146 for the given pressure loading and annular dimensions, the tangential stress component is predicted to be:

	r (cm)	σ_t (MPa)
$r = r_i$	29.75	-67.1
$r = r_a$	30.375	-65.7
$r = r_b$	31.0	-64.4
$r = r_c$	31.625	-63.2
$r = r_o$	32.25	-62.1

4.0 RADIATION SHIELDING PROBLEMS

This section deals with the shielding of neutrons and gamma rays within the waste form and the surrounding waste canister. It contains five problems:

- A simple problem to allow comparison of the "buildup factor" method with more sophisticated transport theory shielding codes
- Measured radiation fields around a PWR fuel assembly in air and water
- Measured radiation levels around a BWR fuel assembly in air and water
- A hypothetical shielding problem for a thick-walled waste package
- A hypothetical shielding problem for a thin-walled waste package

These problems can be used to aid in verifying and validating radiation shielding codes.

4.1 Hypothetical Radiation Shielding Problem

Problem Statement. The problem requires the estimation of the gamma flux and dose at the outer surface of a concrete drum containing a 1 MeV gamma source. Three subproblems are presented: no external shield, a 5 cm steel shield, and a 25 cm steel shield. This is a relatively simple problem that can be solved analytically by the buildup factor method.

Objectives. The purpose of this problem is to compare the predictive capabilities of a simple analytical shielding calculation and a transport theory computer code calculation.

Physical Description. A long concrete cylinder contains a uniformly dispersed 1 MeV gamma emitter with a source strength of 10^7 disintegrations per cubic centimeter per second. The cylinder is 0.60 m in diameter and, for purposes of the analysis, is assumed to be infinitely long. The gamma flux and dose rate are to be calculated for a bare cylinder and for cylinders with 5 cm and 25 cm annular steel shields.

Analytical Solution. This problem can be solved analytically using methods described in Reference RO-56. This method assumes that the shield is a slab. This is a good approximation for the 5 cm thick shield but may be a poor assumption for the 25 cm shield.

For an infinite length cylindrical source, the gamma flux, ϕ , at an exterior point is given by:

$$\phi = \frac{BS_v R_o^2}{2(a+z)} F\left(\frac{\pi}{2}, b_2\right) \tag{147}$$

where:

ϕ = gamma flux, photons/cm^2·sec

B = buildup factor, dimensionless

S_v = volumetric photon source, photons/cm^3·sec

R_o = radius of cylinder, cm

a = distance from cylinder surface to measurement point, cm

z = effective source self-attenuation distance, cm

$(F \frac{\pi}{2}, b_2) = \int_0^{\pi/2} e^{-b_2 \sec\theta} d\theta$, Sieverts integral or secant integral, dimensionless

The buildup factor, B, is defined as the rate of the actual gamma flux compared to that calculated using exponential attenuation with the linear attenuation coefficient. Table 4.1-1 gives dose buildup factors and attenuation coefficients for 1 MeV gamma photons in selected materials.

The effective source self-attenuation distance can be calculated using figures in Reference RO-56. The calculated values of z as a function of shield thickness are given below:

Shield Thickness, cm	Self-Attenuation Factor (cm)
0	25.8
5	26.4
25	23.5

Buildup factors in concrete and iron calculated using values from Table 4.1-1 are given in Table 4.1-2. The total number of relaxation lengths (b_2) can be calculated from the equation:

$$b_2 = \mu_c z + \mu_1 t$$

where:

μ_c = the gamma absorption coefficient for concrete

μ_1 = the gamma absorption coefficient for iron

t = the thickness of the iron shield

Calculated values of b_2 are given below:

t	b_2
0	3.85
5	6.28
25	15.20

The calculated values of b_2 are used to determine $F(\pi/2, b_2)$ from figures in Reference RO-56.

Table 4.1-1

Dose Buildup Factors and Attenuation Coefficients
for 1 MeV Gamma Rays

	Constant					
Material	A_1	α_1	α_2	μ_t	μ_e	ρ
Air	--	--	--	.0000822	.0000362	.001293
Water	13.5	-.100	.01	.0706	.0311	1.00
Iron	8.0	-.0895	.04	.4677	.2051	7.85
Concrete	10.0	-.088	.029	.1492	.0653	2.35

$$B(\mu_t x) = A_1 \exp(-\alpha_1 x) + (1-A_1)\exp(-\alpha_2 x)$$

$$\text{Dose} = E\phi(E)\mu_e/\rho \quad \text{MeV/cm}^3\cdot\text{sec}$$

$$= 5.767 \times 10^{-5}\, E\phi(E)\mu_e/\rho \ \text{Rad/hr}^{*}$$

$$^{*}\ 5.767 \times 10^{-5} = \frac{1.602 \times 10^{-6}\ \text{erg}}{\text{MeV}} \cdot \frac{1\ \text{Rad}}{100\ \text{erg/g}} \cdot \frac{1}{\rho\ \text{g/cm}^3} \cdot \frac{3600\text{g}}{\text{hr}}$$

Source: AN-63

Table 4.1-2

Calculated Buildup Factors

No Shield

Concrete

$$B_C = 10 \exp(.088 \cdot .1492 \cdot 25.8) - 9 \exp(-.029 \cdot .1492 \cdot 25.8)$$
$$= 6.1$$

Iron

$$B_I = 8 \exp(.0895 \cdot .4677 \cdot 0) - 7 \exp(-.04 \cdot .4677 \cdot 0)$$
$$= 1$$

$$B_{system} = B_C \cdot B_I$$
$$= 6.1$$

5 cm Shield

Concrete

$$B_C = 10 \exp(.088 \cdot .1492 \cdot 26.4) - 9 \exp(-.029 \cdot .1492 \cdot 26.4)$$
$$= 6.1$$

Iron

$$B_I = 8 \exp(.0895 \cdot .4677 \cdot 5) - 7 \exp(-.04 \cdot .4677 \cdot 5)$$
$$= 3.5$$

$$B_{system} = B_C \cdot B_I$$
$$= 6.1 \cdot 3.5$$
$$= 21.4$$

25 cm Shield

Concrete

$$B_C = 10 \exp(.088 \cdot .1492 \cdot 23.5) - 9 \exp(-.029 \cdot .1492 \cdot 23.5)$$
$$= 5.6$$

Iron

$$B_I = 8 \exp(.0895 \cdot .4677 \cdot 25) - 7 \exp(-.04 \cdot .4677 \cdot 25)$$
$$= 18.0$$

$$B_{system} = B_C \cdot B_I$$
$$= 5.6 \cdot 18$$
$$= 101.4$$

Table 4.1-2

Calculated Buildup Factors

No Shield

Concrete

$$B_C = 10 \exp(.088 \cdot .1492 \cdot 25.8) - 9 \exp(-.029 \cdot .1492 \cdot 25.8)$$
$$= 6.1$$

Iron

$$B_I = 8 \exp(.0895 \cdot .4677 \cdot 0) - 7(-.04 \cdot .4677 \cdot 0)$$
$$= 1$$

$$B_{system} = B_C \cdot B_I$$
$$= 6.1$$

5 cm Shield

Concrete

$$B_C = 10 \exp(.088 \cdot .1492 \cdot 26.4) - 9 \exp(-.029 \cdot .1492 \cdot 26.4)$$
$$= 6.1$$

Iron

$$B_I = 8 \exp(.0895 \cdot .4677 \cdot 5) - 7 \exp(-.04 \cdot .4677 \cdot 5)$$
$$= 3.5$$

$$B_{system} = B_C \cdot B_I$$
$$= 6.1 \cdot 3.5$$
$$= 21.4$$

25 cm Shield

Concrete

$$B_C = 10 \exp(.088 \cdot .1492 \cdot 23.5) - 9 \exp(-.029 \cdot .1492 \cdot 23.5)$$
$$= 5.6$$

Iron

$$B_I = 8 \exp(.0895 \cdot .4677 \cdot 25) - 7 \exp(-.04 \cdot .4677 \cdot 25)$$
$$= 18.0$$

$$B_{system} = B_C \cdot B_I$$
$$= 5.6 \cdot 18$$
$$= 101.4$$

Shield Thickness, t	Sieverts Integral $F(\pi/2, b_2)$
0	1.2×10^{-2}
5	7.5×10^{-4}
25	7.5×10^{-8}

Substituting these values into the equation for the flux and dose at the center surface, the following are obtained:

Shield Thickness, t	Gamma Flux, ϕ gammas/cm^3·sec	Outer Surface Dose Rate Rad/hr
0	1.28E7	2.29E1
5	2.30E6	4.13E0
25	7.06E2	1.27E-3

Assumptions. The concrete isotopic content in Table 4.1-3 should be used to estimate the gamma flux using a transport theory code.

Output Specifications. The outputs for this problem are the gamma photon flux and the dose rate at the outer shield surface.

Comments. The results given here should be compared with the results from a one-dimensional transport theory calculation and the shielding factor method employed in the codes BARIER and WAPPA. For the 0 cm and 5 cm shields, good agreement ($\sim$20%) between the results given here and code predictions can be expected. For the 25 cm shield, the results predicted in this report may vary from predictions derived from a transport theory code because of the difficulty in calculating attenuation in thick shields using the shielding factor method.

4.2 Pressurized Water Reactor Fuel Assembly Radiation Levels

Problem Statement. This problem presents the results of in-plant test measurements of the radiation field in air and water around a Pressurized Water Reactor (PWR) fuel assembly from Point Beach Unit 2. The problem is based on measurements taken at General Electric's Morris Operation.

Table 4.1-3

Elemental Content of Type 04 Cement*

Isotope	Content (g/cm^3)
H	0.014
O (in H_2O)	0.111
O (in dry mix)	1.062
Mg	0.006
Al	0.107
Si	0.737
K	0.045
Ca	0.194
Fe	0.029
Na	0.040
Density - g/cm^3	2.35

Source: AN-63, p. 660. Na content corrected from 0.400 to 0.040. Water content increased slightly (H from 0.013 to 0.014, O from 0.103 to 0.111) to agree with density of 2.35 g/cm^3.

Objectives. This problem will provide a basis for comparing the radiation field calculated using a source term code and a shielding code with measured experimental data.

Physical Description. Point Beach Unit 2 uses Westinghouse 14x14 fuel assemblies. The fuel was irradiated from August 1972 to March 1977. After discharge from the reactor and cooling, the fuel was shipped to General Electric's Morris Operation for interim storage. As part of an engineering and test support contract funded by the Department of Energy, selected fuel assemblies were characterized. Gamma exposure rates near spent fuel assemblies were measured four years after discharge of the fuel from the reactor.

Fuel assembly design characteristics are given in Table 4.2-1. The initial non-actinide composition of uranium oxide fuel pellets is given in Table 4.2-2. The weight of fuel assembly structural materials is presented in Table 4.2-3, and the elemental composition of structural material is given in Table 4.2-4. Fuel assembly operating conditions are summarized in Table 4.2-5.

The concentrations of fuel assembly structural material located in the end fitting zone should be multiplied by 0.011 to account for the lower activation levels near the ends of the fuel assembly due to flux levels lower than those in the active fuel zone. In addition, the concentrations of manganese, cobalt, and zirconium in the end fitting zone should be multiplied by factors of 0.80, 0.67, and 0.40, respectively. These corrections account for the difference between the neutron energy spectrum in that zone and the spectrum in the active fuel zone. Both kinds of corrections are based on axial spectrum calculations for a Westinghouse PWR fuel assembly as reported in Reference CR-78. With these corrections, the ORIGEN-S calculations should more accurately predict the nuclide activities from the structural materials.

Reference JU-81 gives the results of experimental measurement of gamma dose rate and calculations using the shielding factor code QAD. These

Table 4.2-1
Fuel Design Data for Point Beach 2

Percent theoretical density[a]		91.8
Initial uranium composition (wt. %)	^{234}U	0.027
	^{235}U	3.400
	^{238}U	96.573
Initial uranium loading (kg/assembly)		
Fuel rods per assembly	179 with Zircaloy-4	clad
Rod pitch (cm)		1.41224
Pellet O.D. (cm)		0.92685
Clad I.D. (cm)		0.94844
Clad O.D. (cm)		1.07188
Nominal Envelope (cm)		19.718 19.718
Plenum Length (cm)		16.982
Active Fuel Length (cm)		365.76
Fuel Temperature (°K)		1200
Clad Temperature (°K)		605
Moderator Temperature (°K)		583
Moderator Density (g cm^{-3})		0.706575
VF for Moderator[b]		0.707850
Average boron concentration (wt. ppm)		550

[a] Theoretical UO_2 density is 10.96 g cm^{-3}.

[b] VF is a SAS2 parameter related to volume fraction and/or percent theoretical density (see Reference OR-82).

Table 4.2-2

Typical Non-actinide (Impurity) Composition of LWR Oxide Fuels

Element	Atomic Number	Concentration (ppm)[a]	Element	Atomic Number	Concentration (ppm)[a]
Li	3	1.0	Mn	25	1.7
B	5	1.0	Fe	26	18.0
C	6	89.4	Co	27	1.0
N	7	25.0	Ni	28	24.0
O	8	134,454.0	Cu	29	1.0
F	9	10.7	Zn	30	40.3
Na	11	15.0	Mo	42	10.0
Mg	12	2.0	Ag	47	0.1
Al	13	16.7	Cd	48	25.0
Si	14	12.1	In	49	2.0
P	15	35.0	Sn	50	4.0
Cl	17	5.3	Gd	64	2.5
Ca	20	2.0	W	74	2.0
Ti	22	1.0	Pb	82	1.0
V	23	3.0	Bi	83	0.4
Cr	24	4.0			

Source: MI-83

[a] Parts of element per million parts of heavy metal.

Table 4.2-3

Typical PWR Fuel Assembly Structural Material Mass Distribution

	Material	Mass kg/MTHM	Mass kg/Assembly
Fuel Zone			
Cladding	Zircaloy-4	223.0	102.9
Grid spacers	Inconel-718	12.8	5.9
Grid-spacer springs	Inconel-718		
Grid-brazing material	Nicrobraze 50	2.6	1.2
Miscellaneous	SS 304[a]	9.9	4.6
Fuel-Gas Plenum Zone			
Cladding	Zircaloy-4	12.0	5.5
Plenum spring	SS 302	4.2	1.9
End Fitting Zone			
Top end fitting	SS 304	14.8	6.8
Bottom end fitting	SS 304	12.4	5.7
TOTAL		291.7	134.5

Source: MI-83

[a] Distribution throughout the PWR core in sleeves and so forth.

Table 4.2-4

Typical Elemental Compositions of LWR Fuel Assembly Structural Materials

Element	Atomic Number	Structural Material Composition (Grams per Metric Ton of Metal)				
		Zircaloy-4	Inconel-718	Stainless Steel 302	Stainless Steel 304	Nicrobraze 50
H	1	13	0	0	0	0
B	5	0.33	0	0	0	50
C	6	120	400	1,500	800	100
N	7	80	1,300	1,300	1,300	66
O	8	950	0	0	0	43
Al	13	24	5,992	0	0	100
Si	14	0	1,997	10,000	10,000	511
P	15	0	0	450	450	103,244
S	16	35	70	300	300	100
Ti	22	20	7,990	0	0	100
V	23	20	0	0	0	0
Cr	24	1,250	189,753	180,000	190,000	149,709
Mn[a]	25	20	1,997	20,000	20,000	100
Fe	26	2,250	179,766	697,740	688,440	471
Co[a]	27	10	4,694	800	800	381
Ni	28	20	519,625	89,200	89,200	744,438
Cu	29	20	999	0	0	0
Zr[a]	40	979,110	0	0	0	100
Nb	41	0	55,458	0	0	0
Mo	42	0	29,961	0	0	0
Cd	48	0.25	0	0	0	0
Sn	50	16,000	0	0	0	0
Hf	72	78	0	0	0	0
W	74	20	20	0	0	100
U	92	0.2	0	0	0	0
Density, grams/cm^3	-	6.56	8.19	8.02	8.02	-

Source: MI-83

[a] Value used in source term calculations should be less than this (actual) value if the materials are not in the active fuel zone.

Table 4.2-5

Fuel Assembly Operating Conditions

Operating Period	Days	Average Power MW/MT
1*	210	6
2		
3		0
4		
5		0
6		
7		0

In Development

* After initial startup, the plant operated at 20% power for seven months due to operating license restrictions.

Source:

results are given for measurements taken at several axial locations for the X-Y detector location given in Table 4.2-6. Table 4.2-7 gives the calculated intensities for the gamma radiation source in spent fuel from Reference JU-81.

Table 4.2-8 gives the measured gamma exposure rates at the fuel assembly mid-point along the "B1" profile for three fuel assemblies that were believed to have similar irradiation histories. In addition to measured exposures at each corner, Table 4.2-8 provides an indication of the anisotropy of gamma exposure. For individual fuel assemblies, the measured gamma exposure varied by as much as ±8%. (In calculating the gamma intensity around a fuel assembly, it is commonly assumed that the fuel burnup and therefore the gamma source is evenly distributed.)

Results of additional measurements made along the B1 profile at 1 ft intervals are given in Table 4.2-9. These measurements provide an estimate of the standard error of the exposure rate measurement of about ±4% (one sigma).

Table 4.2-10 gives results of calculated and measured exposure rates in air and water for three detector profiles.

Reference JU-81 includes a discussion of the accuracy and precision of measured results. Based on an analysis of all identified sources of random errors, the overall variability of measurement is estimated to be 3.8%. This reference also states that based on measurements performed by GE, a variance of ±3% (one sigma) between utility-calculated fuel exposures and true exposures may exist. This agrees with generally held beliefs about the accuracy of these calculations and is consistent with IAEA guidelines established for safeguards purposes.

Assumptions. Analyses may be performed using the following assumptions:

- The entire fuel assembly (except end fittings) is a homogeneous mass.
- The two outer rows of fuel rods are modeled discretely; the remaining rods are a homogeneous mass.

Table 4.2-6

Gamma Detector Locations

Detector	X-Y Location*	
	X	Y
A-1	1.6	+ 1.6
B-1	7.0	+ 7.0
E-1	- 3.9	+10
T-1**	- 3.9	- 3.9

* The origin is the corner of the fuel assembly envelope at the top of the active length of the fuel.

** This detector is located above the fuel assembly.

Table 4.2-7

Calculated Gamma Intensities for Gamma Radiation Sources in Spent Fuel

Upper Energy Range	Gamma $MeV/cm^3 \cdot sec$
0.55	1.75E9
0.85	4.28E10
1.25	3.89E9
1.75	8.87E8
2.25	1.62E7
2.65	1.57E8
3.00	3.48E6
4.00	6.70E5
5.00	2.27E2
6.00	5.52E1

Source: JU-81

Table 4.2-8

Exposure Rates from Fuel Assemblies

Fuel Assembly Identification	Exposure Rate (KR/hr) at Fuel Assembly Midpoint along B1 Profile in Water — Edge Measured: N	E	S	W	Average	Figure of Anisotropy 100 (Max-Min)/Max
C56	30.0	32.0	32.1	31.7	31.5	6.5
C64	32.0	29.8	28.0	29.0	29.7	12.5
C67	28.0	30.5	31.0	31.5	30.3	11.1

Source: JU-81

Table 4.2-9

Exposure Rate from Repeated Fuel Assembly Measurements

Fuel Assembly I.D.	Profile	Z* Location Feet-Inches	Number of Independent Measurements	Exposure Rate KR/hr (Mean Standard Deviation)	Measurement Error (%)
C56	B1	0-3	4	6.95 (0.36)	5.2
		0+9	4	21.26 (0.62)	2.9
		1+9	4	26.00 (0.94)	3.6
		2+9	4	27.60 (1.08)	3.9
		3+9	4	28.74 (0.96)	3.3
		4+9	4	29.50 (1.00)	3.4
		5+9	4	30.54 (1.32)	4.3
C64	B1	0-3	2	6.73	-
		0+9	2	20.8	-
		1+9	2	25.7	-
		2+9	2	26.6	-
		3+9	2	28.	-
		4+9	2	28.8	-
		5+9	2	28.8	-
C67	B1	0-3	1	6.7	-
		0+9	1	21.0	-
		1+9	1	26.0	-
		2+9	1	28.0	-
		3+9	1	29.0	-
		4+9	1	30.0	-
		5+9	1	30.5	-

* Distance from the top of the active fuel height.

Source: JU-81

Table 4.2-10

Calculated and Measured Exposure Rates

Shielding Media	Profile	Vertical Position*	Exposure Rate (R/hr) Calculated	Measured
water	B1	0	6,850	7,000
water	B1	3	29,100	28,500
water	B1	6	40,700	31,300
air	B1	0	5,150	10,000
air	B1	3	20,100	33,500
air	B1	6	27,800	34,800
water	A1	0	1,590	1,700
water	A1	3	4,640	5,300
water	A1	6	4,680	5,600
air	A1	0	4,310	6,500
air	A1	3	10,800	18,000
air	A1	6	11,100	18,100
water	E1	0	2,010	2,100
water	E1	3	6,370	6,200
water	E1	6	6,430	6,800
air	E1	0	4,260	5,800
air	E1	3	11,300	18,000
air	E1	6	11,500	18,000
water	T1	-1.75	7	85
air	T1	-1.75	25	475

*Feet below top of fuel assembly active height.

Source: JU-81

Additional simplifying assumptions are:

- Spacer grids are homogenized over the entire assembly.
- Fuel assembly burnup in any X-Y cross-sectional plane is constant.
- The fuel exposure of the uppermost 2 ft and lowermost 2 ft of the fuel assembly is 80% of the fuel assembly average exposure.
- The fuel exposure of the middle 8 ft of the fuel assembly is 110% of the fuel assembly average exposure.

Output Specification. The output for this problem is the gamma radiation dose at the measurement points described earlier. The calculated gamma energy spectrum should be compared with that given in Table 4.2-7 for consistency. The gamma dose should be reported in units of R/hour or KR/hour for comparison with measured values.

Comments. This problem has not been simulated using a Monte Carlo Transport Theory code. Additional problem assumptions may be necessary to perform effective analyses. Reference JU-81 states that the measured results are reproducible to ±4%. Fuel burnups are thought to be accurate to ± 3%. Dose rate instrumentation was biased 18% higher than a calibrated detection system. The reported standard error was ±12R/hour.

From Reference JU-81, we were not able to determine whether the units of the reported gamma dose are Roentgen/hour or Rad/hour (1 Roentgen = 0.88 Rad).

4.3 Boiling Water Reactor Fuel Assembly Radiation Level

Problem Statement. This problem presents the results of in-plant test measurements of the radiation field in air and water around a Boiling Water Reactor (BWR) fuel assembly. The problem is based on measurements taken at General Electric's Morris Operation.

Objective. This problem provides a basis for comparing the radiation field calculated using a source term code and a shielding code with measured experimental data.

Physical Description. Dresden Unit 2 uses General Electric 7x7 fuel assemblies. The fuel was irradiated from April 1970 (first significant power) to January 1971. After discharge from the reactor and cooling, the fuel was shipped to General Electric's Morris Operation for interim storage. As part of an engineering and test support contract funded by the Department of Energy, selected fuel assemblies were characterized. Gamma exposure rates near spent fuel assemblies were measured eight years after discharge of the fuel from the reactor.

Estimated fuel assembly operating conditions are given in Table 4.3-1. Fuel assembly design characteristics are presented in Table 4.3-2. The initial non-actinide composition of uranium fuel oxide pellets is given in Table 4.3-3. The weight of fuel assembly structural materials is presented in Table 4.3-4, and fuel assembly operating conditions are summarized in Table 4.3-5.

The concentrations of fuel assembly structural material located in the end fitting zone should be multiplied by 0.13 to account for the lower activation levels near the ends of the fuel assembly due to flux levels lower than those in the active fuel zone. In addition, the concentrations of manganese, cobalt, and zirconium in the end fitting zone should be multiplied by factors of 0.80, 0.67, and 0.32, respectively. These corrections account for the difference between the neutron energy spectrum in that zone and the spectrum in the active fuel zone. Both kinds of corrections are based on axial spectrum calculations for a General Electric BWR fuel assembly as reported in Reference CR-78. With these corrections, the ORIGEN-S calculations should more accurately predict the nuclide activities from the structural materials.

Reference JU-81 gives the results of experimental measurements of gamma dose rate and calculations using the shielding factor code QAD. These

Table 4.3-1 -- In Development

Table 4.3-2

Fuel Design Data for Dresden 2

Percent Theoretical Density[a] for UO_2	95.0
Initial Uranium Composition (wt. %)[b]	2.12
Initial Uranium Loading (kg/assembly)	
Fuel Rods per Assembly	49
Rod Pitch (cm)	1.87452
Pellet O.D. (cm)	1.23952
Clad I.D. (cm)	1.26746
Clad O.D. (cm)	1.43002
Nominal Envelope (cm)	13.81252
Plenum Length (cm)	28.575
Active Fuel Length (cm)	365.76
Fuel Temperature (^oK)	700.
Moderator Temperature (^oK)	283.
Moderator Density (g cm^{-3})	.46[c]

[a] Theoretical UO_2 density is 10.96 g cm^{-3}.

[b] Fuel assembly average - 30 rods at 2.44%, 16 rods at 1.69%, and 3 rods at 1.20%.

[c] Assuming a 35% void fraction.

Table 4.3-3

Typical Non-actinide (Impurity) Composition of LWR Oxide Fuels

Element	Atomic Number	Concentration (ppm)[a]	Element	Atomic Number	Concentration (ppm)[a]
Li	3	1.0	Mn	25	1.7
B	5	1.0	Fe	26	18.0
C	6	89.4	Co	27	1.0
N	7	25.0	Ni	28	24.0
O	8	134,454.0	Cu	29	1.0
F	9	10.7	Zn	30	40.3
Na	11	15.0	Mo	42	10.0
Mg	12	2.0	Ag	47	0.1
Al	13	16.7	Cd	48	25.0
Si	14	12.1	In	49	2.0
P	15	35.0	Sn	50	4.0
Cl	17	5.3	Gd	64	2.5[c]
Ca	20	2.0	W	74	2.0
Ti	22	1.0	Pb	82	1.0
V	23	3.0	Bi	83	0.4
Cr	24	4.0			

[a] Parts of element per million parts of heavy metal.

[b] Stoichiometric quantity for MO_2 fuel, i.e., two atoms of O per atom of U or Pu.

[c] Average of 1,573 ppm of gadolinium in BWR fuel rods as a burnable poison.

Source: CR-78

Table 4.3-4

Assumed Fuel Assembly Structural Material Mass Distribution in a BWR

	Material	kg/MTHM
Fuel Zone		
Cladding	Zircaloy-2	279.5
Fuel channel	Zircaloy-4	227.5
Grid spacers	Zircaloy-4	10.6
Grid-spacer springs	Inconel X-750	1.8
Fuel-Gas Plenum Zone		
Cladding	Zircaloy-2	25.4
Fuel channel	Zircaloy-4	20.7
Plenum spring	SS 302	6.0
End Fitting Zone		
Top end fitting	SS 304	10.9
Bottom end fitting	SS 304	26.1
Expansion springs	Inconel X-750	2.1
Total		610.6

Source: MI-83

Table 4.3-5

Fuel Assembly Operating Conditions

Operating Period	Days	Average Power MW/MT
1	70	10
2	40	0
3	200	20

results are given for measurements taken at several axial locations for the X-Y detector locations given in Table 4.3-6.

Table 4.3-7 gives the calculated intensities from Reference JU-81 for the gamma radiation source in spent fuel.

Table 4.3-8 gives the measured gamma exposure rates at the fuel assembly mid-point along the "B1" profile for three fuel assemblies that were believed to have similar irradiation histories. In addition to measured exposures at each corner, Table 4.3.8 provides an indication of the anisotropy of gamma exposure. For irradiated fuel assemblies, the measured gamma exposure varied by as much as ±10%. (In calculating the gamma intensity around a fuel assembly, it is commonly assumed that fuel burnup and therefore the gamma source is evenly distributed.)

Results of additional measurements made along the B1 profile at 1 ft intervals are given in Table 4.3-9. These measurements provide an estimate of the standard error of the expsoure rate measurement of about 9% (one sigma).

Table 4.3-10 gives results of calculated and measured exposure rates in air and water for three detector profiles.

Reference JU-81 includes a discussion of the accuracy and precision of measured results. Based on an analysis of all identified sources of random errors, the overall variability of measurements is estimated to be 9.1%. This reference also states that based on its measurements, a variance of ±3% (one sigma) between utility-calculated fuel exposures and true exposures may exist. This agrees with generally held beliefs about the accuracy of these calculations and is consistent with IAEA guidelines established for safeguards purposes.

Assumptions. Analyses may be performed using the following assumptions:

- The entire fuel assembly (except end fittings) is a homogeneous mass.

Table 4.3-6

Gamma Detector Locations

Detector	X-Y Location*	
	X	Y
A-1	1.6	+ 1.6
B-1	7.0	+ 7.0
E-1	-3.9	+10
T-1**	-3.9	- 3.9

* The origin is the corner of the fuel assembly envelope at the top of the active length of the fuel.

** This detector is located above the fuel assembly.

Source: JU-81

Table 4.3-7

Calculated Gamma Intensities for Gamma Radiation Sources in Spent Fuel

Upper Energy Range	Gamma $MeV/cm^3 \cdot sec$
0.55	2.22E7
0.85	2.05E9
1.25	3.09E7
1.75	4.38E6
2.25	5.91E4
2.65	5.63E5
3.00	1.24E4
4.00	2.25E3
5.00	1.90E-1
6.00	4.62E-2

Source: JU-81

Table 4.3-8

Exposure Rates from Fuel Assemblies

Fuel Assembly Identification	Exposure Rate (R/hr) at Fuel Assembly Midpoint Along B1 Profile in Water: Edge Measured N	E	S	W	Average	Figure of Anisotropy 100 (Max-Min)/Max
201	975	910	860	860	900	11.8
686	945	920	880	885	910	6.9
599	1200	1100	1000	1050	1090	16.7

Source: JU-81

Table 4.3-9

Exposure Rate from Repeated Fuel Assembly Measurements

Fuel Assembly I.D.	Profile	Z* Location Feet-Inches	Number of Independent Measurements	Exposure Rate KR/hr (Mean Standard Deviation)	Measurement Error (%)
201	B1	+5	11	108 (10.4)	9.6
686		1+5	11	454 (20.5)	4.5
599		2+5	11	759 (23.3)	3.1
		3+5	11	912 (48.5)	5.3
		4+5	11	961 (126)	13.1
		5+5	11	977 (150)	15.4
		6+5	11	959 (122)	12.8
				Average	9.1

*Distance from the top of the active fuel height.

Source: JU-81

Table 4.3-10

Calculated and Measured Exposure Rates

Shielding Media	Profile	Vertical Position*	Exposure Rate (R/hr) Calculated	Measured
water	B1	0	87	105
water	B1	3	470	940
water	B1	6	510	885
air	B1	0	91	185
air	B1	3	437	1200
air	B1	6	482	1400
water	A1	0	20	30
water	A1	3	97	190
water	A1	6	106	190
air	A1	0	72	160
air	A1	3	262	650
air	A1	6	296	730
water	E1	0	20	40
water	E1	3	103	220
water	E1	6	113	245
air	E1	0	59	130
air	E1	3	232	540
air	E1	6	264	600
water	T1	-1.75	.05	2
air	T1	-1.75	.2	15

* Feet below top of fuel assembly active height.

Source: JU-81

- The two center rows of fuel rods are modeled discretely, the remaining rods are homogenized.

Additional simplifying assumptions are:

- Spacer grids are homogenized over the entire assembly.
- Fuel assembly burnup in the X-Y plane is assumed to be equal.
- The fuel exposure of the uppermost 2 ft of the fuel assembly will be 50% of the fuel assembly average exposure.
- The fuel exposure of the lower 10 ft of the fuel assembly will be 110% of the fuel assembly average exposure.

Output Specification. The output for this problem is the gamma radiation dose at the measurement points described earlier. The calculated gamma energy spectrum should be compared with that given in Table 4.3-7 for consistency. The gamma dose should be reported in units of R/hour or KR/hour for comparison with measured values.

Comments. This problem has not been simulated using a Monte Carlo Transport Theory code. Additional problem assumptions may be necessary to perform effective analyses. Reference JU-81 states that measured results are reproducible to ±4%. Fuel assembly burnups are thought to be accurate to ±3%. However, the axial burnup distribution of low exposure BWR fuel is not easy to estimate without performing coupled depletion/thermal-hydraulic analysis. Dose rate instrumentation was biased 18% higher than a calibrated detector system. The reported standard error was ±12R/hour.

From Reference JU-81, we were not able to determine whether the units of the reported gamma dose rates are Roentgens/hour or Rad/hour (1 Roentgen = .88 Rad).

4.4 Hypothetical Thin-Walled Waste Package Shielding Problem

Problem Statement. This problem requires the estimation of the gamma flux and neutron flux and dose around a hypothetical thin-walled, high-level radioactive waste package. The hypothetical waste package is conceptually similar to packages that the Department of Energy has proposed for use in a salt repository. The flux and dose will be estimated at points within the shield and at points exterior to the shield.

Objective. The purpose of this problem is to provide a baseline for prediction of the gamma and neutron flux and dose in an environment similar to that which may exist around a waste package in a repository for high-level radioactive waste.

Physical Description. The waste package consists of a 2-3/4 in cylindrical carbon steel structural member covered by a 0.25 cm Ticode-12 overpack. Waste package design characteristics are summarized in Table 4.4-1. The gamma flux and dose rate are to be calculated at points in the structural component, in the Ticode-12 overpack, and at points in a salt host rock surrounding the waste package. Figure 4.4-1 shows a typical waste package emplacement environment.

Problem Solution. This problem will be solved using a transport theory computer program. It should be assumed that the spent BWR fuel rods had an initial enrichment of 2.7% and were irradiated at constant power over a three-year period to a discharge exposure of 27,000 megawatt days per metric ton of uranium. Subsequent calculations should be performed for time periods of 30, 100, 300, and 1,000 years following waste package emplacement.

Assumptions. In modeling the spent fuel rods contained in the waste package, it is adequate to analyze discretely the outermost two rows of fuel rods. The innermost fuel rods can be analyzed using the properties for a homogenized material composition. The problem may be analyzed in either one or two dimensions. Isotopic compositions of materials for this problem are given in Table 4.2-2.

Table 4.4-1

Summary of Waste Package Design Characteristics

Design Parameters	Reference BWR
Waste Form	
Diameter (cm)	49
Length (m)	4.11
Weight of Waste (kgU)	3402
Total Waste Form Weight (kg)	6260
Waste Package	
Overpack Material	TiCode-12
Overpack Thickness (cm)	0.25
Outside Diameter (cm)	64.5
Length (m)	4.45
Empty Weight (tonnes)	4.8
Loaded Weight (tonnes)	11.1
Repository	
Package Pitch (m)	10.0
Tunnel Height (m)	7.2
Tunnel Width (m)	4.0
Borehole Diameter (cm)	68
Borehole Depth (m)	5.6
Performance Parameters	
Surface of Overpack (mrem/hr)	10^6
Surface of Tunnel (mrem/hr)	1.3
Structural Component Thickness	
Cylinder Wall (cm)	7
Actual Top Head (cm)	20
Actual Bottom Head (cm)	12

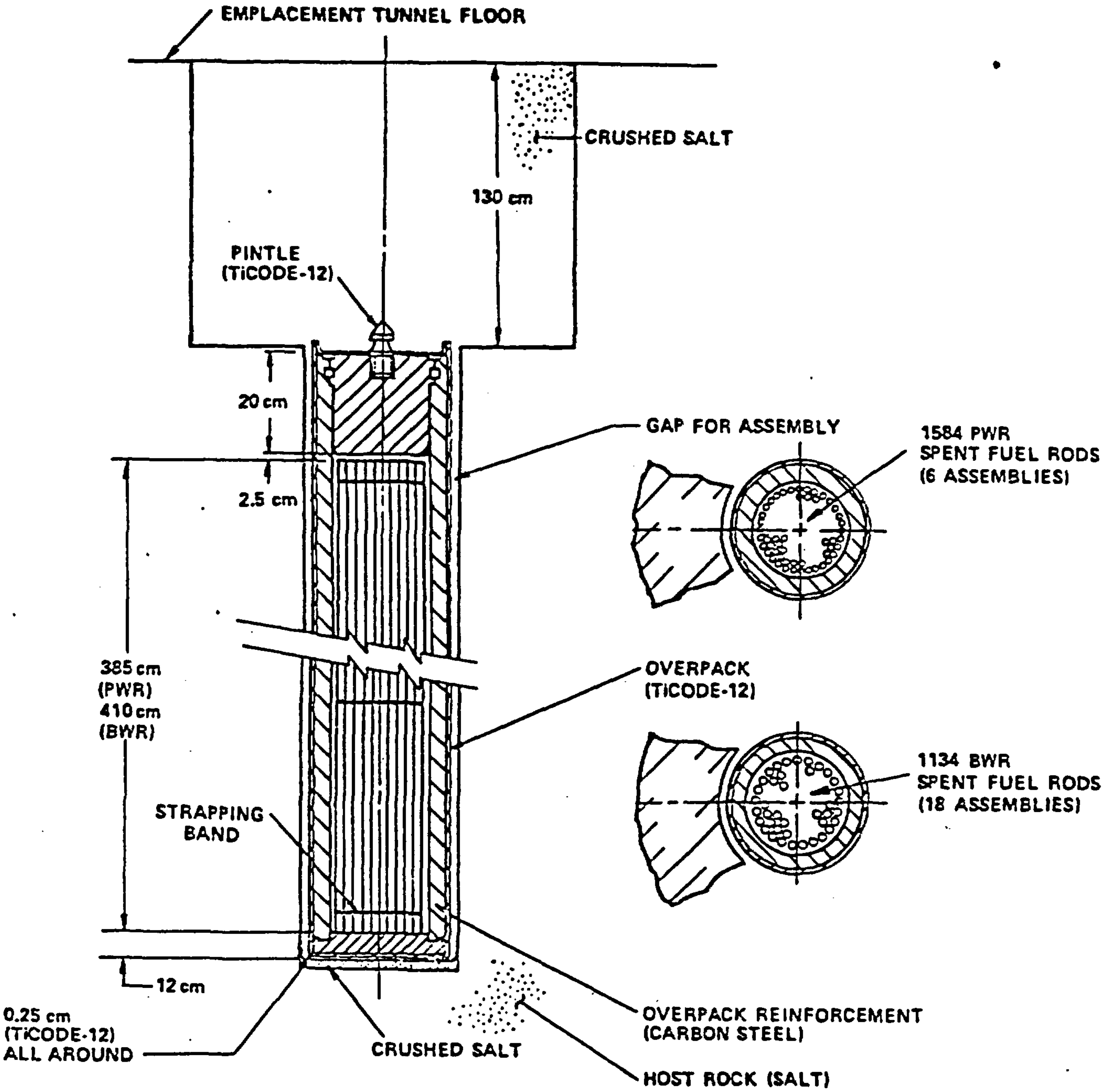

Figure 4.4-1

Reference Spent Fuel Waste Package for Borehole Emplacement

Output Specifications. The outputs for this problem are the gamma photon flux and the neutron flux at the waste package centerline, at the outer carbon steel overpack surface, at the outer Ticode-12 surface, and at points 5, 10, 20, 50, 100, and 500 cm from the waste canister surface in the host rock.

Comments. This problem has not yet been analyzed. However, assessments performed by Westinghouse using a one-dimensional transport theory code estimated that the dose for 10-year cooled BWR fuel at the surface of the overpack would be approximately 10^6 millirems per hour.

4.5 Hypothetical Thick-Walled Waste Package Shielding Problem

Problem Statement. This problem requires the estimation of the gamma flux and neutron flux around a hypothetical thick-walled, high-level radioactive waste package. The hypothetical waste package is conceptually similiar to packages that the Department of Energy has proposed for use in the BWIP facility. The flux will be estimated at points within the shield and at points exterior to the shield.

Objective. This problem is designed to provide a baseline for prediction of the gamma and neutron flux in an environment similar to that which may be seen around a waste package in a repository for high-level radioactive waste.

Physical Description. The waste package consists of a 38 cm thick triangular cast iron container. Waste package design characteristics are summarized in Tables 4.5-1 and 4.5-2. The gamma flux is to be calculated at points in the waste package and at points in a bentonite backfill surrounding the waste package. Figures 4.5-1 and 4.5-2 show a typical waste package emplacement environment.

Problem Solution. This problem will be solved using a transport theory computer program. It should be assumed that the waste form is commercial

Table 4.5-1

Summary of Alternate II (SSP) Waste Package Design Features

Conceptual Design Feature	CHLW
Waste Form Features	
Number of Waste Forms	3
Waste Form Diameter, cm	32.5
Waste Form Length, cm	305
Waste Form Weight, kg	2,535
Waste Content per Package, kg	1,785
Package Heat Load, W	6,630
Package Features	
Cross Section Geometry	Modified Triangle
Inside Dimension(s), cm	70
Outside Dimension(s), cm	146
Overpack Length, cm	400
Overpack Empty Weight, tonne	39.0
Overpack Loaded Weight, tonne	41.5
Package Surface Radiation (mrem/hr)	100

Table 4.5-2

CHLW Characteristics

Canister Dimensions	0.324 m dia. x 3.05 m long
Glass[a] Thermal Conductivity	0.8-1.3 W/m°C 0 to 500°C
Glass Specific Heat	700-800 J/kg°C
Glass Density	3.1 g/cm^3
Canister Average Heat Output at Emplacement	2.2 kW
Limiting Glass Temperature During Package Design Life[b]	500°C
Limiting Glass Temperature After Containment Life[c]	100°C
Glass Total Weight	595 kg
Canister Radioactivity Content	6.58 x 10^5 @ 10 years out of reactor
Canister Active Glass Volume	0.19 m^3
Leach Rate	2.0 x 10^{-6} g/cm^2 day[d]

(a) Glass refers to HLW in glass matrix.
(b) These limits represent the glass softening point beyond which glass devitrification is possible.
(c) This temperature limit may not be applicable to the NWRB where the backfill is used to control post-containment radionuclide release rates.
(d) 24-day value. Leach rate is expected to go to 2 x 10^{-9} g/cm^2 day after 400 days

Source: WE-82

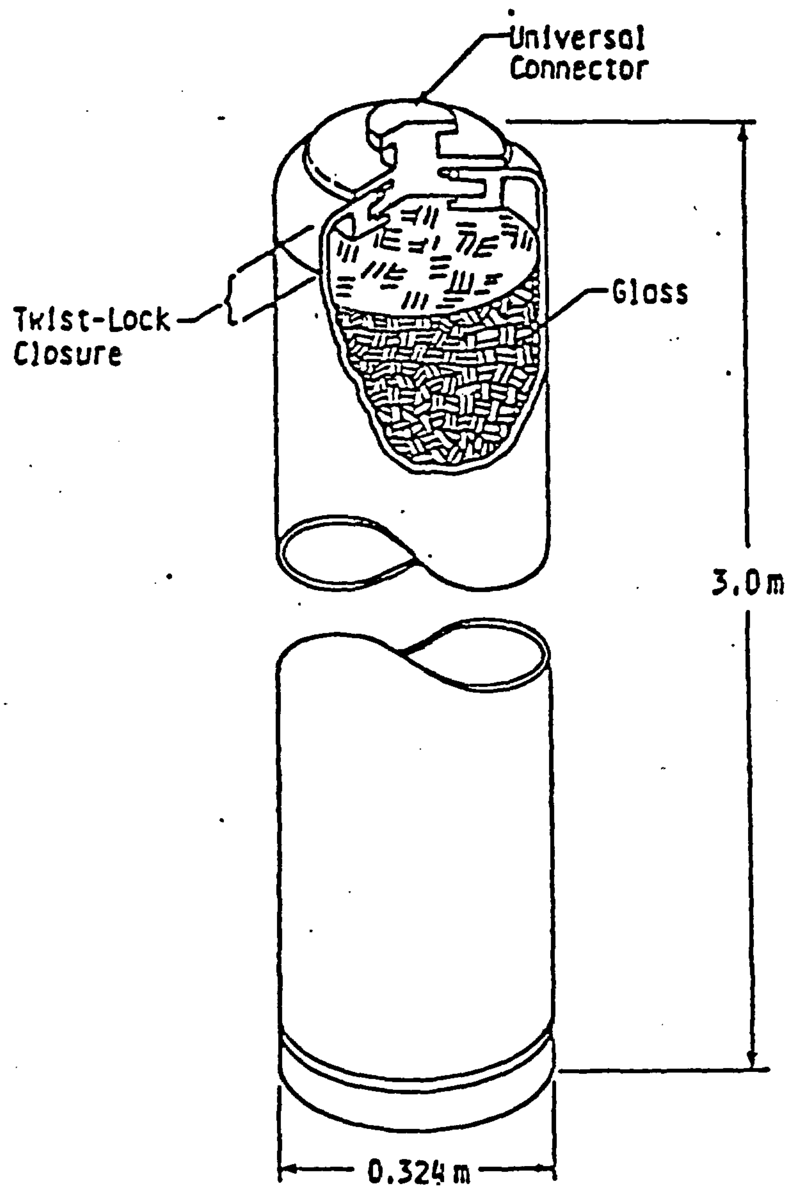

Figure 4.5-1

Reference Commercial High Level Waste Form

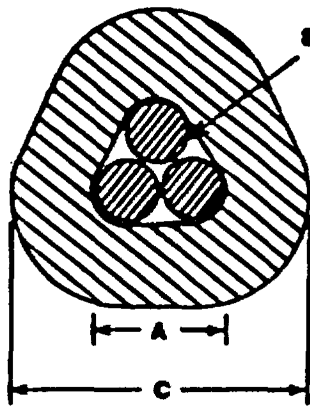

	CHLW	
	Gray Iron	Steel
Overpack Dimensions, cm		
A	70	70
B	--	--
C	146	161
D	--	--
Overpack Length, m	4.0	4.1
Wall Thickness, cm	38*	45.5
Overpack Weight, tonnes	39	60.1
Waste per Package, kg	1785	1785
Total Package Wt., tonnes	41.5	62.6

*High carbon content of cast iron provides better neutron attenuation: thus thinner wall is required.

Figure 4.5-2

Typical Thick-Walled Waste Package

high-level waste from PWR fuel with an initial enrichment of 3.5% irradiated at constant power over a three-year period to a discharge exposure of 35,000 MWD/MTU. Calculations should be performed for waste cooling times of 10, 30, and 100 years following spent fuel discharge.

Assumptions. The problem may be analyzed in either one or two dimensions. Isotopic compositions of materials in this problem are given in Table 4.5-3.

Output Specifications. The outputs for this problem are the gamma photon flux, gamma photon dose, the neutron flux, and the neutron dose at the points given in Table 4.5-3.

Comments. This problem has not yet been analyzed. However, assessments performed by Westinghouse using a one-dimensional transport theory code estimated that the dose for 10-year cooled commercial high-level waste at the surface of the overpack would be approximately 100 millirems per hour.

Table 4.5-3 -- In Development

5.0 EMPIRICAL CORROSION AND LEACHING PROBLEMS

This section contains two verification problems for corrosion and leaching that can be used in the verification of the computer code WAPPA. Although the problems in this section are useful in showing that certain parts of the numerical algorithms of the code WAPPA function as designed, the code WAPPA relies heavily on empirical data, and its predictions will never be better than the empirical constants used in the code.

The first problem is based on test problems developed under the SCEPTER project. This problem is designed to allow sensitivity analyses on selected input parameters related to corrosion and leaching. The second problem is an analytical solution for solute transport by diffusion across an infinitely long cylindrical segment. This problem can be used to assess the acceptability of WAPPA's backfill leaching calculation.

5.1 Simple and Complex Waste Package Concepts Used in the Verification of the WAPPA Code

Problem Statement. The 7 barrier and 17 barrier test problems used in the verification of the WAPPA code under the SCEPTER project will be used to benchmark WAPPA. The simple and complex test problem configurations are summarized in Tables 5.1-1 and 5.1-2 respectively. Once the test problem results have been found to agree with those obtained under the SCEPTER project, the code will be run a number of times with selected changes made to the inputs related to corrosion and leaching. These changes will be within the range of uncertainty commonly associated with these data values.

Objectives. The first objective of this problem is to ensure that the version of the code on hand can reproduce the results from the earlier verification study. A more important objective, however, is to evaluate the sensitivity of code results to changes in corrosion and leaching parameters and uncover possible errors in the program logic which could be revealed by these changes.

Table 5.1-1

Verification Test for a Simple Waste Package Concept

Barrier Counter	Material	Material Code ISMAT (I)	Barrier Radii SRADII (I)
1	WF glass	012	0.1555
2	SST - 304L canister	101	0.1619
3	oxide	500	0.1619
4	air	203	0.1683
5	Ticode-12 overpack	108	0.1746
6	oxide	508	0.1746
7	sand bentonite backfill	402	0.5080

Table 5.1-2

Verification Test for Complex Waste Package Concept

Barrier Counter (I)	Material	Material Code ISMAT (I)	Barrier Radii SRADII (I)
			0
1	WF glass	012	0.1500
2	air gap	203	0.1510
3	SST - 304L canister	101	0.1750
4	oxide	501	0.1750
5	argon gap	204	0.1780
6	SST - 316L overpack	102	0.1980
7	oxide	502	0.1980
8	helium gap	205	0.2000
9	C-steel overpack	106	0.2240
10	oxide	506	0.2240
11	air gap	203	0.2260
12	Ticode-12 overpack	108	0.2360
13	oxide	508	0.2360
14	air gap	203	0.2370
15	lead sleeve	115	0.2470
16	oxide	515	0.2470
17	sand/bentonite backfill	402	0.5000

Analytical Solution. The solution to this problem can not be expressed analytically.

Assumptions. The assumptions are identical to those of the WAPPA code (see Reference MI-83 for a description).

Input Specifications. The input data for the simple and complex configurations are listed in Appendix A.

Output Specifications. In addition to an echo print of input data and data base values, the output will include:

- Barrier radii
- Temperature as a function of radius
- Ratio of the heat energy generated or deposited in a barrier or in the waste package to the total heat energy generated in the waste package
- Barrier status (intact, breached, or failed)
- Areal degradation factor
- Nuclide concentrations

5.2 Solute Transport by Diffusion Across an Infinitely Long Cylindrical Segment

Problem Statement. A constant flux of F and a constant concentration of zero are specified for the inner and outer surface, respectively, of an infinitely long cylindrical segment (see Figure 5.2-1) with inner radius a and outer radius b. The solute diffusion coefficient, D, is assumed to be constant throughout the segment. No solute is assumed to be present in the segment initially. The values to be calculated as a function of time are (1) the concentration profile across the segment, (2) the average concentration within the segment, and (3) the concentration gradient at the radius b.

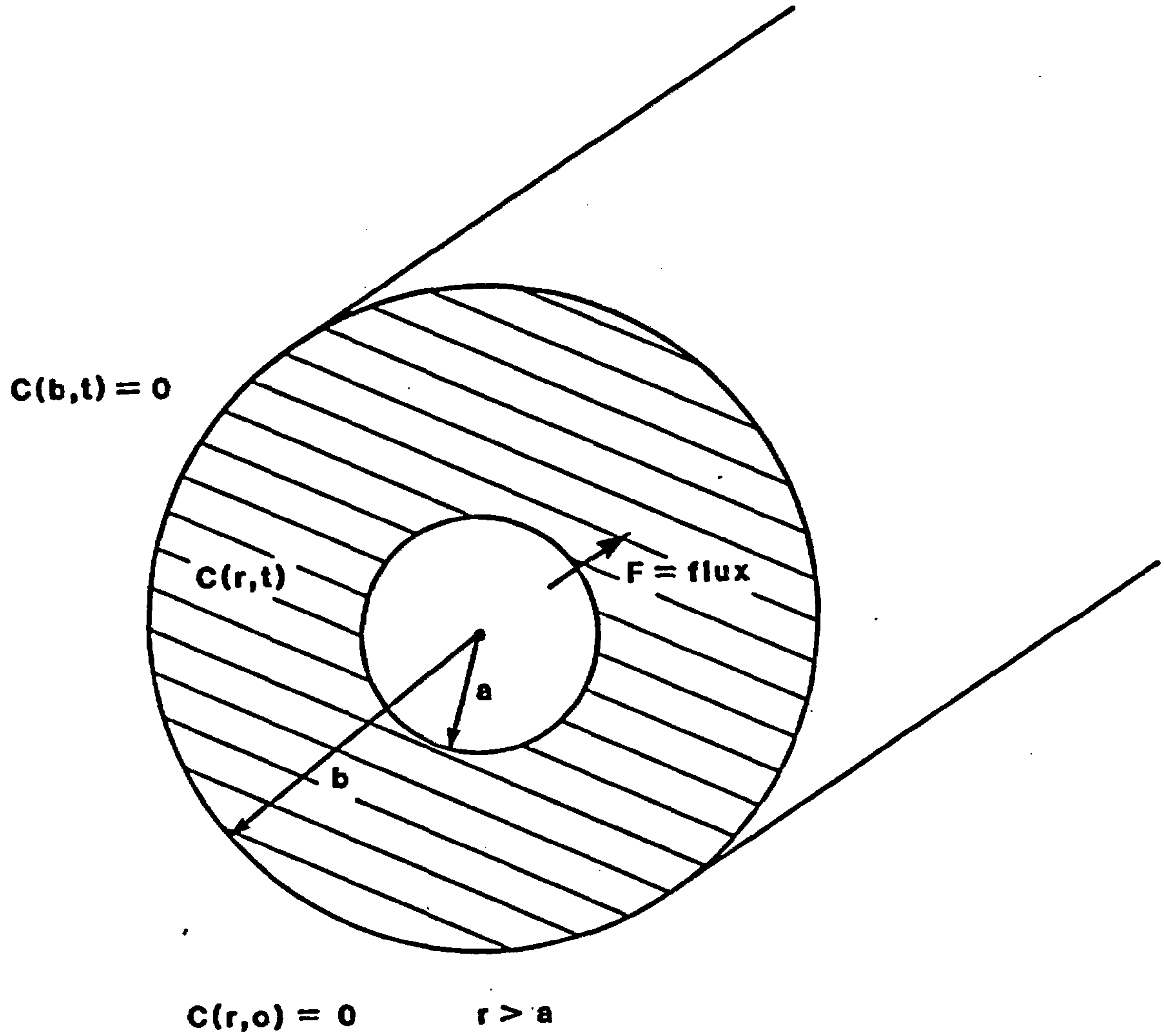

Figure 5.2-1

Diagram for Benchmark Problem 5.2

Objectives. This problem is designed to test the backfill leaching calculation used in WAPPA and the assumption that the backfill can be treated as a single, uniformly mixed cell.

Analytical Solution. The concentration of solute as a function of time can be described by the diffusion equation in cylindrical coordinates:

$$\frac{\partial^2 C}{\partial r^2} + \frac{1}{r}\frac{\partial C}{\partial r} = \frac{1}{D}\frac{\partial C}{\partial t} \tag{148}$$

with the following boundary conditions:

$$-D\left(\frac{\partial C}{\partial r}\right)_{r=a} = F \text{ (a constant)}$$

$$C(b,t) = 0$$

$$C(r,o) = 0 \text{ for } r \geq a$$

The analytical solution to this equation is given as follows:

$$C(r,t) = \frac{aF}{D}\ell n\left(\frac{b}{r}\right) + \frac{\pi F}{D}\sum_{m=1}^{\infty}\exp(-D\alpha_n^{2}t) \times \frac{J_o^{2}(b\alpha_n)\left[J_o(r\alpha_n)Y_1(a\alpha_n)-Y_o(r\alpha_n)J_1(a\alpha_n)\right]}{\alpha_n\left[J_1^{2}(a\alpha_n) - J_o^{2}(b\alpha_n)\right]} \tag{149}$$

where α_n are the positive roots of

$$J_1(a\alpha)Y_0(b\alpha) - Y_1(a\alpha)J_0(b\alpha) = 0$$

Assumptions. There is no variation of solute concentration with the angle or along the axis of the cylindrical segment. Also, solute advection, adsorption, and decay within the segment are neglected.

Input Specification. Calculations are to be performed for a wide range of values of inner radius a, outer radius b, diffusion coefficient D, and flux F at radius a.

Output Specifications. The solute concentration as a function of time is calculated for a range of distances between a and b. Also, the average concentration within the cylindrical segment is calculated as a function of time. Finally, the concentration gradient at r = b is calculated as a function of time. Concentration profiles for different values of b/a were calculated by use of Equation 149 and are displayed in Figures 5.2-2 through 5.2-4. The associated average concentrations and concentration derivatives at r = b are given in Table 5.2-1. In reporting these results, all concentrations, distances, and times have been normalized as indicated in Figures 5.2-2 through 5.2-4.

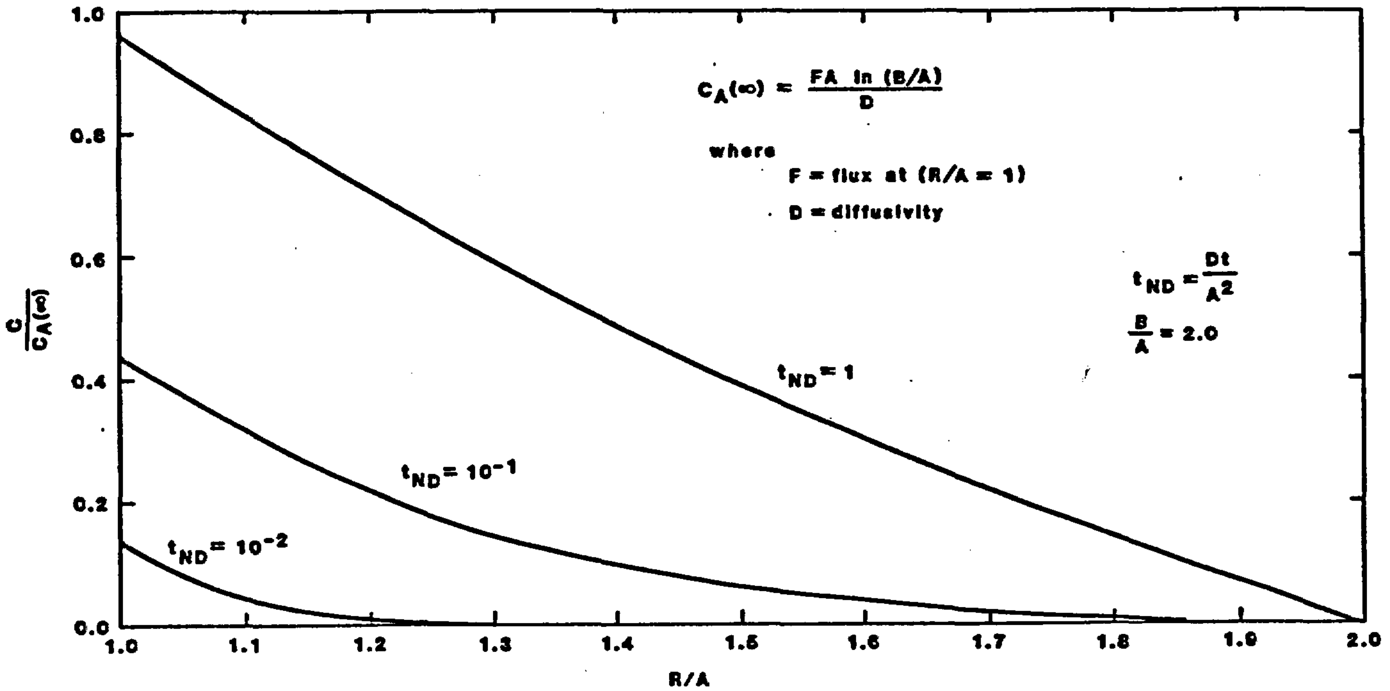

Figure 5.2-2

Normalized Concentration Curve for B/A = 2

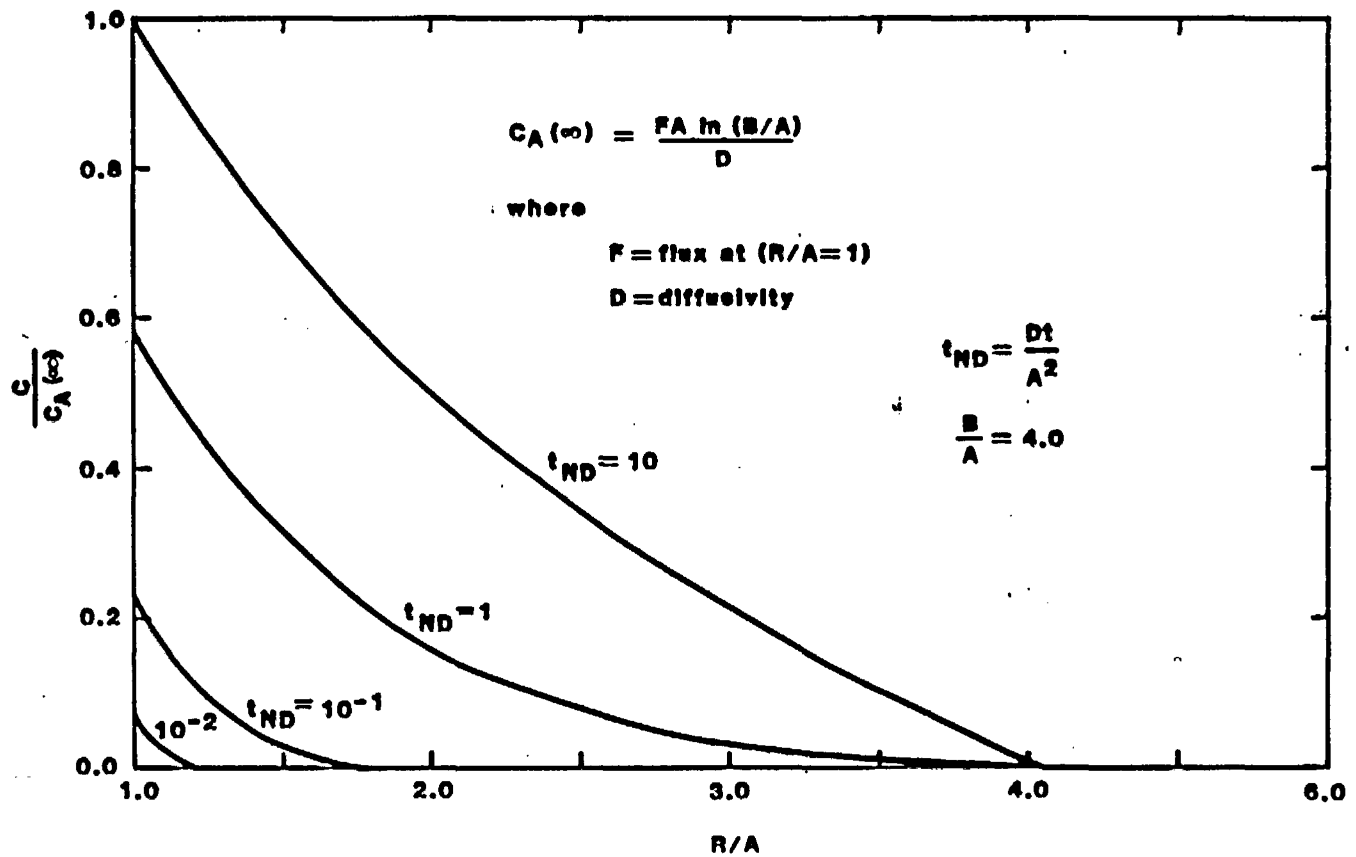

Figure 5.2-3

Normalized Concentration Curve for B/A = 4

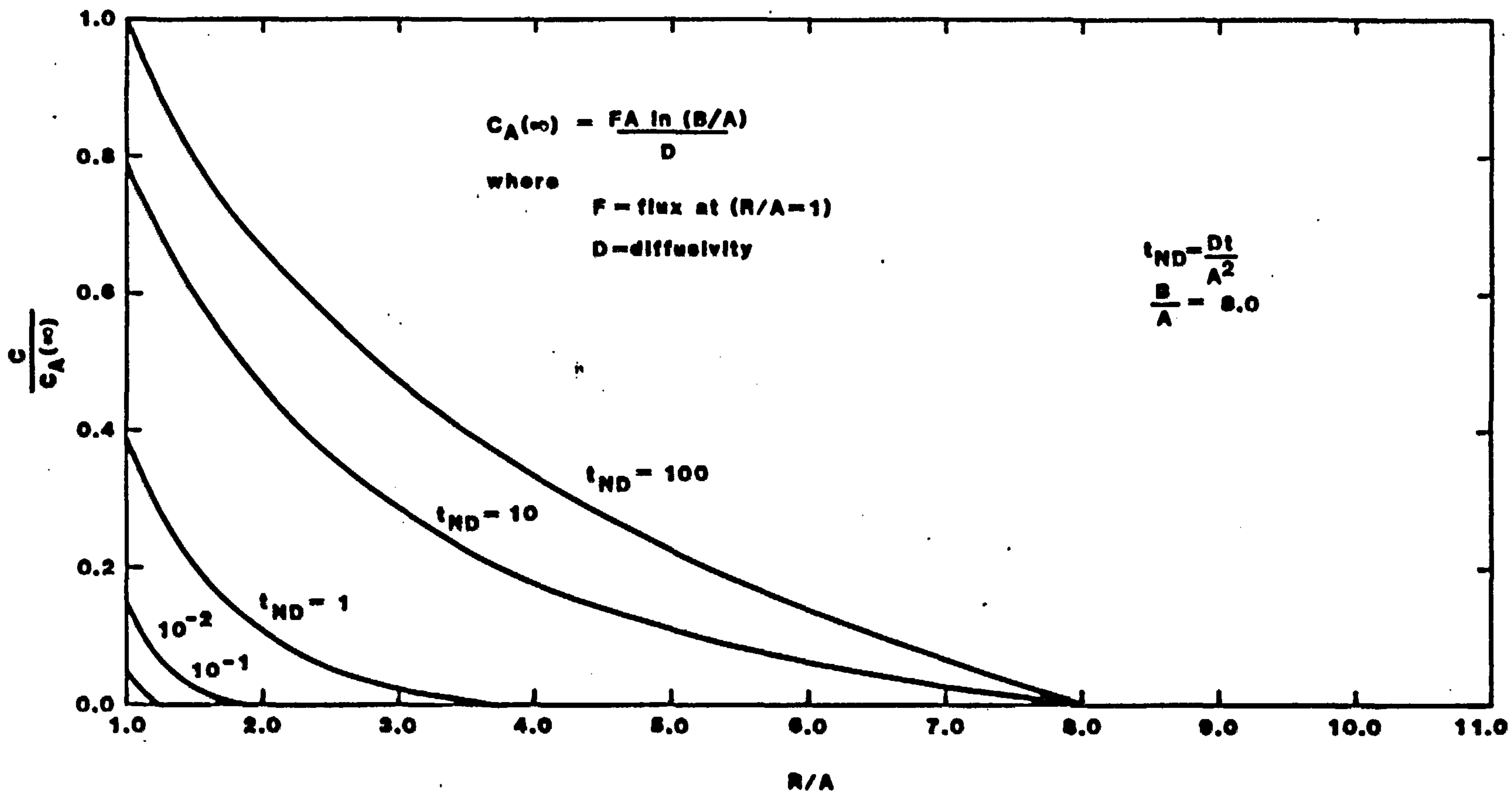

Figure 5.2-4

Normalized Concentration Curve for B/A = 8

Table 5.2-1

Average Normalized Concentrations and Boundary Derivatives for Different Values of b/a*

Non-dimensionalized Time $t_{ND} = Dt/a^2$	Average Non-dimensionalized Concentration $C_{ND} = \frac{CD}{F_a \ln (b/a)}$ b/a = 2.0	4.0	8.0	Negative Derivative of Non-dimensionalized Concentration** $-\left(\frac{\partial C_{ND}}{\partial (r/a)}\right)_{(r/a) = b/a}$ b/a = 2.0	4.0	8.0
0.01	0.99×10^{-2}	0.93×10^{-3}	0.24×10^{-3}	-	-	-
0.1	0.0950	0.96×10^{-2}	0.16×10^{-2}	0.05	-	-
1.0	0.372	0.936×10^{-1}	0.154×10^{-1}	0.69	0.021	-
10	0.388	0.290	0.131	0.73	0.18	0.025
100	0.388	0.294	0.225	0.73	0.18	0.061

* Results based on the evaluation of 40 terms in the Equation 149 summation.

** Slope based on the last two points plotted in each of the Figures 5.2-2 through 5.2-4.

6.0 WASTE PACKAGE GEOCHEMICAL CODE BENCHMARK PROBLEMS

Numerical models may be used to simulate geochemical processes in the high-temperature regions around waste packages in a nuclear repository. Benchmarking the geochemical codes that may be considered for such use requires appropriate test problem data sets. Ideally, a test problem will evaluate the utility of each code and verify the code algorithms for the geochemical processes being modeled.

Geochemical models should provide input to analyses of the effects of near-field geochemistry on waste form solubility and leaching, canister corrosion, and backfill properties. The usefulness of geochemical models to the analysis of these effects will depend not only on the development of the necessary algorithms and thermodynamic data, but also on the data to verify and validate the codes.

Since there is no direct experience with the complex interactions of high-level waste packages with backfill material, host rock, and groundwaters, data must be obtained from other sources. For example, laboratory studies have been conducted on representative samples of waste form, canister backfill, and host rocks related to repository media (References AP-82, CH-83a and b, GO-81, GR-83, KE-84, KU-81, MO-83, MY-83, RE-82, SE-84, and WO-82). Laboratory studies may provide useful information as controlled experiments, although certain drawbacks exist. For example, problems in laboratory methods raise significant questions about the usefulness and viability of some early experiments (References KE-84 and CR-84).

Shortcomings in laboratory experiments often arise from difficulty in formulating synthetic groundwater representative of that found in the candidate host rock; obtaining unaltered, representative samples of repository rock; and reproducing the temperature, redox, and degree of openness of the system. In addition, laboratory-scale tests are restricted in time, raising the possibility that kinetically controlled reactions will prevent the attainment of equilibrium conditions, an all-important assumption with state-of-the-art geochemical models. For these reasons, laboratory experiments have not been utilized as potential test problems in benchmarking equilibrium-based geochemical models.

If the methodological problems can be surmounted, laboratory experiments may prove to be valuable test problems for the benchmarking of kinetically based geochemical models now in the developmental stage. A kinetic benchmark problem is offered in Problem 6.5 in anticipation that a kinetic model may be developed. Even here, an understanding of the long-term behavior of repository systems over hundreds of years may be satisfied only partially by such short-term experiments (Reference EL-83).

One approach to dealing with uncertainties in extrapolating from the laboratory scale to the repository scale (both in time and space) is to investigate comparable geologic systems found in nature. These "natural analogs" may contribute to understanding the processes that will occur in a repository over many hundreds of years (Reference EL-83):

- The Oklo, Gabon, uranium ore body achieved criticality naturally about two billion years ago. Researchers have measured the extent of migration of radionuclides similar to those derived from high-level waste.
- Metamorphic haloes surrounding igneous intrusives can be studied to observe the effects of heat on clay backfill and host rock.
- Metamict effects on minerals show crystal structure damage from radiation.
- Geothermal systems allow the study of mineral alteration products due to elevated temperatures.

Natural analogs that are similar to geochemical processes in high-level radioactive waste repositories should provide fairly complete data on the chemistry of water, mineralogy, and effects of changing temperature. Temperature and pressure of the natural analog should be in the range of 50^{o}-$300^{o}C$ and up to about one hundred bars of hydrostatic pressure. Ideally, stable mineral assemblages under known water chemistry and temperature conditions should be well documented. The natural analog selected for a given candidate repository also should exhibit petrology, mineralogy, and groundwater chemistry similar to those of the candidate repository.

Based on these criteria, proposed natural analogs may be selected for use in the development of geochemical code benchmark problems. A search of the literature has revealed that sufficiently detailed studies of the geochemistry of geothermal systems are available to provide potentially valuable natural analogs. With temperature typically ranging from ambient to over 300°C and pressures under hydrostatic conditions ranging up to about one hundred bars, geothermal systems provide natural analogs of water-rock interactions within a pressure and temperature range similar to that anticipated for high-level waste repositories. In addition, the variety of geologic terrains in which geothermal systems occur provides petrologic, mineralogic, and hydrogeochemical conditions similar to those in the candidate repository media under consideration. Table 6-1 lists several geothermal systems, the host rock to which they are similar, and a qualitative rating of the degree to which they have been studied.

The candidate media for a deep geologic repository for high-level waste in the United States include at least four rock types*:

1. Basalt (Hanford Reservation, Washington)
2. Tuff (Nevada Test Site)
3. Salt (Gulf Coast salt domes and bedded salt in Palo Duro Basin, Texas, and Paradox Basin, Utah)
4. Granite (not selected yet)

* In addition, the United States is involved in research on the feasibility of seabed disposal. This research is conducted jointly with seven other countries under the auspices of the Nuclear Energy Agency of the Organization for Economic Cooperation and Development.

Table 6-1

Candidate Geothermal Systems as Natural Analogs for High-Level Radioactive Waste Repositories

Geothermal System	Analogous Host Media	Level of Study*
Iceland	Basaltic	High
Newberry Volcano, OR	Basaltic	Moderate
La Grande, OR	Basaltic	Low
Yellowstone, WY	Rhyolitic	High
New Zealand	Rhyolitic	High
Valles Caldera, NM	Rhyolitic	Low
Roosevelt, UT	Granitic	Moderate
Marysville, MT	Granitic	Low
Salton Trough, CA	Brine Salt	High
Red Sea	Brine Salt	Low
Raft River, ID	Shale	Moderate

*Level of study refers to a subjective evaluation of the amount of research and the degree of understanding of the system.

Although the DOE has devoted most of its efforts to studying the basalt site at the Hanford Reservation (BWIP), the tuff site at the Nevada test site (NTS), and bedded and dome salt sites, the Department has initiated the screening process to select candidate sites in granite for further study. Furthermore, the DOE is well along in the evaluation of bedded salt at the Waste Isolation Pilot Program (WIPP) in New Mexico.

These potential media present different problems in understanding the physical and chemical processes that will control the repository environment. Rock types being considered include mafic (basalt) and silicic (rhyolite and granite) igneous rocks, sedimentary evaporites (bedded salt), and diapiric salt domes (Gulf Coast salt domes).

In the near-field environment of a repository, consisting of a waste package and backfill emplaced within a mined opening, geochemical interactions must be simulated in an environment where temperature may rise as high as 200°-$300^{\circ}C$ for several years, then gradually decline over several hundred years as shown in Figure 6-1 for the spent fuel case in a basalt repository (Reference RO-82).

During the life of a basalt repository, the near-field environment will initially be under oxygenated, dry conditions. As the temperature drops, resaturation is predicted to occur after 360 to 390 years (Reference RO-82), and anoxic conditions will return.

Thus, during the early, unsaturated high-temperature period, dehydration will be the most important process, while after resaturation of the backfill and host rock, water-rock interactions will be important, especially at elevated temperatures.

To simulate geochemical processes in a changing thermal regime requires not only that the aqueous speciation, redox potential, and degree of mineral saturation be calculated but also that temperature effects be

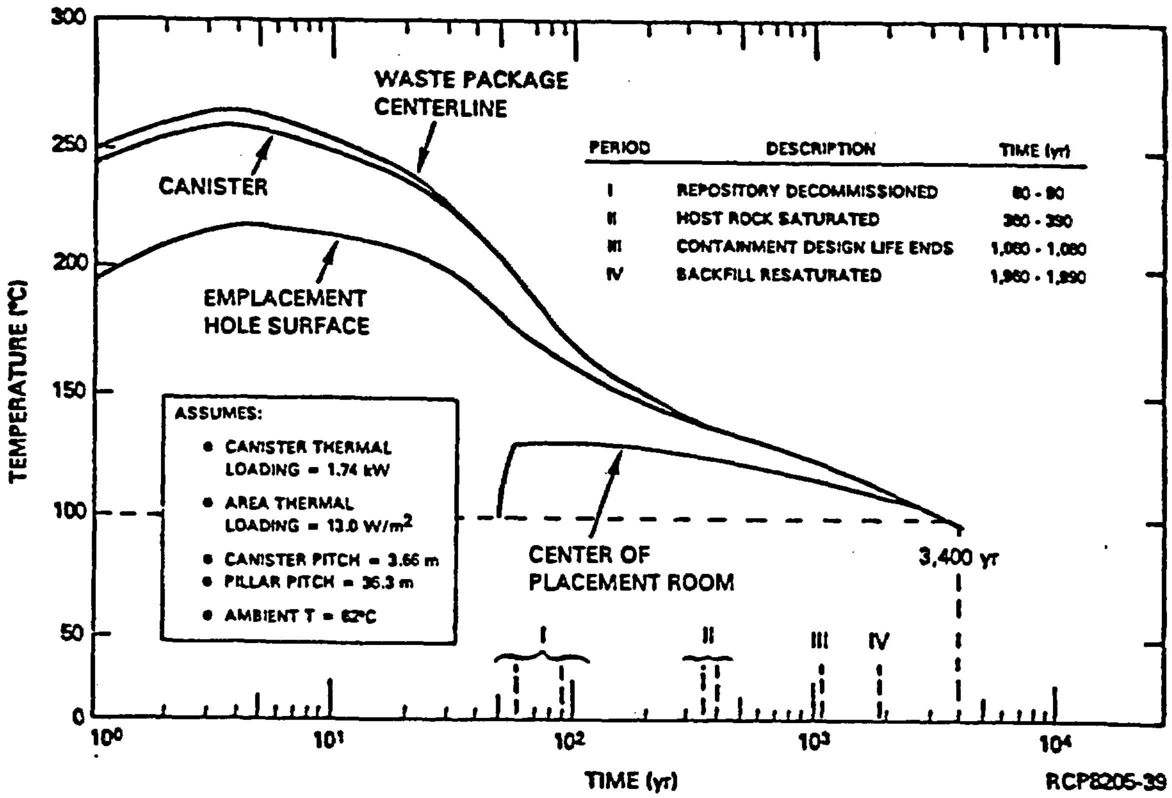

Figure 6-1

Temperature-Versus-Time Curves for Different Components of a Vertically Emplaced Spent-Fuel Waste Package in a Repository Located in Basalt (RO-82) incorporated. Therefore, the benchmark problems have been designed to test the effects of temperature within the full range expected for the near-field, as well as to test the algorithms for deriving speciation, redox, and saturation indices. In addition, some geochemical codes (reaction path models) may be used to simulate water-rock interactions in systems that have changed from one equilibrium condition to another, either through heating or cooling or through the migration of water to a different mineral regime.

The benchmark problems designed for near-field geochemical codes are:

Problem 6.1:	Two-phase, water-rock system at low temperature (less than 150°C) with no boiling
Problem 6.2:	Three-phase, vapor-water-rock system at high temperature (greater than 150°C)
Problem 6.3:	Hypothetical radionuclide equilibrium speciation and mineral solubility
Problem 6.4:	Reaction path incorporating effects of changing temperatures on mineral-water equilibria
Problem 6.5:	Reaction kinetics based on experimental results

6.1 Low-Temperature (<150°C) Basalt Analog without Boiling

<u>Problem Statement</u>. This problem requires the calculation of aqueous speciation, mineral saturation indices (SI), and redox potential (Eh) for a low-temperature (<150°C) geothermal groundwater. The temperature-pressure conditions are such that only two phases, liquid and solid, are considered. Coexisting mineral assemblages for the groundwater are presented as confirmation of the calculated SIs.

Objective. This problem provides a benchmark test of the routines for solving the equilibrium aqueous speciation and mineral solubility products or saturation indices for a two-phase, liquid water-rock system at a temperature of 100°-150°C.

Physical Description. This problem uses the data presented by Arnorsson and his coworkers (References AR-78, AR-82, and AR-83) on the hydrogeochemistry of the geothermal fields in southwest Iceland. Both the fluid chemistry and hydrothermal mineral alteration of this region have been studied intensely.

Table 6.1-1 presents a comparison of the range and average major-element composition of the middle Sentinel Bluffs and Umtanum flows and Icelandic basalt. This comparison indicates that, although there are variations in the percent distribution of the oxides of major elements, especially magnesium, the basaltic rocks of the Grande Ronde and Iceland are essentially similar, especially considering that the ranges overlap for most oxides. In comparing altered versus unaltered Icelandic basalts, Kristmannsdottir (Reference KR-75) found that the major changes in the altered rock are hydration and oxidation, with enrichment of SiO_2 in some samples.

The comparison of groundwater chemistry between the Grande Ronde and Icelandic basalts is presented in Table 6.1-2. The groundwater chemistry is very similar, although minor variations are again present. The Icelandic waters tend to be slightly more dilute with a mean total dissolved solids (TDS) content of almost 400 milligrams per liter (mg/l) while the Grande Ronde averages 900 mg/l. The maximum TDS in both the Icelandic and Grande Ronde samples is about 1,000 mg/l.

A major difference between the two waters is the fluoride content. The Icelandic groundwaters have only about 2 mg/l of fluoride, on average, while the Grande Ronde groundwaters have 8 to 16 times as much. This probably is due to a greater abundance of apatite minerals, although there is some question about apatite as the source of fluoride in Grande

Table 6.1-1

Comparison of Major-Element Composition
of Basaltic Rock of the Umtanum and Middle
Sentinel Bluffs Flow at the Hanford Site with
Basaltic Rock of Southwest Iceland (in weight percent)

Constituent	Umtanum[a]		Middle Sentinel Bluffs[a]		Icelandic Basalts[b]	
	Range	Mean	Range	Mean	Range	Mean
SiO_2	54.45-55.45	54.90	52.43-54.21	53.41	43.71-51.73	48.64
Al_2O_3	14.08-14.59	14.43	14.26-15.66	15.00	10.59-14.29	12.95
FeO	12.70-13.39	13.10	11.10-12.50	11.73	8.03-14.83	12.76
MgO	3.38- 3.71	3.48	4.46- 5.34	4.99	5.52-8.35	7.13
CaO	7.14- 7.64	7.30	8.16- 9.31	8.86	8.36-12.90	11.08
Na_2O	1.86- 2.95	2.66	1.44- 2.92	2.48	1.94- 4.31	2.58
K_2O	0.94- 1.71	1.48	0.51- 1.40	1.03	0.11- 1.13	0.32
TiO_2	2.12- 2.23	2.17	1.67- 2.11	1.79	0.50- 3.27	2.04

[a] From Reference RO-82, Table 6.1.

[b] Calculated from data in Reference KR-75, Tables 1 and 2.

Table 6.1-2

Major Ion Chemistry of Groundwaters in the Umtanum and Middle Sentinel Bluffs Flow at Hanford Site Compared to the Geothermal Waters in the Icelandic Basalts

Constituent	Umtanum Flow[a]		Middle Sentinel Bluffs[a]		Icelandic Basalts[b]	
	Range (mg/l)	Mean (mg/l)	Range (mg/l)	Mean (mg/l)	Range (mg/l)	Mean (mg/l)
HCO_3^-	45 - 102	60	64 - 118	89	6 - 326 [c]	32[c]
CO_3^{-2}	4 - 55	19	8 - 24	18		
Cl^-	98 - 289	194	117 - 297	199	5 - 390	51
SO_4^{-2}	4.2 - 191	121	4 - 197	133	6 - 302	48
NO_3^-	0.5	0.5	0.5	0.5	NR	NR
F^-	13 - 42	32	11 - 22	17	0.14 - 12	1.6
SiO_2 [d]	77 - 220	158	114 - 194	158	30 - 252	105
Na^+	161 - 360	274	163 - 350	247	24 - 185	74
K^+	3.3 - 8.1	5.9	12 - 16	14	0.1 - 5.1	2.9
Ca^{+2}	0.8 - 4.5	2.4	1.6 - 10	5.5	1 - 68	7.3
Mg^{+2}	0.01 - 0.15	0.04	0.08 - 0.17	0.14	0.01 - 5.6	0.17
pH [e]	8.8 - 10.1	9.5	9.3 - 9.6	9.5	6.63 - 10.48	9.78
TDS	626 - 1,071	886	600 - 1,201	857	90 - 965	363
Temperature (^oC)		58		51	18 - 157	76.5

(a) From Reference RO-82.

(b) From Reference AR-83.

(c) Reported as total carbonate.

(d) The values for the Umtanum and Middle Sentinel Bluffs flows were obtained by combining the molarity of $H_3SiO_4^-$ and $H_4SiO^o{}_4$ and converting to mg/l SiO_2.

(e) The values for the Umtanum and Middle Sentinel Bluffs flows were reported as determined in the field. The temperature at which pH was measured is not given. The Icelandic values are reported for a given temperature in the range of 11-25^o C.

Ronde groundwater (Reference RO-82). Finally, the pH and temperature range of the Icelandic groundwater represented in Table 6.1-2 bracket the ranges for the Grande Ronde analyses.

Alteration zones, or stable mineral assemblages versus temperature, have been described for the Icelandic geothermal systems (References KR-75 and AR-83). In general, for the low-temperature systems (<150°C), four zones of mineral alteration have been established based on temperature. Figure 6.1-1 presents the alteration zones described by Kristmannsdottir (Reference KR-75).

Although the temperature ranges of the zones in Figure 6.1-1 are very approximate, they do provide an estimate of the stable mineral assemblages that would be anticipated in the Icelandic basalts under low-temperature conditions. Even though this figure shows zones for only two locations in Iceland, comparison to other areas in Iceland has shown similar alteration zones (Reference KR-75).

Chabazite (a zeolite) and opal with minor calcite, levyne (a zeolite), smectite, and mixed-layer clays characterize Zone I in the temperature range up to about 70°-80°C. Between 70°-80°C and about 90°C, mesolite and scolecite (zeolites) are the alteration minerals characteristic of Zone II. Calcite and smectite also are found in Zone II along with minor amounts of several other zeolites and mixed-layer clays. Zone III occurs between about 90°C and 110°-120°C and is characterized by the dominance of the zeolite stilbite. Above about 120°C, Zone IV is characterized by laumontite, the stable zeolite, along with quartz, calcite, smectite, and minor mixed-layer clays.

<u>Assumptions</u>.

- The water sample represents a water from a single horizon.
- The water sample did not boil.

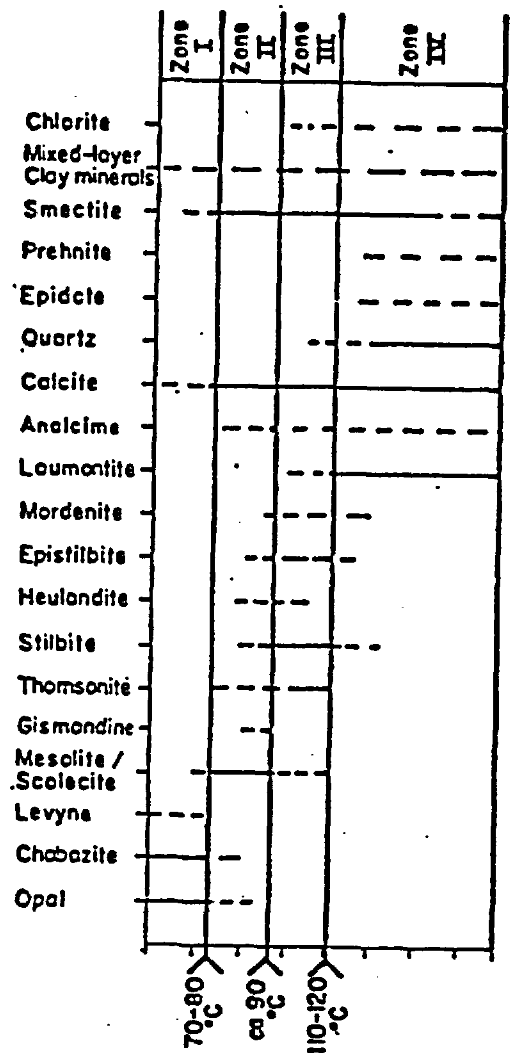

Figure 6.1-1

Alteration Mineral Zones found in the Reykjavik and Reykir Low-Temperature Area. The Rock Temperatures of the Zone Borders are Very Approximate (KR-1975)

- The mineral assemblage represents prograde alteration only.
- The water and minerals are at equilibrium.
- The redox system is at equilibrium and well poised.
- The Debye-Huckel theory adequately describes non-ideal behavior of dissolved ions.
- Mineral dissolution is congruent.
- Minerals are stoichiometric.
- The water has not interacted with casing or minerals nor solutes precipitated out of solution on the way to the surface.
- No degassing of the water sample occurred.

Input Specifications. The input data consist of measurements made on the surface. The input data for the low-temperature benchmark problem are presented in Table 6.1-3.

Output Specifications. The output for this problem will include the activity coefficients of the solutes, molal activities of aqueous species, ionic strength, ionic balance, Eh based on the H_2S-SO_4 redox couple, temperature based on the quartz and sodium-potassium geothermometers, and solubility products or saturation indices of important minerals.

6.2 Three-Phase, High-Temperature (>150°C) Equilibrium Speciation

Problem Statement. This problem requires the calculation of aqueous speciation, mineral saturation indices (SI), and redox potential (Eh) for a high-temperature (>150°C) geothermal groundwater. The temperature-pressure conditions are such that the water boils as it is withdrawn from the well prior to sampling. The model must calculate the geochemistry (i.e., temperature, aqueous speciation, SI, and Eh) of the water as it occurs in the aquifer. Alteration mineral assemblages for the host rock are presented as a confirmation of calculated SIs.

Table 6.1-3

Input Data for Low-Temperature Basalt Analog Benchmark Problem (Reykjavik, Iceland, Well 11)

Constituent	Concentration (in ppm unless otherwise noted)
SiO_2	147.8
B	0.05
Na	57.1
K	2.60
Ca	2.56
Mg	0.024
Fe	0.018
Al	0.18
CO_2 (total)	17.5
SO_4	19.4
H_2S (total)	0.41
Cl	36.4
F	0.82
TDS	345.0
pH, standard units at 20°C	9.44
Temperature, °C	129
Pumped Flow Rate at Sampling, l/s	25
Total Depth of Well, m	928

Source: Reference AR-82

Objectives. This problem is a test of the routines for calculating the activity coefficients, aqueous speciation, ionic strength, ionic balance, Eh based on the H_2S-SO_4, CH_4-CO_3, H_2-H_2O, and NH_3-NO_3 redox pairs; and the solubility products or saturation indices for important minerals in a three-phase, steam-water-mineral system. The problem also requires the code to back-calculate the original, in-situ chemical composition of the water by incorporating the chemical data on the steam sample collected with the water sample.

Physical Description. This problem uses the data presented by Arnorsson, et al., (Reference AR-82) on the analyses of the Krafla geothermal field (Well 7) in northern Iceland. Well 7 is 2,165 m deep, with producing zones at 825, 1,163, 1,700, and 2,000 m, having temperatures of 160, 206, 287, and 340°C, respectively. The chemical analysis for Well 7 is presented in Table 6.2-1.

The stable mineral assemblage for high-temperature geothermal systems determined from core samples in Iceland is presented in Figure 6.2-1. Minerals that may occur at temperatures over 250°C include quartz, calcite, fluorite (which may not be present), anhydrite, low albite, microcline (potassium feldspar), mixed-layer clays, chlorite, wairakite or prehnite, pyrite, iron hydroxides, and epidote.

Asssumptions.

- The water sample represents water from a single horizon.
- Flashing to steam due to pumping does not extend into the aquifer.
- The mineral assemblage represents prograde alteration only.
- The water and minerals are at equilibrium.
- The redox system is at equilibrium and well poised.
- The water has not interacted with or precipitated any substances on its path to the surface.
- The amount of degassing of the water sample can be closely estimated.

Table 6.2-1

Input Data for High-Temperature Basalt Analog Benchmark Problem (Krafla, Iceland, Well 7)

Constituent	Concentration (in ppm unless otherwise noted)
<u>Water Sample</u>	
SiO_2	766.8
B	1.50
Na	193.0
K	36.0
Ca	1.90
Mg	0.067
Fe	8.78
Al	0.21
CO_2 (total)	186.6
SO_4	143.0
H_2S (total)	22.2
Cl	52.0
F	1.03
TDS	1,389.0
pH	--
<u>Condensate Sample</u>	
CO_2	14,680.0
H_2S	381.0
<u>Gas with Condensate (Vol. %)</u>	
CO_2	--
H_2S	--
H_2	2.5
CH_4	0.1
N_2	0.7
Liters gas/kg condensate/^oC	8.50/20
Sampling pressure, bars abs	5.5
Discharge enthalpy, kcal/kg	383.0
Flow, kg/sec	12.0
Quartz Geothermometer, ^oC	269.5

Source: Reference AR-83

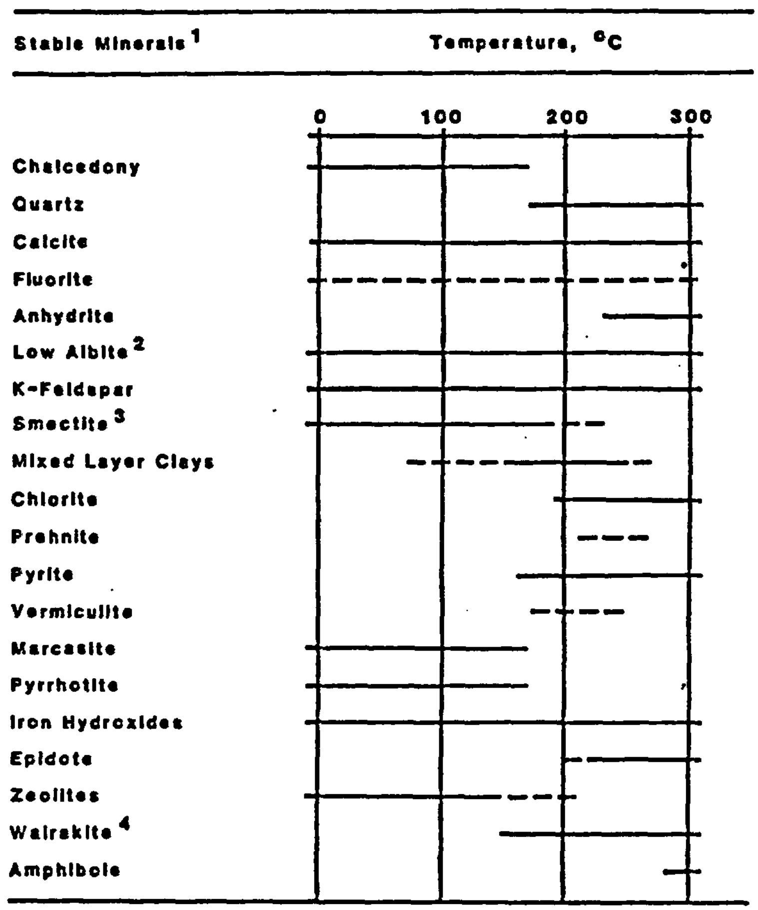

[1] Modified from AR-83 and KR-75.

[2] Upon cooling when under 100°C, analcime may become stable, especially in olivine basalts.

[3] Smectite gradually alters to chlorite between 200-240°C via mixed layer clay minerals. Mixed layer clays begin to appear at about 100°C.

[4] May also have prehnite.

Figure 6.2-1

Empirically Determined Stable Mineral Assemblages for Geothermal Waters in Icelandic Basalts in the Temperature Range of 0-300°C and Pressure Less Than 14 MPa

Input Specifications. The input chemical data for this problem are presented in Table 6.2-1.

Output Specifications. A solution to this problem has been calculated previously (Reference AR-82) and is presented in Table 6.2-2, which lists the input data (i.e., the chemical analysis and deep-water temperature and pressure); the calculated deep-water chemistry after the vapor phase is recombined with the liquid; and the activity coefficients for the various species, the activities, ionic strength, ion balance, geothermometric temperatures, Eh, and the solubility products for 26 minerals. Table 6.2-3 lists the saturation indices (SI) computed from data in Table 6.2-2 and compares the SI values with the mineral assemblage determined empirically.

6.3 Hypothetical Radionuclide Equilibrium Speciation and Mineral Solubility

Problem Statement. This test problem presents data on a hypothetical case involving the determination of solubility contols under high temperatures on radionuclides in groundwater in clastic sedimentary strata. This problem requires the calculation of aqueous speciation and mineral saturation indices for major constituents and radionuclides at temperatures ranging from ambient (50° to 100°C) to a maximum of about 400°C. Pressures vary from about 30 to 300 MPa.

Objectives. This test problem serves as a benchmark of a geochemical code for the calculation of the aqueous speciation and mineral saturation indices for radionuclides in a high-temperature environment similar to the near-field.

Problem Description. The Oklo uranium ore district in Gabon, Africa, reached criticality through natural processes about two billion years ago and maintained a nuclear reaction for an estimated 500,000 years. The ore formed initially at about the same time as the formation of the host

Table 6.2-2

Output of the Program WATCH1 Showing Original Input Data, Correction of Surface Sample to Deep Water, and Calculation of Aqueous Speciation and Solubility Products for 26 Minerals

3049 KRAFLA WELL 7

PROGRAM WATCH1.

WATER SAMPLE (PPM)		STEAM SAMPLE				
pH/DEG.C	8.52/20.0	GAS (VOL.%)		REFERENCE TEMP.	DEGREES C.	0.0 (QTZ)
SiO_2	766.80	CO_2	94.00			
NA	193.00	H_2S	2.70	Sampling Pressure	BARS ABS.	5.5
K	36.00	H_2	2.50	Discharge Enthalpy	MJOUL/KG	1.601 (Measured)
CA	1.90	O_2	0.00	Discharge	KG/SEC.	12.0
MG	0.067	CH_4	0.10			
CO_2	186.60	N_2	0.70	Measured Temperature	Degrees C	0.0
SO_4	143.00			Resistivity/Temp.	OHMM/DEG.C	11.1/20.0
H_2S	22.20			EH/Temp.	MV/DEG.C	0.000/0.0
CL	52.00					
F	1.03	Liters Gas Per Kg				
Diss. Solids	1389.00	Condensate/Deg.C	8.50/20.0			
AL	0.2100					
B	1.5000					
FE	8.7800	Condensate (PPM)				
NH_3	0.0950	pH/Deg.C	0.00/0.0			
NO_3	0.001	CO_2	0.00			
PO_4	0.002	H_2S	0.00			
O		NA	0.00			
		Condensate with NAOH (PPM)				
		CO_2	14680.00			
		H_2S	380.80			

Measured Downhole Temp. Degrees C	Meters	Fluid Inflow Depth (Meters)
112.0	200.0	825.0
147.0	600.0	1163.0
176.0	900.0	1700.0
197.0	1100.0	2000.0
213.0	1300.0	0.0
231.0	1500.0	0.0
242.0	1600.0	0.0
287.0	1700.0	0.0
335.0	1800.0	0.0
342.0	1900.0	0.0
342.0	2100.0	0.0

(continued)

Table 6.2-2 (continued)

Ionic Strength = 0.01143

Ionic Balance:

Cations	(Mol. Eq.)	0.00962867
Anions	(Mol. Eq.)	0.00981502
Difference	(%)	-1.92

Deep Water (PPM)				Deep Steam (PPM)		Gas Pressures (Bars ABS.)	
SiO_2	569.32	CO_2	2102.43	CO_2	19816.86	CO_2	0.443E+00
NA	143.28	H_2S	126.83	H_2S	346.18	H_2S	0.999E-02
K	26.72	H_2	0.71	H_2	28.34	H_2	0.138E-01
CA	1.41	O_2	0.00	O_2	0.00	O_2	0.183E-34
MG	0.050	CH_4	0.15	CH_4	9.21	CH_4	0.565E-03
SO_4	106.16	N_2	2.33	N_2	111.19	N_2	0.390E-02
CL	38.60	NH_3	0.06	NH_3	0.03	NH_3	0.180E-05
F	0.76					H_2O	0.546E+02
Diss. S	1031.19					Total	0.551E+02
AL	0.1559						
B	1.1135			H_2O (%)	26.14		
FE	6.5186			Boiling Portion	0.26		

Gas Solubility Multiplying Factor: 0.10

(continued)

Table 6.2-2 (continued)

ACTIVITY COEFFICIENTS IN DEEP WATER

H^+	0.849	KSO_4	0.834	FE^{++}	0.491	$FECL^+$	0.828
OH^-	0.826	F^-	0.826	FE^{+++}	0.229	AL^{+++}	0.229
$H_3SiO_4^-$	0.828	CL^-	0.823	$FEOH^+$	0.833	$ALOH^{++}$	0.485
$H_2SiO_4^{--}$	0.485	NA^+	0.828	$FE(OH)_3^-$	0.833	$AL(OH)_2^+$	0.834
$H_2BO_3^-$	0.821	K^+	0.823	$FE(OH)_4^{--}$	0.481	$AL(OH)_4^-$	0.830
HCO_3^-	0.828	CA^{++}	0.491	$FEOH^{++}$	0.481	$ALSO_4^+$	0.830
CO_3^{--}	0.476	MG^{++}	0.510	$FE(OH)_2^+$	0.834	$AL(SO_4)_2^-$	0.830
HS^-	0.826	$CAHCO_3^+$	0.837	$FE(OH)_4^-$	0.834	ALF^{++}	0.485
S^{--}	0.481	$MGHCO_3^+$	0.828	$FESO_4^+$	0.833	ALF_2^+	0.834
HSO_4^-	0.830	$CAOH^+$	0.837	$FECL^{++}$	0.481	ALF_4^-	0.830
SO_4^{--}	0.470	$MGOH^+$	0.839	$FECL_2^+$	0.833	ALF_5^{--}	0.476
$NASO_4^-$	0.834	NH_4^+	0.821	$FECL_4^-$	0.828	ALF_6^{---}	0.188

CHEMICAL COMPONENTS IN DEEP WATER (PPM AND LOG MOLE)

H^+(ACT.)	0.00	-6.692	MG^{++}	0.01	-6.425	$FE(OH)_3$	1.42	-4.878
OH^-	0.97	-4.244	NACL	0.74	-4.899	$FE(OH)_4^-$	12.82	-3.985
H_4SiO_4	907.17	-2.025	KCL	0.05	-6.136	$FECL^+$	0.00	-12.622
$H_3SiO_4^-$	3.21	-4.472	$NASO_4^-$	12.44	-3.981	$FECL_2$	0.00	-16.690
$H_2SiO_4^{--}$	0.00	-9.149	KSO_4^-	12.04	-4.050	$FECL^{++}$	0.00	-23.451
NAH_3SiO_4	0.33	-5.554	$CASO_4$	1.33	-5.011	$FECL_2^+$	0.00	-25.819

(continued)

Table 6.2-2 (continued)

H_3BO_3	6.34	-3.989	$MGSO_4$	0.16	-5.864	$FECL_3$	0.00	-28.935
$H_2BO_3^-$	0.03	-6.357	$CACO_3$	0.05	-6.265	$FECL_4^-$	0.00	-32.395
H_2CO_3	2748.07	-1.354	$MGCO_3$	0.00	-8.741	$FESO_4$	0.00	-11.926
HCO_3^-	210.42	-2.462	$CAHCO_3^+$	2.05	-4.692	$FESO_4^+$	0.00	-21.412
CO_3^{--}	0.01	-6.945	$MGHCO_3^+$	0.01	-7.019	AL^{+++}	0.00	-25.071
H_2S	111.60	-2.485	$CAOH^+$	0.00	-7.220	$ALOH^{++}$	0.00	-16.562
HS^-	14.78	-3.350	$MGOH^+$	0.01	-6.691	$AL(OH)_2^+$	0.00	-8.958
S^{--}	0.00	-11.265	NH_4OH	0.12	-5.463	$AL(OH)_3$	0.45	-5.239
H_2SO_4	0.00	-11.778	NH_4^+	0.00	-7.314	$AL(OH)_4^-$	0.00	-8.239
HSO_4^-	3.70	-4.419	FE^{++}	0.00	-11.555	$ALSO_4^+$	0.00	-23.571
SO_4^{--}	82.84	-3.064	FE^{+++}	0.00	-26.768	$AL(SO_4)_2^-$	0.00	-23.946
HF	0.05	-5.579	$FEOH^+$	0.00	-10.110	ALF^{++}	0.00	-19.822
F^-	0.71	-4.425	$FE(OH)_2$	0.00	-9.600	ALF_2^+	0.00	-16.395
CL^-	38.13	-2.968	$FE(OH)_3^-$	0.00	-9.675	ALF_3	0.00	-15.364
NA^+	140.53	-2.214	$FE(OH)_4^{--}$	0.00	-15.008	ALF_4^-	0.00	-16.540
K^+	23.21	-3.226	$FE(OH)^{++}$	0.00	-17.479	ALF_5^{--}	0.00	-19.181
CA^{++}	0.18	-5.346	$FE(OH)_2^+$	0.00	-9.450	ALF_6^{---}	0.00	-23.506

(continued)

Table 6.2-2 (continued)

IONIC STRENGTH = 0.00770 IONIC BALANCE : CATIONS (MOL.EQ)0.00673669
ANIONS (MOL.EQ)0.00692810
DIFFERENCE (%) -2.80

CHEMICAL GEOTHERMOMETERS DEGREES C 1000/T DEGREES KELVIN = 1.84

QUARTZ	269.5
CHALCEDONY	999.9
NAK	258.9

OXIDATION POTENTIAL (VOLTS) : EH H_2S = -0.601 EH CH_4 = -0.643 EH H_2 = -0.731 EH NH_3 = -0.608

LOG SOLUBILITY PRODUCTS OF MINERALS IN DEEP WATER

	THEOR.[a]	CALC.[b]		THEOR.	CALC.		THEOR.	CALC.
ADULARIA	-14.371	-14.705	ALBITE LOW	-13.939	-13.690	ANALCIME	-11.571	-11.665
ANHYDRITE	-8.469	-9.047	CALCITE	-13.281	-12.922	CHALCEDONY	-1.919	-2.025
MG-CHLORITE	-86.501	-84.913	FLUORITE	-11.065	-14.670	GOETHITE	3.371	0.263
LAUMONDITE	-24.733	-24.393	MICROCLINE	-14.992	-14.705	MAGNETITE	-15.026	-19.992
CA-MONTMOR.	-72.582	-72.752	K-MONTMOR.	-33.855	-36.860	MG-MONTMOR.	-74.088	-73.815
NA-MONTMOR.	-34.140	-35.844	MUSCOVITE	-17.838	-16.690	PREHNITE	-38.016	-36.676
PYRRHOTITE	-9.942	-25.522	PYRITE	-27.340	-29.908	QUARTZ	-2.025	-2.025
WAIRAKITE	-24.946	-24.393	WOLLASTONITE	7.165	5.704	ZOISITE	-38.875	-37.669
EPIDOTE	-38.541	-36.414	MARCASITE	-11.186	-29.908			

[a]THEOR = Logarithm of the theoretical solubility product at equilibrium, which is equivalent to the logarithm of the equilibrium constant (log K).

[b]CALC = Logarithm of the calculated solubility product (log Q).

Source: Reference AR-82

Table 6.2-3

Calculated Mineral Saturation Indices (SI) for Benchmark Problem 6.2 and Comparison with Empirical Stable Mineral Assemblages from Figure 6.2-1

Mineral	SI[a]	Empirical Assemblages[b]
Adularia	-0.334	
Albite, Low	+0.249	+
Analcime	-0.094	
Anhydrite	-0.578	+
Calcite	+0.359	+
Chalcedony	-0.106	
Mg-Chlorite	+1.588	+
Epidote	+2.127	+
Fluorite	-3.605	+
Goethite	+3.108	+
Laumondite	+0.340	
Microcline	+0.287	+
Magnetite	-4.966	
Marcasite	-18.722	
Ca-Montmorillonite	-0.170	
K-Montmorillonite	-3.005	
Mg-Montmorillonite	+0.273	
Na-Montmorillonite	-1.704	
Muscovite	+1.148	
Prehnite	+1.340	+
Pyrrhotite	-15.580	
Pyrite	-2.568	+
Quartz	0.000	+
Wairakite	+0.553	+
Wollastonite	-1.461	
Zoisite	+1.206	+

[a] SI = log Q - log K

[b] "+" means mineral is generally present, and a blank means it is absent at the temperature range under consideration.

rock, an argillaceous sandstone-shale-carbonate-conglomerate sequence named the Francevillian Series. The primary host rocks were argillaceous sandstones and sandy shales. Tilting and fracturing of the host rock soon after its formation created open fractures that were later filled in with clay. At about the same time, the uranium ore in the argillaceous sandstone was remobilized. As the remobilized uranium migrated through the clay-filled fractures, reducing conditions caused the uranium to precipitate, resulting in an enriched pitchblende of 50 to 70 percent uranium content. Major gangue minerals associated with the enriched ore include chlorite, illite, carbonates, barite, chalcopyrite, pyrite, and hematite (Reference BR-84a).

During the nuclear reactions that occurred, temperatures in the ore body are thought to have reached over 400°C while, in the host rock, the temperatures probably remained under 250°C and rapidly decreased away from the ore body. It has been estimated that temperatures beyond 1 m of the ore body were below 200°C (Reference BR-84a). The ambient temperature of this region is thought to range from 50° to 150°C due to a regional geothermal gradient of 40°-50°C per kilometer of depth (Reference BR-84a).

Although no data on groundwater chemistry are known to have been published, or collected (Reference BR-84b), some idea of the ambient groundwater quality has been formulated. The Oklo hydrothermal system was low in chloride, ammonia, and cyanide and relatively low in sulfur (Reference BR-84b).

Since there are similarities between the primary Oklo ore genesis and the uranium ore genesis in the Grants Mineral Belt of New Mexico, it is possible to construct a hypothetical groundwater analysis for the Oklo site prior to the nuclear reaction. Table 6.3-1 presents a typical chemical analysis for groundwater from the Westwater Canyon Member of the Morrison Formation in the Grants Mineral Belt. The depth of samples comparable to that in Table 6.3-1 is about 250 m. This analysis compares favorably with the qualitative estimates of Brookins (Reference BR-84a) as stated above.

Table 6.3-1

Chemical Analysis of Groundwater from the Westwater Canyon Member of the Morrison Formation, Grants Mineral Belt, New Mexico

Constituent	Concentration mg/l
Ca	35.0
Mg	15.0
Na	100.0
K	6.0
HCO_3	250.0
SO_4	200.0
Cl	10.0
F	1.0
Si	16.0
Fe	0.2
B	0.2
NH_4	0
pH	8.0
Eh	-0.3
Temperature	21°C
Depth	250 m

Source: Modified from Reference ST-83

Brookins (Reference BR-84a) has developed Eh-pH diagrams for several constituents. Figure 6.3-1 presents an Eh-pH diagram for the system uranium-silicon-sulfur-carbon-hydrogen-oxygen at 25°C and 1 bar (10^5 Pa) pressure. The stability region for uraninite (UO_2), the ore in both the Oklo and Grants districts, is in the pH range of about 7 to 9 and the Eh range below about -0.1 volts.

Assumptions.

- The hypothetical chemical analysis presented in Table 6.3-1 represents an analysis of major chemical components in groundwater of the Francevillian sedimentary rocks at Oklo.
- The pH-Eh can be approximated from the stability diagram of Figure 6.3-1.
- Equilibrium between minerals and solution is maintained at all temperatures in the hypothetical system.
- The production and release of fission products at Oklo can be approximated as an instantaneous event (this is a reasonable assumption considering the 2 billion year total time scale).
- The temperature of the pitchblende immediately increased to 400°C. A zone out to about 1 m attained an average temperature of 250°C, and beyond about 1 m from the ore, the temperature was ambient.

Input. The initial input data for the test problem are presented in Table 6.3-1. The beginning mineral assemblage is quartz, chlorite, illite, carbonate, barite, chalcopyrite, pyrite, hematite, and pitchblende.

Fission products include those listed in Table 6.3-2.

Output. The output consists of activities of aqueous species for the major constituents listed in Table 6.3-1 and the products listed in Table 6.3-2. Mineral saturation indices for solid phases incorporating those constituents are calculated.

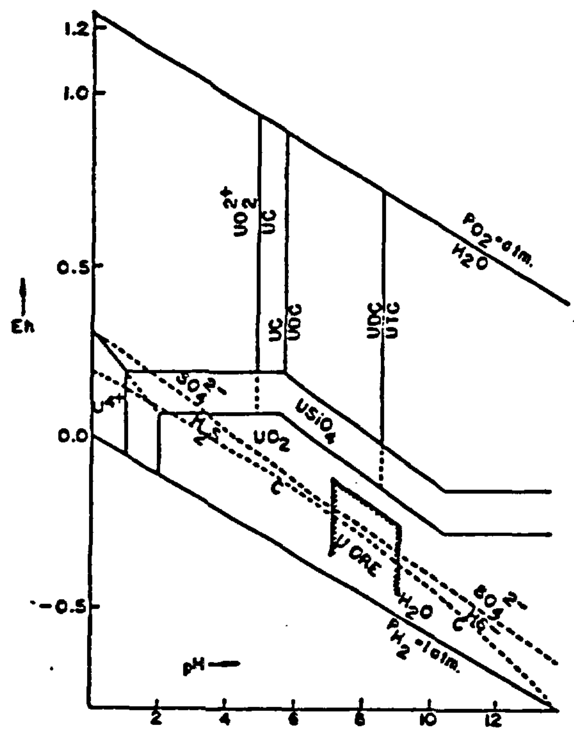

Figure 6.3-1

Eh-pH Diagram for Part of the System U-Si-S-COH-O at 25°C and 10^5 Pa Pressure (BR-84)

Table 6.3-2

Fission and Nonfission Products from the
Oklo Nuclear Reaction

Selenium
Bromine
Rubidium
Strontium
Yttrium
Zirconium
Niobium
Molybdenum
Technetium
Ruthenium
Rhodium
Palladium
Silver
Cadmium
Indium
Tin
Antimony
Tellurium
Iodine
Xenon
Cesium
Barium
REE[a,b]
Lead
Bismuth
Thorium
Uranium
Transuranics[b]

[a] Rare earth elements

[b] Transuranic elements and REE are each combined since the elements in each group behave similarly.

For comparison, studies of the Oklo site have indicated the relative mobility of the reaction products. Based on field observations and predictions from Eh-pH diagrams, Brookins prepared the analyses presented in Table 6.3-3 (Reference BR-84a).

6.4 Reaction-Path Problem with Cooling

Problem Statement. This problem requires the calculation of aqueous speciation, mineral saturation indices, and the mass transfer of minerals and gases as the result of cooling along the flow path for a high-temperature brine. Comparisons between predicted and observed water chemistry and between predicted mineral-water reactions and known mineralogy serve to validate the geochemical mass transfer code.

Objectives. The features of the code being tested are the calculations of aqueous speciation, activities of species, mineral saturation, mass balance, and mass transfer. The mass transfer calculations predict the reactions of minerals and gases within the water-rock system and the associated transfer of mass into or out of the aqueous solution. Predictions of mineral dissolution, precipitation, or alteration are considered a function of temperature.

Problem Description. A geochemical model of the evolution of deep-sea brines in the Red Sea geothermal systems by Shanks and Bischoff (Reference SH-77) is used as a near-field test problem for the benchmarking of reaction-path geochemical models. The problem involves the analysis of the geochemistry of a natural geothermal brine and the subsequent alteration of that brine as it cools, but does not mix with Red Sea waters, upon exiting the subsurface at the bottom of the Atlantis II Deep in the central Red Sea. The changes in the brine chemistry are to be used in the predictions of mass transfer, i.e., mineral precipitation or dissolution, that occurs during cooling.

Although accurate determinations of the subsurface brine are not available, data for deep Red Sea brine just above the sediment-water interface have allowed the extrapolation back to the original brine chemistry

Table 6.3-3

Observed Mobility of Important Elements at Oklo Compared to Predicted Mobilities Based on Eh-pH Diagrams

Element	Observed Relative Mobility	Predictions of Relative Mobility Based on Diagrams 25°C	200°C
Krypton	Most migrated	Not applicable	Not applicable
Rubidium	Probable local redistribution	Not applicable	Not applicable
Strontium	Probable local redistribution	Not applicable	Not applicable
Yttrium	Most retained	Retention	Retention
Zirconium	Most retained; some local redistribution	Retention	Some migration
Niobium	Most retained	Retention	Retention
Molybdenum	Most migrated	Migration	Migration
Technetium	Local redistribution	Retention	Migration (?)
Ruthenium	Local redistribution	Retention	Minor migration
Rhodium	Most retained	Retention	Retention
Palladium	Most retained	Retention	Retention
Silver	Most retained	Retention	Retention
Cadmium	Most migrated	Migration	Migration
Indium	Most retained	Retention	Retention
Tin	Not yet studied	Retention	Retention
Antimony	Not yet studied	Possible migration	Some migration
Tellurium	Not yet studied	Retention	Retention
Iodine	Most migrated	Not applicable	Not applicable
Xenon	Most migrated	Not applicable	Not applicable
Cesium	Most migrated (?; perhaps locally)	Not applicable	Not applicable
Barium	Local redistribution	Not applicable	Not applicable
REE	Most retained	Retention	Retention

(continued)

Table 6.3-3 (continued)

Element	Observed Relative Mobility	Predictions of Relative Mobility Based on Diagrams 25°C	200°C
Lead	Variable migration	Retention or local redistribution	Some migration
Bismuth	Most retained	Retention or local redistribution	Some migration
Polonium	Most retained	Retention	Retention
Thorium	Most retained	Retention	Retention
Uranium	Some local redistribution	Retention or local redistribution	Retention
Neptunium	Most retained	Retention	Retention
Plutonium	Most retained	Retention	Retention
Americium	Not measureable	Retention	Retention

Source: Reference BR-84a

and temperature. The brine chemistry in the lower layer of the Red Sea in Atlantis Deep II has a chlorinity of 156 parts per thousand and essentially represents original brine unmixed with sea water (Reference SH-77).

The initial brine temperature has been estimated by several methods to range from 150-261°C. A temperature of 250°C for the original geothermal brine has been assumed (Reference SH-77). The temperature of the brine after entering the Red Sea has been measured at 60°C.

A second major assumption concerns the presence of hydrogen. Although hydrogen sulfide has not been detected in the brine, some sulfide minerals are forming. Since the sulfate concentration (840 ppm) in the brine is high, the hydrogen sulfide concentration should be very low (Reference SH-77).

The sulfate-sulfide equilibrium distribution and the concentration of sulfide species can be obtained from the oxygen fugacity determined by the magnetite-hematite equilibrium:

$$\underset{\text{Hematite}}{3Fe_2O_3} = \underset{\text{Magnetite}}{2Fe_3O_4} + 1/2\ O_2 \qquad (150)$$

The temperature-dependent equilibrium constant for this reaction can be determined from the data supplied by Helgeson (Reference HE-69).

Finally, the pH of the brine as a function of temperature has been estimated using an experimentally determined pH of 5.5 for cooled brine samples at 25°C, plus a mass balance relation for hydrogen-bearing species at higher temperatures.

The reaction path model requires the calculation of saturation indices to indicate the controlling mineral-water reactions. Mass balances for those controlling reactions are calculated to determine the mass transfer such that the change in the number of moles of an aqueous species along a flow path is equal, but of opposite sign, to the change in moles of the solid mineral phases that incorporate that species. In this case, the flow path is from the subsurface region with a temperature of 250°C to the Red Sea brine at the sediment-seawater interface where the temperature of the brine has cooled to 60°C.

Assumptions. All the assumptions of the reaction path model incorporate those of the equilibrium speciation model:

- Homogeneous equilibrium is maintained throughout the reaction paths.
- The Debye-Huckel theory adequately describes the non-ideal behavior of dissolved ions.
- Mass and charge are conserved.
- Mineral dissolution is congruent.
- Mineral formulas are stoichiometric.

In addition, it is assumed for this test problem:

- That the maximum temperature of the original brine is accurately estimated to be 250°C
- That the activity of hydrogen sulfide can be accurately estimated from the oxygen fugacity that is fixed by the magnetite-hematite equilibrium
- That the oxygen fugacity determined as a function of temperature is valid
- That the pH as a function of temperature can be accurately estimated on the basis of the empirical method described above
- That the overall chemical composition of the brine has not changed

Input. The input data are presented in Table 6.4-1.

Table 6.4-1

Input Data for the Red Sea Brine

Constituent	Vented Brine Concentration (mg/kg)	Red Sea Brine Concentration (mg/kg)
Na	92,600	92,600
K	1,870	1,870
Mg	764	764
Ca	5,150	5,150
Cl	156,030	156,030
SO_4	840	840
Total CO_2 (as HCO_3)	140	140
Ba	0.9	0.9
Cu	0.26	0.26
F	less than 0.02	less than 0.02
Fe	81.0	81.0
Li	4.4	4.4
Mn	82.0	82.0
Pb	0.63	0.63
Si	27.6	27.6
Zn	5.4	5.4
Temperature	250°C	60°C
log fO_2	-33	-60
pH	4.0	5.4

Source: Reference SH-77

Output. Output for this test problem includes aqueous speciation and activities, mineral saturation indices (ion activity product divided by the equilibrium constant), and mass transfer calculations. The mass transfer calculations will consist of changes in the mass of each dissolved constituent per unit mass of water (i.e., moles per kilogram of water).

As a partial validation, saturation indices for important minerals have been calculated as a function of temperature (Reference SH-77) and are presented in Figure 6.4-1.

6.5 Reaction Kinetics Problem

Problem Statement. This problem requires the solution of the rate of change over time in the concentration of an aqueous species or the rate of change over time in the mass per unit volume of a solid. The rate of change in concentration or mass is to be solved at an elevated temperature. Experimental results are provided for comparison.

Objectives. The features of a kinetics code being tested are the data base of rate constants utilized for the reactions, the temperature functions of the rate constants, and the aqueous speciation and activities under nonequilibrium conditions.

Problem Description. Experimental work has been completed on the water-rock-spent fuel interactions under controlled temperatures ranging from 100°C to 300°C and 30 MPa (Reference MY-83). The experimental method involved an essentially closed system using gold bags heated in an autoclave. During the run of an experiment, samples of fluid were periodically withdrawn for chemical analysis. The ratio of groundwater to basalt to simulated spent fuel was 20:1:1.

Alteration minerals observed in the experimental mixture of groundwater, basalt, and simulated spent fuel included saponite (smectite), illite, microcline, and poorly crystalline silica. The spent fuel was largely unaltered except for a surface alteration product that was tentatively

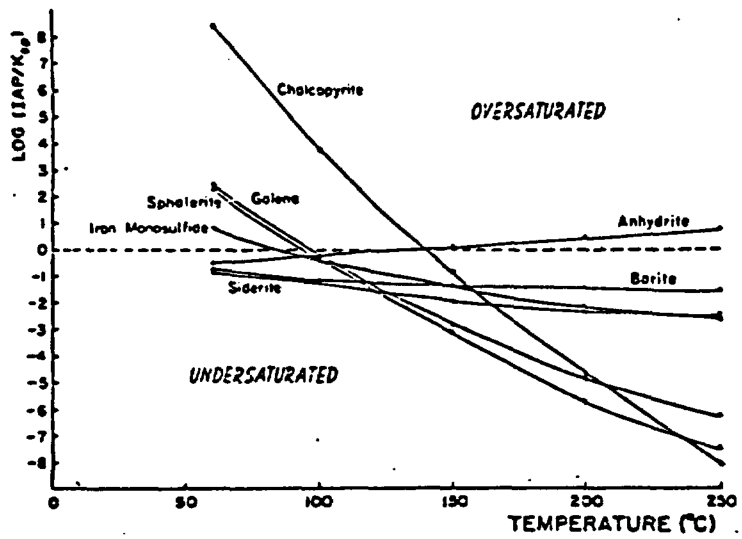

Figure 6.4-1

Degree of Saturation of the Red Sea Geothermal Brine with Respect to Various Hydrothermal Minerals, Expressed as a Ratio of Ion Activity Product to Solubility Product Constant (IAP/Ksp) For Each Mineral (SH-77) identified as weeksite ($K_2(UO_2)_2(Si_2O_5)_3 \cdot 4H_2O$) or boltwoodite ($K_2(UO_2)_2(SiO_3)_2(OH)_2 \cdot 5H_2O$). A minor amount of scheelite ($CaWO_4$) also was detected as an alteration product.

Results of the chemical analyses indicated concentrations arrived at approximate equilibrium values in the closed system during the run of the experiments (Reference MY-83).

Assumptions.

- The experimental method represents a closed system. Fluid samples withdrawn periodically are small enough so that the overall chemical composition of the fluid is not affected.
- The closed system of the experimental setup approximates the real physico-chemical conditions of the near-field environment, i.e., fluid residence times are very long and local equilibrium between solution and minerals is approached.
- Experimental apparatus is inert with respect to all components in the simulated spent fuel-groundwater-basalt mixture.
- Simulated components such as spent fuel and groundwater are representative of the actual components.

Input. The mass ratio of the spent fuel to groundwater to basalt is 1:20:1. Three constant temperature conditions, 100°, 200°, and 300°C, and a single pressure condition, 30 MPa, are applied to the experimental mixture.

The basalt is from the entablature of the Umatanum flow of the Grande Ronde Basalt with the chemical and mineralogic composition shown in Table 6.5-1.

The synthetic groundwater, representative of that occurring in the Grande Ronde Basalt, has the chemical composition presented in Table 6.5-2.

Table 6.5-1

Chemical Analysis of Grande Ronde Basalt Sample RUE-1

Component	Weight %	Estimated (wt. %) Uncertainty
SiO_2	55.59	0.88
TiO_2	2.21	0.04
Al_2O_3	13.71	0.27
Fe_2O_3	3.68	0.07
FeO	10.24	0.25
MnO	0.24	0.02
MgO	3.79	0.26
CaO	7.31	0.11
Na_2O	2.95	0.29
K_2O	1.63	0.06
P_2O_5	0.35	0.02
Total	101.70	

Modal Mineralogy

	Weight %
Plagioclase (AN_{40})	28.7
Pyroxene	17.1
Mesostasis	47.7
Titaniferous magnetite	5.12
Chlorophaeite	1.65
	100.27

Source: Reference MY-83

Table 6.5-2

Composition of Synthetic Groundwater

Dissolved Constituent	Concentration in mg/L GR-3
Na^+	358
K^+	3.4
Ca^{2+}	2.8
Mg^{2+}	0.032
Cl^-	312
CO_3^{2-}	12.9
HCO_3^-	42.9
F^-	33.4
SO_4^{2-}	173
SiO_2	76.2
pH	9.9

Source: Reference MY-83

The simulated spent fuel chemical composition is presented in Table 6.5-3.

Output. The output consists of the change in concentration over time of aqueous species, the dissolution/precipitation rates of initial solid-phase components, and the precipitation rates of new solid-phase components.

Figure 6.5-1 presents results of experiments on the pH as measured in a sample cooled to 25°C, and Figure 6.5-2 presents the pH values as corrected to the original temperature of 100°, 200°, or 300°C (Reference MY-83).

Figure 6.5-3 presents plots of concentration in solution versus time for sodium and silicon at the three temperatures. Figures 6.5-4 through 6.5-7 present similar plots for chloride and sulfate, iodine, strontium and uranium, and cesium and molybdenum, respectively.

Table 6.5-3

Chemical Analysis of Simulated Spent Fuel*

Component	Weight %	Component	Weight %
UO_2	96.09	Te	0.05
ThO_2	0.95	Sr	0.07
Y_2O_3	0.05	Ba	0.15
CeO_2	0.26	Pr	0.10
Mo	0.30	Sm	0.56
Pd	0.30	Zr	0.32
Cs	0.26	Re	0.13
I	0.02		

* Minor components have been tabulated as the element for use in inventory calculations.

Source: Reference MY-83

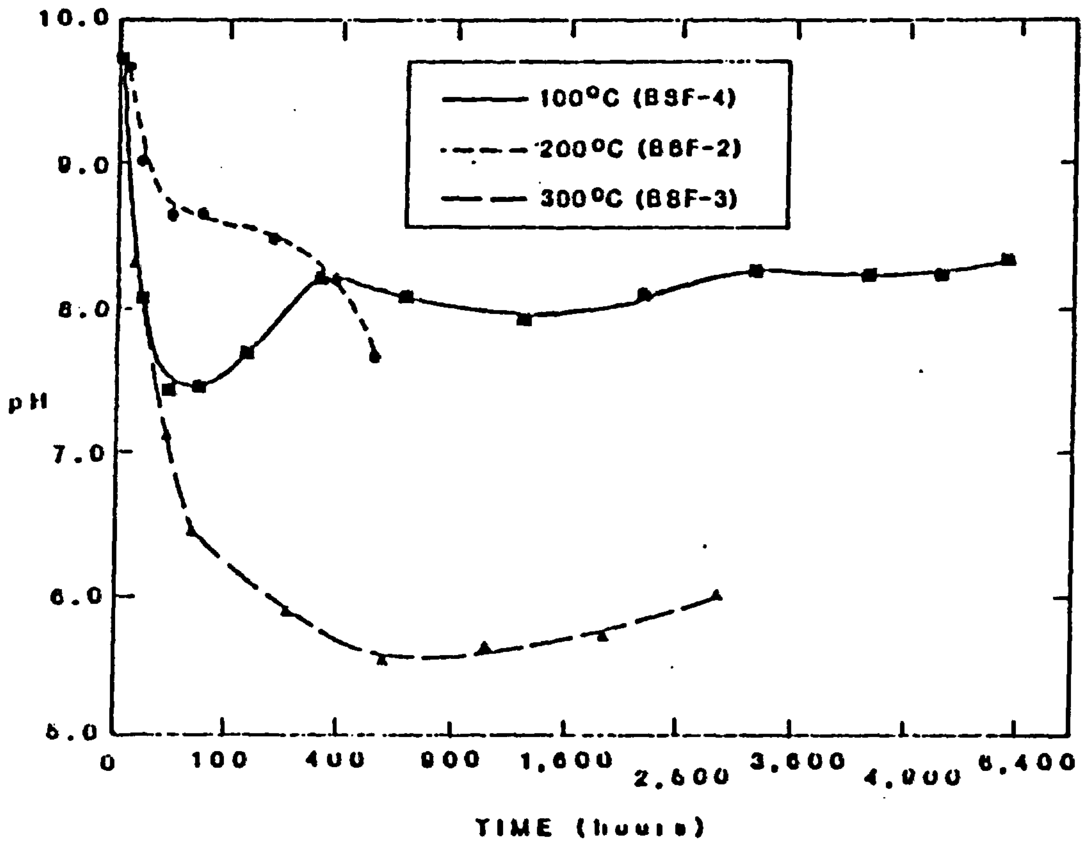

Figure 6.5-1

Effect of Temperature on Measured pH Values for Simulated Spent Fuel Plus Basalt (AP-83)

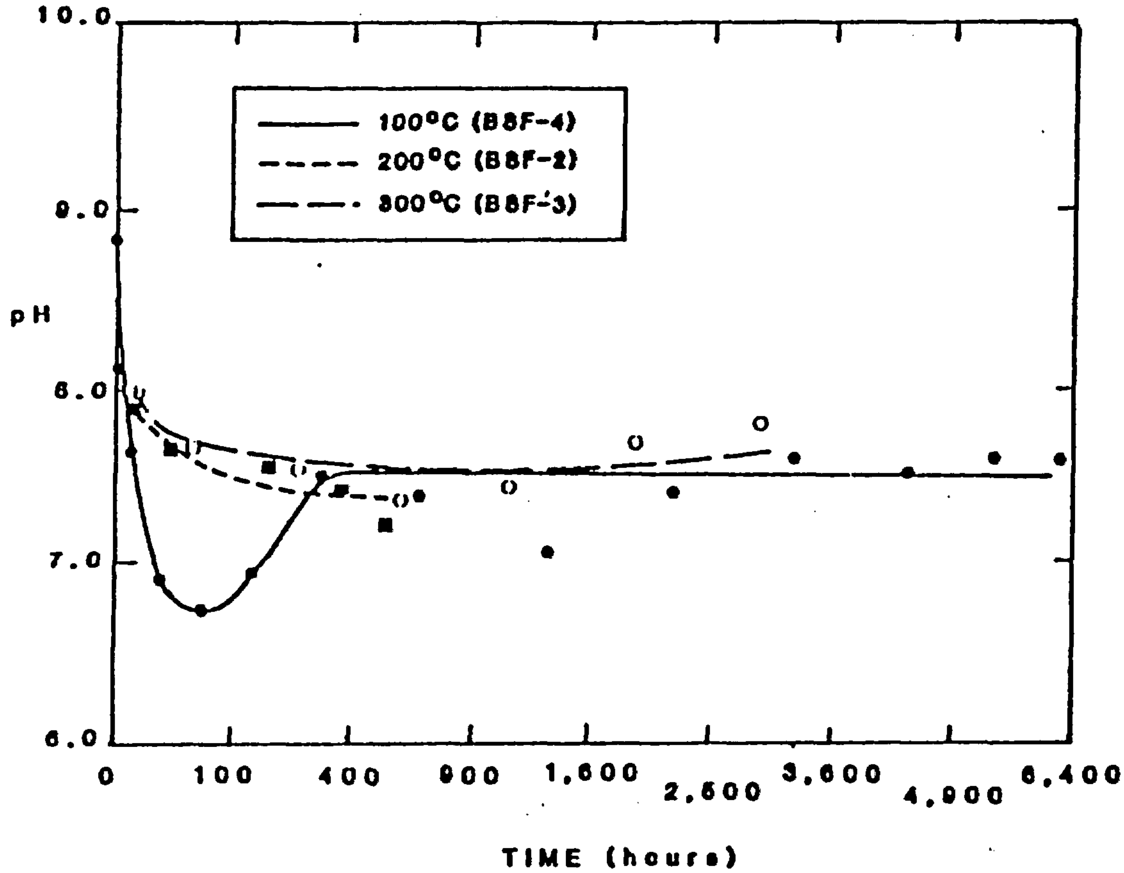

Figure 6.5-2

Effect of Temperature on Calculated pH Values for Simulated Spent Fuel Plus Basalt (AP-83)

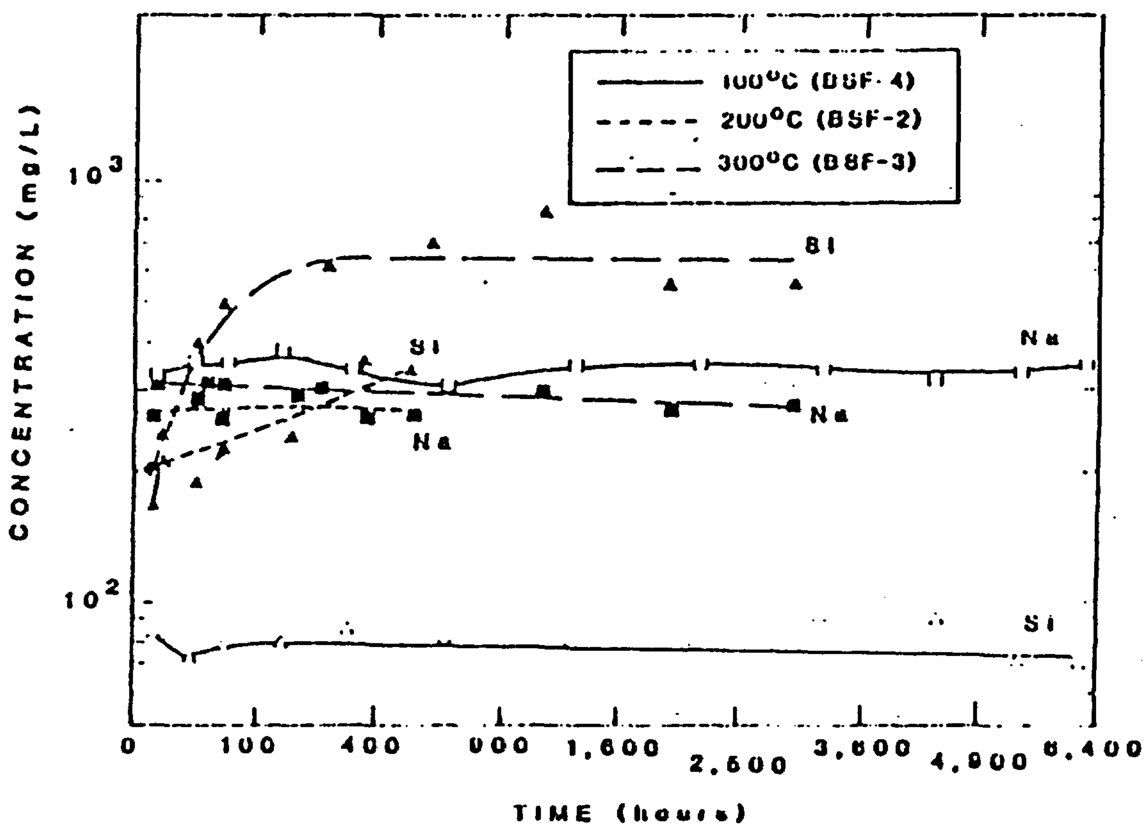

Figure 6.5-3

Effect of Temperature on Sodium and Silicon Concentrations for Simulated Spent Fuel Plus Basalt (AP-83)

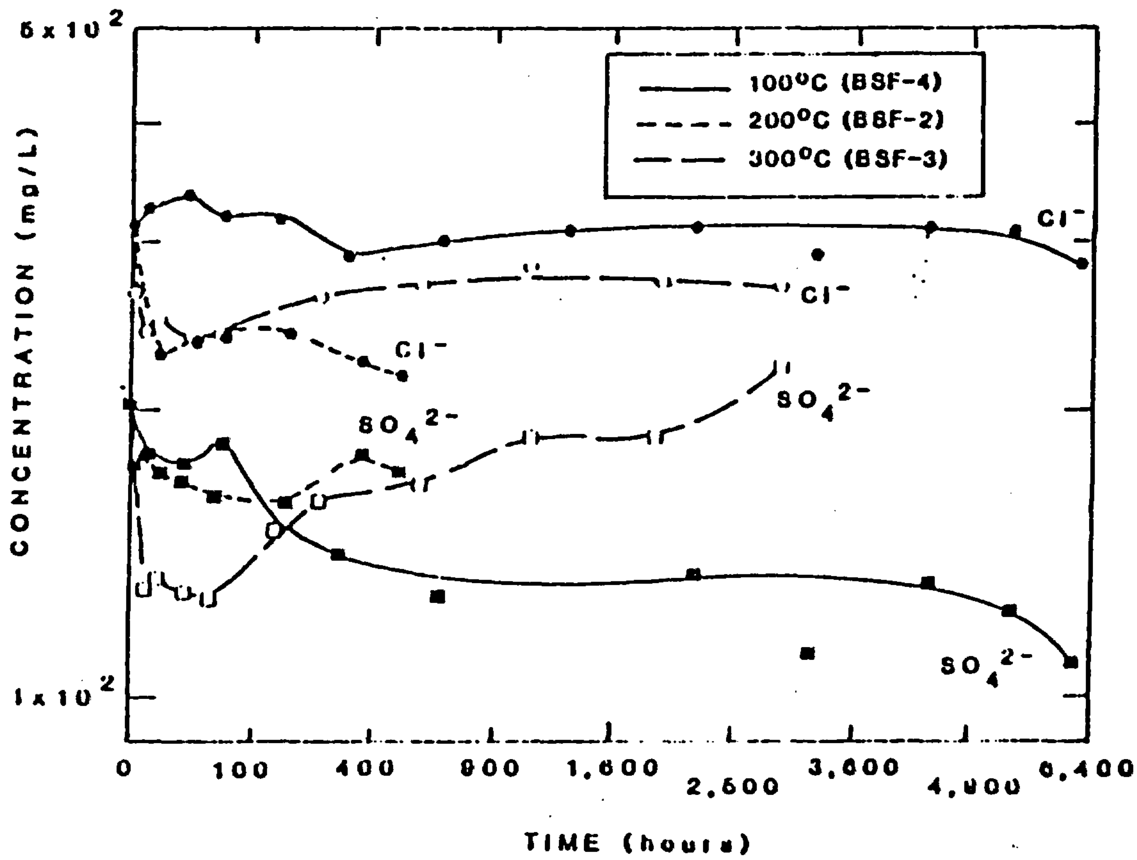

Figure 6.5-4

Effect of Temperature on Chloride and Sulfate Concentrations for Spent Fuel Plus Basalt (AP-83)

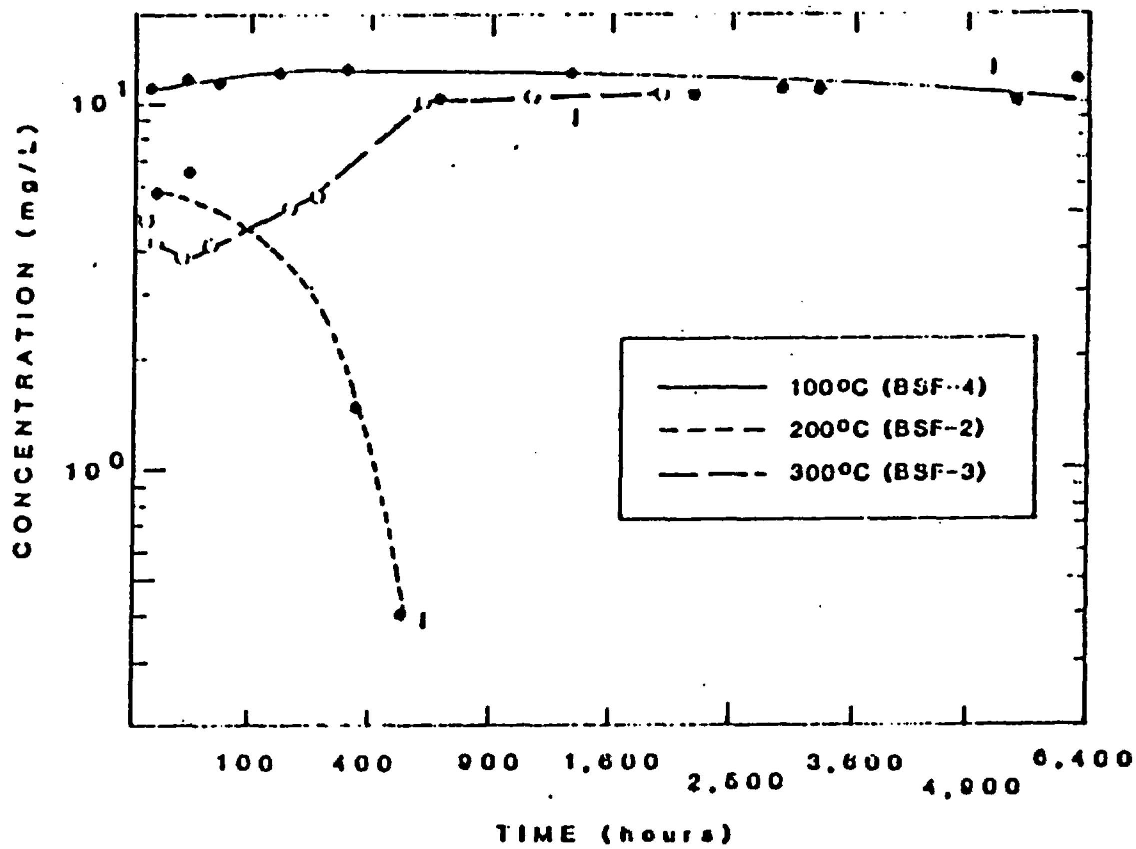

Figure 6.5-5

Effect of Temperature on Iodine Concentrations for Simulated Spent Fuel Plus Basalt (AP-83)

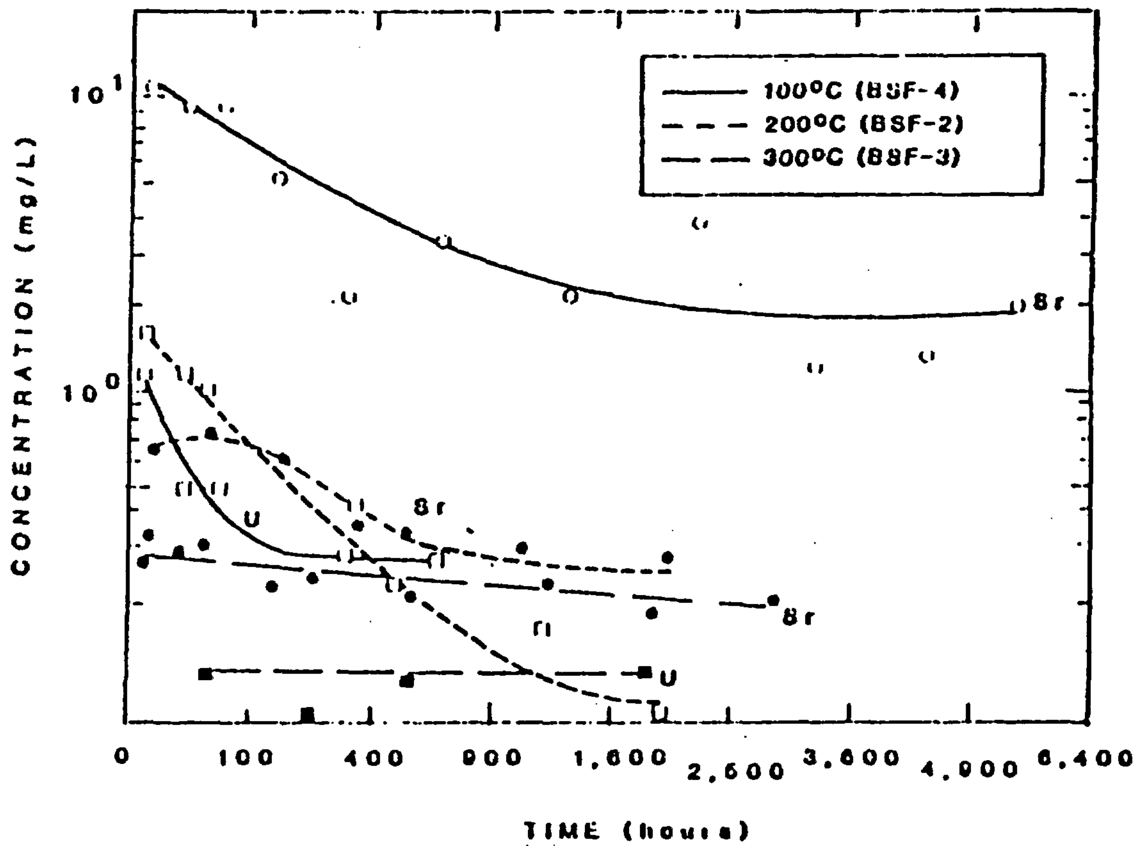

Figure 6.5-6

Effect of Temperatures on Strontium and Uranium Concentrations
for Simulated Spent Fuel Plus Basalt (AP-83)

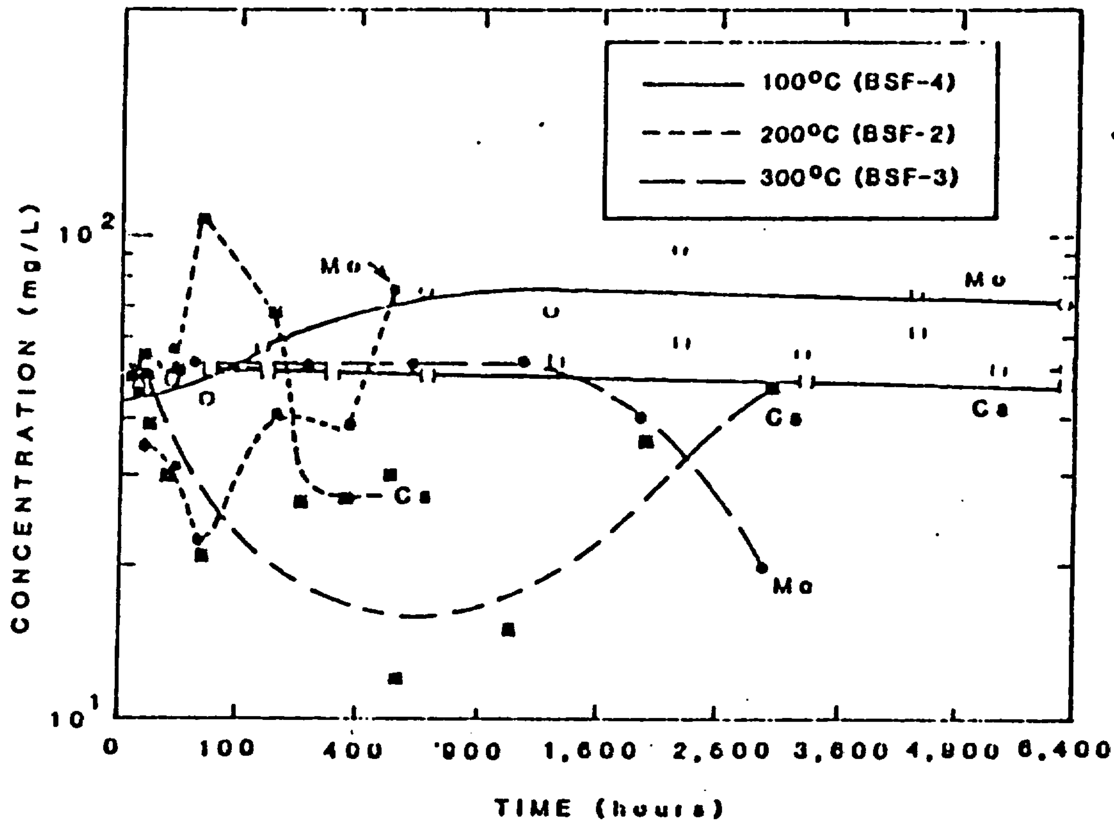

Figure 6.5-7

Effect of Temperature on Cesium and Molybdenum Concentrations for Simulated Spent Fuel Plus Basalt (AP-83)

REFERENCES

AN-63 Argonne National Laboratory, "Reactor Physics Constants," ANL-5800, July 1963.

AP-82 Apted, M.J. and J. Myers, "Comparison of the Hydrothermal Stability of Simulated Spent Fuel and Borosilicate Glass in a Basaltic Environment," Rockwell Hanford Operations, RHO-BW-ST-38P, July 1982.

AR-78 Arnorsson, S., K. Gronwold, and S. Sigurdsson, "Aquifer Chemistry of Four High-Temperature Geothermal Systems in Iceland," Geochim. Cosmochim. Acta, Vol. 42, pp. 523-536, 1978.

AR-82 Arnorsson, S., S. Sigurdsson, and H. Svarvarsson, "The Chemistry of Geothermal Waters in Iceland. I. Calculation of Aqueous Speciation from 0^{o} to $370^{o}C$," Geochim. Cosmochim. Acta, Vol. 46, pp. 1513-1532, 1982.

AR-83 Arnorsson, S., E. Gunnlaugsson, and H. Svarvarsson, "The Chemistry of Geothermal Waters in Iceland. II. Mineral Equilibria and Independent Variables Controlling Water Compositions," Geochim. Cosmochim. Acta, Vol. 47, pp. 547-566, 1983.

BI-64 Biggs, J.M., Introduction of Structural Dynamics, McGraw-Hill Book Co., New York, 1964.

BO-42 Boelter, L.M.K., V.H. Cherry, and H.A. Johnson, Heat Transfer, 3rd Edition, University of California Press, Berkeley, 1942.

BR-84a Brookins, D.G., Geothermal Aspects of Radioactive Waste Disposal, Springer-Verlag, New York, 1984.

BR-84b Brookins, D.G., personal communication with Lyle R. Silka, July 9, 1984.

CA-59 Carslaw, H.S. and J.C. Jaeger, Conduction of Heat in Solids, Clarendon Press, Oxford, England, 1959.

CH-83a Charles, R.W. and G.K. Bayhurst, "Sentinel Gap Basalt Reacted in a Temperature Gradient," LA-9481-MS, Los Alamos National Laboratory, January 1983.

CH-83b Charles, R.W. and G.E. Bayhurst, "Rock-Fluid Interactions in a Temperature Gradient: Biolite Granodiorite + H_2O," Jour. Volcanol. Geotherm. Res., Vol. 15, 137-166, 1983.

CO-84 Coffman, W., D. Vogt, and M. Mills, "A Summary of Computer Codes for Waste Package Performance Assessments," NUREG/CR-3699, March 1984.

CR-78 Croff, A.G., M.J. Bjerke, G.W. Morrison, and L.M. Petrie, "Revised Uranium-Plutonium Cycle PWR and BWR Models for the ORIGEN Computer Code," ORNL/TM-6051, Oak Ridge National Laboratory, September 1978.

CR-84 Croff, A.G., A.D. Kelmers, and S.K. Whatley, "Laboratory Evaluation of DOE Radionuclide Solubility Data and Selected Retardation Parameters, Experimental Strategies, Laboratory Techniques and Procedures," Program review and seminar, ORNL, April 12, 1984.

DE-82 De Salvo, G.J., "ANSYS Engineering Analysis System Verification Manual," Swanson Analysis Systems, Inc., 1982.

EL-83 Elders, W.A. and L.H. Cohen, "The Salton Sea Geothermal Field, California, as a Near-Field Natural Analog of a Radioactive Waste Repository in Salt," Office of Nuclear Waste Isolation, BMI/ONWI-513, 146 pp., November 1983.

GO-81 Goff, F.E., C.O. Grigsby, P.E. Trujillo, Jr., D. Counce, and A. Kron, "Geology, Water Geochemistry and Geothermal Potential of the Jemez Springs Area, Canon De San Diego, New Mexico," Jour. Volcanol. Geotherm. Res., Vol. 10, pp. 227-244, 1981.

GR-67 Griffin, D.S. "Deformation and Collapse of Fuel Rod Cladding Due to External Pressure," WAPD-TM-591, Bettis Atomic Power Laboratory, January 1967.

GR-83 Grigsby, C.O., J.W. Tester, P.E. Trujillo, Jr., D. Counce, J. Abbott, C.E. Holley, and L.A. Blatz, "Rock-Water Interactions in Hot Dry Rock Geothermal Systems: Field Investigations of In-situ Geochemical Behavior," Jour. Volcanol. Geotherm. Res., Vol. 15, pp. 101-136, 1983.

HE-47 Heisler, M.P., "Temperature Charts for Induction and Constant Temperature Heating," Trans. ASME, Vol. 69, pp. 227-236, 1947.

HE-69 Helgeson, H.C., "Thermodynamics of Hydrothermal Systems at Elevated Temperatures and Pressures," Am. Jour. Sci., Vol. 267, pp. 729-804, 1969.

HO-81 Holman, J.P., Heat Transfer, 5th Edition, McGraw-Hill Book Co., New York, 1981.

JU-81 Judson, B.F., H.R. Strickler, and K.J. Eger, "In-Plant Test Measurements for Spent Fuel at Morris Operation," NEDG-24922-2, September 1981.

KE-84 Kelmers, A.D., R.J. Clark, N.H. Cutshall, G.K. Jacobs, J.S. Johnson, J.H. Kessler, and R.E. Meyers, "Evaluation of Radionuclide Geochemical Information Developed by DOE High-Level Nuclear Waste Repository Site Projects," NUREG/CR-3730, 1984.

KR-58 Kreith, F., Principles of Heat Transfer, International Textbook Company, Scranton, Pennsylvania, 1958.

KR-75 Kristmannsdottir, H., "Hydrothermal Alteration of Basaltic Rocks in Icelandic Geothermal Areas," Proc. 2nd U.N. Symp. on Development and Use of Geothermal Resources, Vol. 1, pp. 441-445, U.S. Government Printing Office, 1975.

KU-81 Kusabe, H., H. Minato, M. Utado, and T. Yamenaka, "Phase Relations of Clinoptilolite, Mordenite, Analcine and Albite with Increasing pH, Sodium Ion Concentration and Temperature," Scientific papers of the College of General Education, Univ. of Tokyo, Vol. 31, pp. 39-59, 1981.

MI-83 Mills, M., D. Vogt, and B. Mann, "Parameters and Variables Appearing in Radiological Assessment Codes," NUREG/CR-3160, June 1983.

MO-83 Moore, D.E., C.A. Morrow, and J.D. Byerlees, "Chemical Reactions Accompanying Fluid Flow through Granite Held in a Temperature Gradient," Geochim. Cosmochim. Acta, Vol. 47, pp. 445-453, 1983.

MY-83 Myers, J., M.J. Apted, and J.J. Mazer, "Hydrothermal Reaction of Simulated Waste Forms with Barrier Materials under Conditions Expected in a Nuclear Waste Repository in Basalt," SD-BWI-TI-141, Rockwell Hanford Operations, September 1983.

ON-83 Office of Nuclear Waste Isolation, "Conceptual Waste Package Design for Disposal of Nuclear Waste in Tuff," ONWI-439, April 1983.

OR-82 Oak Ridge National Laboratory, "SCALE, A Modular Code System for Performing Standardized Computer Analysis for Licensing Evaluation," Vols. 1-3, NUREG/CR-0200, January 1982.

RE-82 Reardon, E.J. and J.D. Reimer, "A Laboratory Investigation of Crystalline Rock-Water Interactions," TR-137, Atomic Energy of Canada, Ltd., March 1982.

RO-56 Rockwell, T., ed., "Reactor Shielding Manual," TIO-7004, March 1956.

RO-65 Roark, R.J., Formulas for Stress and Strain, 4th Edition, McGraw-Hill Book Co., New York, 1965.

RO-82 Rockwell Hanford Operations, "Site Characterization Report for the Basalt Waste Isolation Project," DOE/RL 82-3, November 1982.

SE-84 Seitz, M., G. Vandegrift, T. Gerding, D. Bowers, S. Fried, and C. Wilbur, "Laboratory Analog Program" in Steindler, M.J., ed., "Fuel Cycle Programs Quarterly Progress Report, January-March 1983," pp. 34-36, Argonne National Laboratory, ANL-83-68, January 1984.

SH-77 Shanks, W.C. and J.L. Bischoff, "Ore Transport and Deposition in the Red Sea Geothermal System: A Geothermal Model," Geochim. Cosmochim. Acta, Vol. 41, pp. 1507-1519, 1977.

ST-83 Stone, W.J., F.P. Lyford, P.F. Frenzel, N.H. Mizell, and E.T. Padget, "Hydrogeology and Water Resources of San Juan Basin, New Mexico," Hydrologic Report 6, New Mexico Bureau of Mines and Mineral Resources, Socorro, New Mexico, 1983.

TH-65 Thomson, W.T., Vibration Theory and Applications, Prentice Hall, Inc., Englewood Cliffs, New Jersey, 2nd Printing, 1965.

TI-56 Timoshenko, S., Strength of Materials, Part 1, Elementary Theory and Problems, 3rd Edition, D. Van Nostrand Co., New York, 1956.

UN-82 Unterzuber, R., et al., "Spent Fuel Dry Storage Testing at E-MAD," PNL-4533, AESD-TME-3162, Westinghouse Electric Corporation, Advanced Energy Systems Division, Pittsburgh, Pennsylvania, 1982.

WE-82 Westinghouse Electric Corporation, "Waste Package Conceptual Designs for a Nuclear Repository in Basalt," RHO-BW-CR-136P, Rockwell Hanford Operations, October 1982.

WO-82 Wood, M.I. and G.D. Aden, "Evaluation of Sodium Bentonite and Crushed Basalt as Waste Package Backfill Materials," RHO-BW-ST-21P, Rockwell Hanford Operations, October 1982.

APPENDIX A

Will be Obtained from NRC